Effect of Inter-critical Annealing Parameters on the Recrystallization, Austenite Formation and Stabilization in a Dual Phase Steel

A Dissertation Submitted
In Partial Fulfillment of the Requirements
for the Degree of

Master of Engineering

in

Production Engineering

by

Mayank Mittal
Regd. No. 801282013

Under the guidance of

Dr. Tarun Nanda
Assistant Professor,
MED, TU, Patiala

Dr. B. Ravi Kumar
Scientist (E_2),
NML, Jamshedpur

to the

MECHANICAL ENGINEERING DEPARTMENT
THAPAR UNIVERSITY, PATIALA
JULY, 2014

Declaration

I, hereby declare that the thesis entitled '**Effect of Inter-critical Annealing Parameters on the Recrystallization, Austenite Formation and Stabilization in a Dual Phase Steel**' is an authentic record of thesis work carried out as requirement for the award of degree of **Master of Engineering** in **Production Engineering** at **Thapar University, Patiala** under the supervision of **Dr. Tarun Nanda**, Assistant Professor, MED, Thapar University, Patiala and **Dr. B. Ravi Kumar**, Scientist E-II, MST Division, National Metallurgical Laboratory (NML), Jamshedpur, during July, 2012 to July, 2014.

The matter embodied in this report has not been submitted in any other University/Institute for award of Masters of Engineering or any other degree.

Mayank Mittal

Mayank Mittal

Place: PATIALA

Date: 18/07/14

Certificate

This is to certify that the thesis entitled, **'Effect of Inter-critical Annealing Parameters on the Recrystallization, Austenite Formation and Stabilization in a Dual Phase steel'**, being submitted by Mayank Mittal (Regd. No. 801282013), in partial fulfilment of the requirements for the award of degree of Master of Engineering in Production Engineering of Mechanical Engineering Department, Thapar University, Patiala, is a record of candidate's own work carried out by him under our supervision. To the best of our knowledge, the content of this thesis does not form a basis for the award of any previous degree to anyone else.

Dr. Tarun Nanda
Assistant Professor
MED, TU, Patiala

Dr. B. Ravi Kumar
Principle Scientist (E_2)
NML, Jamshedpur

(Countersigned by)

Dr. Ajay Batish
Professor and Head
MED, TU, Patiala

Dr. S.K. Mohapatra
Dean of Academics Affairs
TU, Patiala

ii

Acknowledgements

This thesis is the end of my journey in obtaining my M.E. degree. I have not travelled in a vacuum in this journey. This thesis has been kept on track and been seen through to completion with the support and encouragement of numerous people including my well-wishers, my family and my dear friends. At the end of my thesis I would like to thank the Almighty and all those people who made this thesis possible.

At this moment of accomplishment, first of all I would like to thank my guide **Dr. Tarun Nanda,** *Assistant Professor, Mechanical Engineering Department, Thapar University, Patiala for his continuous guidance, support and encouragement. Despite of his busy schedule, he used to review my thesis progress, gave his valuable suggestions and made corrections.*

I am also extremely indebted to my guide **Dr. B. Ravi Kumar,** *Scientist (E-II), Material Science & Testing division, National Metallurgical Laboratory (NML), Jamshedpur for providing necessary infrastructure and resources to accomplish this work. I am very much thankful to him for picking me up has his student. I warmly thank him for his invaluable suggestions, constructive criticism and his extensive discussion around my work.*

My sincere thanks to **Dr. Ajay Batish,** *Professor and Head, MED, TU, Patiala and* **Dr. S.K. Mohapatra,** *Dean of Academic Affairs, TU, Patiala for providing me with the opportunity to conduct this work and bring it out in the present form.*

I take this opportunity to sincerely acknowledge the **National Metallurgical Laboratory (NML),** *Jamshedpur for giving me an opportunity to conduct this work quite comfortably.*

My special acknowledgements go to **Rao Ji** *and* **Mr. Ranjit Prasad** *who made possible the difficult task of 'Sample preparation' for my experiments.*

Mayank Mittal

Mayank Mittal

Abstract

Advanced high strength steels (AHSS) have been developed in the last few decades especially for automotive applications due to their remarkable properties combining high strength and good ductility. DP steels are the most common grade of advanced high strength steels which are produced through inter-critical annealing of a low carbon steel followed by an accelerated cooling to obtain the ferrite-martensite (dual phase) microstructure. The strength of DP steels is manipulated by the amount of martensite and ductility by the size and distribution of this phase. The fraction of martensite formed depends upon the austenite amount available during the inter-critical annealing process. So, it is always important to understand the kinetics of ferrite recrystallization and austenite formation during the annealing of cold rolled sheets. The present work focuses on understanding the effect of intercritical annealing parameters (viz. annealing temperature, soaking time periods etc.) on ferrite recrystallization, austenite formation and its stabilization during the production of dual phase steel from a low carbon cold rolled steel. The main effort of this research work has been to arrive at the combination of annealing process parameters to produce the desired ferrite-martensite structures. For the study, commercial software viz. Thermo-Calc (3.0) and JMat-Pro (7.0) have been used to predict the various annealing parameters. The predicted values have been compared with the experimental values and a significant variation has been observed in the results. It has been concluded that the annealing parameters clearly affect the phenomenon of ferrite recrystallization, and austenite formation and its stabilization during the production of dual phase steels. Hence, this study is very helpful in understanding the synergistic effect of ferrite recrystallization and austenite phase transformation behaviour in dual phase steels to tailor design the mechanical properties by microstructure control.

Table of Contents

Declaration……(i)
Certificate……(ii)
Acknowledgement……...(iii)
Abstract……(iv)
Table of Contents……(v)
List of Figures……(viii)
List of Tables……...(x)
List of Acronyms……(xi)

Chapter 1 INTRODUCTION……..1–8
1.1 General……1
1.2 Advanced High Strength Steels……1
1.2.1 Common AHSS Types……...2
A) Dual-Phase Steels……...3
B) Transformation Induced Plasticity Steels……..3
C) Complex Phase Steels……4
D) Martensitic Steels……...4
E) Twinning Induced Plasticity Steels……4
1.3 Manufacturing Aspects of DP Steels.....4
1.4 Inter-Critical Annealing of Dual Phase Steels……5
1.5 Properties and Applications of Dual Phase Steels……..……..……...6
1.6 Effect of Alloying Elements in Dual Phase Steels……7
1.7 Current Trends in the Field of Dual Phase Steels……..7
1.8 Summary of the Chapter……8

Chapter 2: LITERATURE REVIEW……9–24
2.1 Introduction.....9
2.2 Review of the Literature.....9
2.3 Gaps in the Existing Literature……..23

Chapter 3: DESIGN OF THE STUDY……25–39
3.1 Introduction……25
3.2 Establishment of the Objective Function……...25
3.3 Experimental Procedure ……26
3.3.1 Material and Processing……..26
A) Starting Material……..26
B) Characterization of Pearlite Phase Mixture…….27
3.3.2 Estimation of Annealing Parameters…….27
3.3.3 Recrystallization Studies……...27
3.3.4 Study of Austenite Formation……..28
3.3.5 Tensile Properties Evaluation……...28
3.4 Machines and Equipment…….29
3.4.1 Precision Cutter……...29
3.4.2 Tensile Testing Machine……..29
3.4.3 Hardness Testing Machine……..31
3.4.4 Muffle Furnace……....31
3.4.5 Sample Preparation for Metallography……...32
A) Mounting…….32
B) Grinding……..33
C) Polishing……..33
D) Etching…….…...35
E) Levelling…….……35
3.4.6 Microstructural Evaluation…….35
A) Optical Microscope……..35
B) Scanning Electron Microscope…….…...37
3.4.7 Annealing Simulator……...37
3.4.8 Commercial Software…….38
A) Thermo-Calc…….…....38
B) JMat-Pro……....…..39
C) ImageJ…….....39
3.5 Summary of the Chapter……39

Chapter 4: RESULTS AND DISCUSSION…….40–62
4.1 Introduction……40
4.2 Microstructure of the as-Received Steel……40
4.3 Prediction of Annealing Parameters ……...42
4.3.1 Thermo-Calc Predictions for Annealing Parameters……...42
4.3.2 JMat-Pro Predictions for Annealing Parameters…….……42
4.4 Recrystallization Kinetics…..……..……43
4.4.1 Calculation of Recrystallization Fraction…….44
4.4.2 Calculation of Activation Energy ……50
4.5 Kinetics of Austenite Formation ……52
4.6 Annealing Under Optimum Conditions in the Simulator……59
4.7 Tensile Property Evaluation……61
4.8 Summary of the Chapter……..62
Chapter 5: CONCLUSIONS …….....63–66
5.1 Introduction……..…….…..63
5.2 Results and Conclusions……..……....63
5.3 Major Conclusions and Recommendations……65
5.4 Scope of Future Work……66
REFERENCES …….....….....67–69
APPENDICES……70-80

List of Figures

Figure No.	Description	Page No.
Figure 1.1	Classification of Advanced High Strength Steels	2
Figure 1.2	Phase transformations during manufacturing of dual phase steels	6
Figure 3.1	Low Speed Precision Cutter	29
Figure 3.2	Tensile testing machine	30
Figure 3.3	Drawing of the Tensile Testing Specimen	30
Figure 3.4	Hardness Testing Machine	31
Figure 3.5	Muffle Furnace	32
Figure 3.6	Mounting Press	33
Figure 3.7	Abrasive Papers	34
Figure 3.8	Polishing Machine	34
Figure 3.9	Levelling Machine	36
Figure 3.10	Optical Microscope	36
Figure 3.11	Scanning Electron Microscope	37
Figure 3.12	Annealing Simulator	38
Figure 4.1	Optical micrographs of as-received steel in (a) rolling plane and (b) transverse plane	41
Figure 4.2	SEM micrographs of as-received steel showing (a) different pearlite colonies (b) distribution of colonies (c) destruction of lamellar structure	41
Figure 4.3	Result window of Thermo-Calc for a) Equilibrium phase diagram b) Phase fraction diagram for the as-received material	42
Figure 4.4	Result window of JMat-Pro (a) Phase Fraction diagram (b) TTT diagram (c) TTA diagram (d), CCT diagram for equilibrium heating conditions	43

Figure 4.5	Variation in recrystallization fraction with different annealing temperatures and holding time periods.	45
Figure 4.6	JMAK plot of ln(ln(1/(1-X)) vs. ln(t) for different temperatures	51
Figure 4.7	Plot of $ln(b)$ vs.$1/T$	52
Figure 4.8	SEM micrographs of sample annealed at 775 ℃ for 3 min showing martensite along grain boundaries.	53
Figure 4.9	Optical micrographs of steel containing (a) fully ferritic and (b) fully martensitic microstructures	54
Figure 4.10	Martensite volume fraction obtained at a given annealing temperature with different soaking periods	58
Figure 4.11	Tensile specimen (a) before annealing (b) after annealing and tensile testing	59
Figure 4.12	Cooling curve for sample annealed in the simulator	60
Figure 4.13	Optical micrographs of the specimen annealed at 825 ℃, 3 min holding (a) annealing simulator (b) muffle furnace.	60
Figure 4.14	Stress-strain curves for the as-received and annealed steel	61

List of Tables

Table No.	Description	Page No.
Table 1.1	Effect of Alloying Elements in DP Steels	7
Table 3.1	Chemical composition of the investigated steel	27
Table 4.1	Austenite phase fraction at different inter-critical temperatures from JMat-Pro	44
Table 4.2	Optical Micrographs for the Recrystallization Studies	46
Table 4.3	Austenite fraction obtained under various annealing conditions and JMat-Pro predictions	55
Table 4.4	Optical micrographs for austenite fraction under various annealing conditions	56

Acronyms

Acronym	Full Name
ACST	Accelerated-Cooling Start Temperature
AHSS	Advanced High Strength Steels
ASS	Austenitic Stainless Steels
ATMP	Advanced Thermo Mechanical Processing
CA	Continuous Annealed
CCT	Continuous Cooling Transformation
CG	Coarse Grained
CP	Complex Phase
CR	Cold Rolled
DBTT	Ductile To Brittle Transition Temperature
DP	Dual Phase
EBSD.	Electron Backscatter Diffraction
F	Ferrite
FBDP	Ferrite/Bainite Dual Phase
FG	Fine Grained
FH	Fast Heated
FMDP	Ferrite/Martensite Dual Phase
IcQ	Inter-Critical Quenching
ImQ	Intermediate Quenching
JMAK	Johnson-Mehl-Avrami-Kolmogorov
L-IP	Light Weight with Induced Plasticity
M-A	Martensite–Austenite
MART	Martensitic
M-TRIP	**m**artensite based TRIP
PLC	Programmable Logic Controller
Q&P	Quenching and Partitioning
SB-TRIP	Super Bainite TRIP
SFE	Stacking Fault Energy
SEM	Scanning Electron Microscope
S-IP	Shear band formation Induced Plasticity
SPD	Severe Plastic Deformation
SQ	Step Quenching
TEM	Transmission Electron Microscopy
TMCP	Thermo Mechanical Controlled Processing

TRIP	Transformation Induced Plasticity
TS-EI	Tensile Strength–Elongation
TTA	Temperature Transformation of Austenite
TTT	Time Temperature Transformation
TWIP	Twinning Induced Plasticity
UFC	Ultra-Fast Cooling
UFG	Ultra-Fine Grained
UTS	Ultimate Tensile Strength
X-AHSS	Extra Advanced High Strength Steels
YS	Yield Strength

Symbols

Symbol	Full Name
℃	Degree Celsius
α	Ferrite
γ	Austenite
%	Percentage
Ac_1	Lower Critical Temperature during heating
Ac_3	Upper Critical Temperature during heating
Ar_1	Lower Critical Temperature during cooling
Ar_3	Upper Critical Temperature during cooling
b	Temperature Dependent Value (JMAK Analysis)
b_0	A Constant (JMAK Analysis)
B_f	Bainitic Ferrite Transformation Finish
e	Exponential
H_0	Initial Microhardness of As-received Steel
H_t	Microhardness after Heat Treatment
H_{Rex}	Microhardness of Fully Recrystallized Ferrite
ln	Natural Log
M_S	Martensite Start Temperature
M_f	Martensite Finish Temperature
n	Strain Hardening Coefficient; Avrami Constant
Q	Activation Energy for Ferrite Recrystallization
R	Universal Gas Constant
$R_{t1.5}$	Stress corresponding to 1.5% total engineering strain
$R_{t0.5}$	Stress corresponding to 0.5% total engineering strain
r_m	Plastic Strain Ratio
s	Second
t	Time

T	Temperature
T_c	Coiling Temperature
T_{iso}	Isothermal Temperature
X	Recrystallized Fraction

Chapter 1

Introduction

1.1 General

Despite the development of sophisticated composite materials in recent years, steel is still the basic construction material for industrial applications. While classical single phase steels either have good formability (ferritic steels) or strength (martensitic steels), modern multiphase steels like dual-phase (DP) or Transformation Induced Plasticity (TRIP) steels have shown high potential especially for automotive applications due to their remarkable properties combining high strength and good formability [Homeberg et al., 2011]. The current demands in the automobile industry for vehicle weight reduction for improved fuel economy while maintaining crash performances requires development of new and advanced high strength steels with extraordinary combination of strength and toughness. This requires new and innovative concepts of alloy design and novel processing for creation of unique microstructures in steels known as Advanced High Strength Steels (AHSS). The development of dual-phase (DP) steels has become an area of interest in the automobile industry because of potential weight reduction by using inexpensive alloying without sacrificing mechanical properties [Saleh and Priestner, 2001]. DP steel possesses combination of special mechanical properties such as high tensile strength, high work hardening rate at early stages of plastic deformation as well as very good ductility [Wang and Wei, 2013]. In DP steels, combination of these properties is achieved by obtaining a ferrite/bainite or ferrite/martensite microstructure, where ferrite forms the ductile and deformable element and the second phase bainite or martensite strengthens the steel [Cornet and Herman, 2003].

1.2 Advanced High Strength Steels

Advanced High Strength Steels (AHSS) are characterised by improved formability and crash worthiness as compared to conventional steel grades. AHSS derive their properties from multi-phase complex microstructure. AHSS can be broadly classified into three main categories as shown in Fig. 1.1.

The First Generation AHSSs include Dual-Phase (DP) steels, Transformation Induced Plasticity (TRIP) Steels, Complex Phase (CP) steels and Martensitic (MART) Steels. The

first generation AHSS concepts were developed in fairly lean compositions and are primarily ferritic-based multi-phase microstructures.

The austenitic stainless steels (ASS), Twinning Induced Plasticity (TWIP) steels, Light-weight steels with induced plasticity (L-IP) and Shear band formation Induced Plasticity steels (SIP) are referred to as Second Generation AHSS. The second generation AHSS steels exhibit superior mechanical properties, but these are highly alloyed resulting in a significant cost increase.

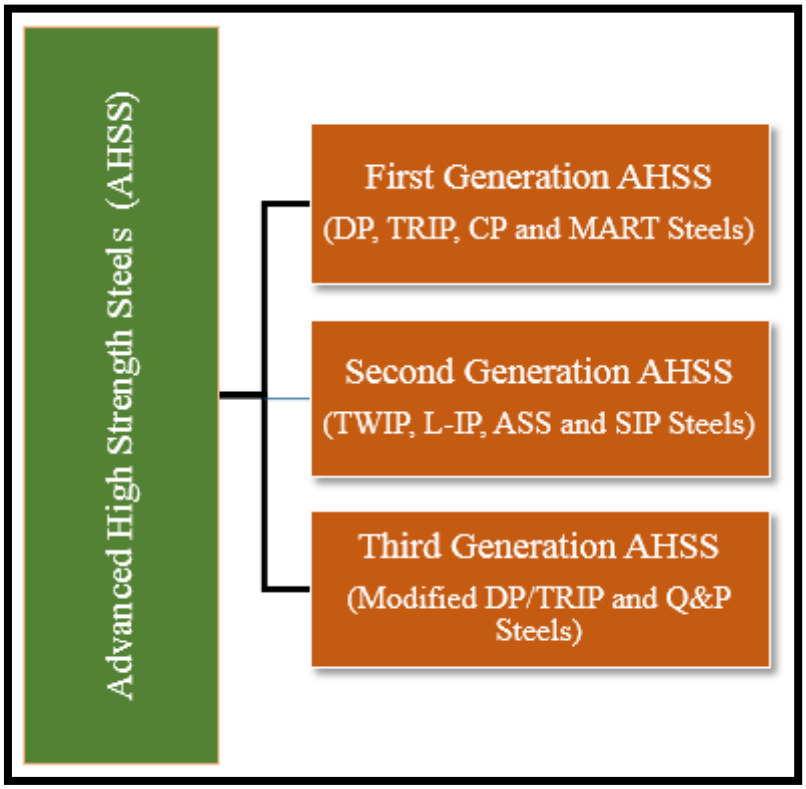

Fig. 1.1 Classification of Advanced High Strength Steels

Third generation AHSS are focused on increasing strength and/or ductility to higher level than exhibited by the first generation AHSS without significantly enriching the alloy compositions. Thus third generation is aimed at reducing the alloying levels in second generation AHSS grades. These steels include modified DP and TRIP steels which are modified to enhance their mechanical properties further. These modifications include methods like implementation of new processing routes, ultrafine microstructure and quenching and partitioning etc. [Matlock et al., 2012].

1.2.1 Common AHSS Types

Some of the commonly used types of AHSS include DP steels, TRIP steels, CP steels, MART steels and TWIP steels. Among these five AHSS steels, DP steels and TRIP steels are most

common which are used in the automobile industry due to their high energy absorption potential during car crashes or collisions [Kuziak et al., 2008]. These common types of AHSS are discussed in the following sections.

A) Dual-Phase Steels

Dual-Phase (DP) Steels are the steels having microstructure composed of ferrite matrix and hard bainite or martensite phase. This type of microstructure allows achieving an ultimate tensile strength in the range of 500–1200 MPa. The strength of the DP steel microstructure is controlled by the amount of martensite/bainite and ductility by the size and distribution of this phase. These steels do not exhibit yield point elongation and possess low YS/UTS ratio (around 0.5). The DP steels show high strain hardening characteristics (high *n* value), especially at the beginning of plastic deformation. The microstructure of DP steels do not allow obtaining high plastic strain ratio (r_m), which means that these steels are not good candidates for applications that require high drawability. DP steels with martensite phase usually exhibit poor hole expansion ratio values which can be improved by adding titanium which reduces the differences in hardness between the two phases i.e. ferrite and martensite. These steels can be welded with all conventional welding methods [Kuziak et al., 2008].

B) Transformation Induced Plasticity Steels

Transformation Induced Plasticity (TRIP) Steels are based on the phenomenon that the strain or stress induced transformation of retained austenite present in the microstructure in a sufficient amount can substantially harden the steel during deformation. This phenomenon results in higher ductility of these steels. The mechanical properties of TRIP steels are derived from their dispersed multi-phase microstructure which is composed of ferrite (50–55%), bainite (30–35%), retained austenite (7–15%), and martensite (1–5%). Among these phases, retained austenite is the most important phase constituent of TRIP steels. During deformation, retained austenite transforms to martensite. The TRIP steels are characterized by a relatively low content of alloying elements. The carbon content plays a fundamental role in TRIP steel composition design, since its distribution among the main microstructural constituents is fundamental to the steel properties. To obtain the best mechanical properties in a product, first of all, carbon should be distributed to austenite to enrich this phase as much as possible to preserve the M_S lower (near room temperature) value [Kuziak et al., 2008].

C) Complex Phase Steels

Complex phase (CP) steels belong to a group of steels with very high ultimate tensile strength of 800 MPa or even greater. The chemical composition and microstructure of these steels is very similar to that of TRIP steels, but, additionally it contains some quantities of Nb, Ti and or V to cause the precipitation strengthening effect. CP steels have no retained austenite in the microstructure, but contain more hard phases like martensite and bainite. The CP steels are characterized by continuous yielding and high uniform elongation. CP steels with the bainitic matrix have superior formability because the difference between hardness of bainite and martensite is relatively small. The bainitic CP microstructure exhibits better strain hardening and strain capacity than that for fully bainitic microstructure [Kuziak et al., 2008].

D) Martensitic Steels

Martensitic (MART) steels provide the highest ultimate strength of upto 1500 MPa. Microstructure of martensitic steels is mainly composed of lath martensite, which is developed by the transformation of austenite during quenching after hot rolling or annealing. They are often subjected to post-quench tempering with the aim of improving ductility and provide good formability even at very high ultimate strength. The concept of chemical composition of martensitic steels is based upon the proper carbon content adoption, since this element increases hardenability and strength [Kuziak et al., 2008].

E) Twinning Induced Plasticity Steels

Twinning Induced Plasticity (TWIP) Steels are based on the potential mechanism of obtaining the superior balance of tensile strength and elongation using twinning induced plasticity effect. This superior mechanical performance is obtained by gradual twinning during deformation. The formation of twins partitions the austenite grains and induces the continuous strain hardening, resulting in improved ductility. The strain hardening behavior is strongly dependent on the stacking fault energy (SFE), which determines the deformation mechanism of the material. Due to lower stacking fault energy of TWIP steels, the twinning behavior is enhanced during deformation and, thereby, increases ductility [Kwon et al., 2010].

1.3 Manufacturing Aspects of DP Steels

Dual Phase (DP) steels, as the most common type of AHSS have been increasingly used in vehicles and structural parts due to the combination of special mechanical properties such as high tensile strength and good ductility [Wang and Wei, 2013]. Microstructure of dual phase

steels is composed of ferrite which is a ductile or deformable phase and bainite or martensite as the second phase which provides strength [Cornet and Herman, 2003]. Significant work on production of DP steels was started during late 1970's and early 1980's. These DP steels containing ferrite and martensite were formed by inter-critical annealing followed by quenching [Matlock et al., 2012]. Modern DP steels which contain ferrite as the primary and martensite as the secondary phase are produced by complex processes involving thermomechanical processing followed by controlled cooling [Kuziak et al., 2008]. The cooling rate affects the microstructure and final properties of the DP steels. On a conventional laminar cooling table, it is not possible to control the cooling rate of the hot rolled strip. The cooling rate depends on the speed and the thickness of the strip and also on the external variables like temperature of the cooling fluid etc. [Cornet and Herman, 2003; Tan et al., 2012]. The chemical composition of the steel is adopted as a function of the microstructure to be achieved [Cornet and Herman, 2003; Kuziak et al., 2008].

1.4 Inter-critical Annealing of Dual Phase Steels

The processing route for the production of dual phase steel involves heating the low carbon steel into the inter-critical region, where a ferrite-austenite mixture is formed followed by fast cooling to room temperature to produce ferrite-martensite dual phase microstructure [Huang et al., 2004]. Two major events that occur during the inter-critical annealing of cold rolled steel are recrystallization of deformed ferrite grains and the austenite formation. Normally under the conventional continuous annealing conditions, recrystallization of ferrite completes before inter-critical temperature range. However, under the high rates of heating, recrystallization temperature shifts above Ac_1. The formation of austenite is a nucleation and grain growth process. The formation of austenite starts at the ferrite-cementite interfaces within the pearlite colonies and later at the recrystallized ferrite boundaries. The process of austenite formation can be separated into three main stages viz. (i) very rapid growth of austenite into pearlite until pearlite dissolution is complete; (ii) slower growth of austenite into ferrite controlled by carbon diffusion rate, and (iii) very slower final equilibration of ferrite and austenite. After quenching or fast cooling, martensite is formed in the austenite grains available at a given annealing temperature. Fig. 1.2 shows the transformation of phases during manufacturing of DP steels [Souza et al. 1982; Huang et al., 2004; Li et al., 2013]

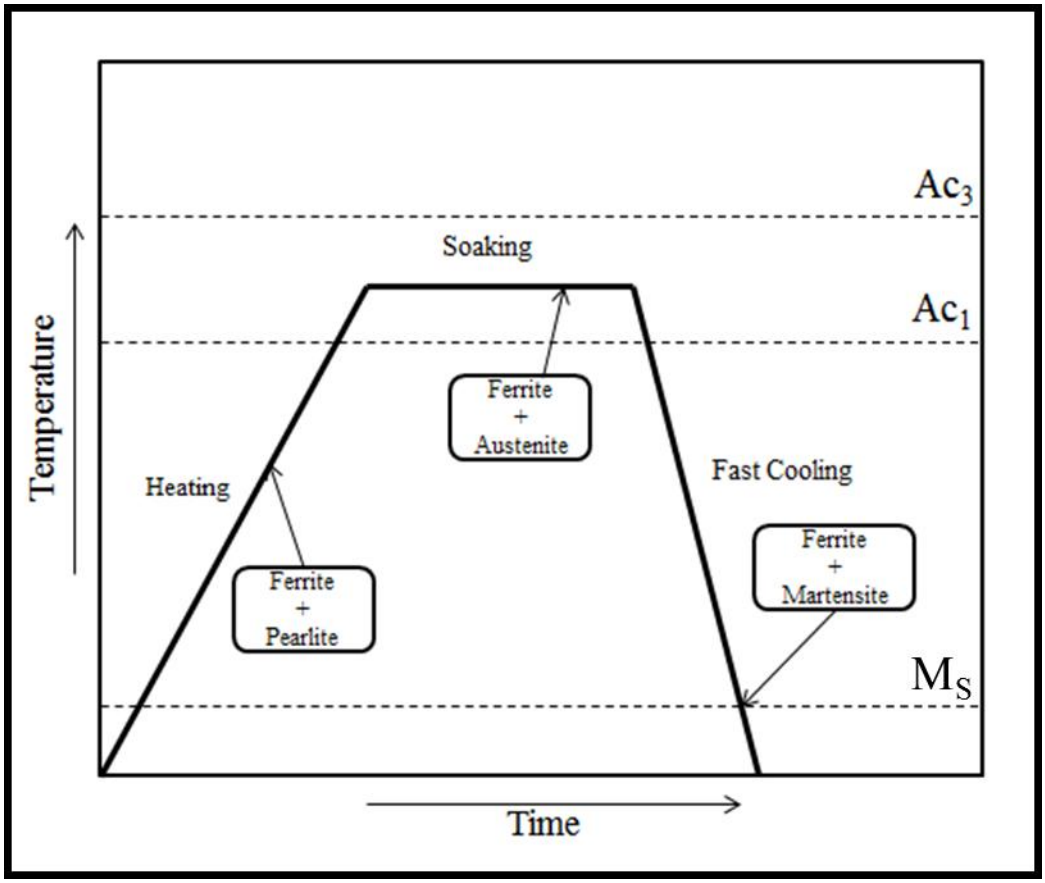

Fig. 1.2 Phase transformations during manufacturing of dual phase steels

1.5 Properties and Applications of Dual Phase Steels

The combination of high strength and ductility in modern AHSS can allow thinner components to be used in car construction and also to improve the safety due to their high energy-absorption capabilities. Dual-phase steels developed over the past few decades offer impressive mechanical properties, such as continuous yielding behavior and superior strength–ductility combination, in addition to the advantage of reduced cost, better formability, and excellent surface finish [Kumar et al., 2008; Dziedzic and Turczyn; 2010, Sayed and Kheirandish, 2012]. The most important features influencing the mechanical properties of dual-phase microstructure comprises shape, size, amount and distribution of ferrite and bainite/martensite phases [Kuziak et al., 2008]. This type of microstructure allows achieving an ultimate tensile strength in the range of 500−1200 MPa. DP steels possess low YS/UTS ratio (around 0.5) and high strain hardening characteristics (high *n* value). The enhancements in formability with strength and ductility combinations make DP steels strong candidates for structural applications [Kang et al., 2013]. The usage of dual phase steels for automotive applications is increasing, because they can meet the formability requirements

and other properties such as high tensile strength, fatigue resistance, hole expansion, good drawing and welding properties [Cai et al., 2014].

1.6 Effect of Alloying Elements in Dual Phase Steels

The microstructure obtained in DP steels depends primarily on the chemical composition. The major elements constituting the DP steels are Carbon, Manganese, Silicon, Chromium and Molybdenum etc. The effects and the reasons due to which these elements are added in the dual phase steels are discussed in Table 1.1.

Table 1.1 Effects of Alloying Elements in DP Steels [Kuziak et al., 2008]

S. No.	Alloying Element	Effects and Reason of Adding
1.	Carbon (C)	• Austenite Stabilizer • Strengthens Martensite • Determines the Phase Distribution
2.	Manganese (Mn)	• Austenite Stabilizer • Solid Solution Strengthener of Ferrite • Retards Ferrite Formation
3,	Silicon (Si)	• Promotes Ferrite Formation
4.	Chromium, Molybdenum (Cr, Mo)	• Austenite Stabilizer • Retards Pearlite and Bainite Formation
5.	Vanadium (V)	• Austenite Stabilizer • Precipitation Strengtheners • Refines Microstructure
6.	Niobium (Nb)	• Austenite Stabilizer • Reduces M_S Temperature • Refines Microstructure and Promotes Ferrite Formation

1.7 Current Trends in the Field of Dual Phase Steels

Since the introduction of ultrafast cooling (UFC) technology, DP steels have been mostly produced using the combination of laminar cooling and ultrafast cooling and this technology also increases the controllability of the microstructures. The first laminar cooling at low cooling rate allows regulating accurately the intermediate temperature. The ultrafast cooling (UFC) regulates the coiling temperature, and consequently the nature of the second phase [Cai et al., 2014]. In view of the increasing demands for occupant safety and fuel efficiency, further strengthening of DP steels without a loss in ductility is also required. Grain

refinement is a promising tool to achieve this aim. In recent years, a variety of new processing routes have been developed to produce ultrafine grained (UFG) low carbon steels with a ferrite grain size of 1μm and below. It is consistently found that yield strength and tensile strength are increased due to grain refinement [Calcagnotto et al., 2010]. Therefore, ultrafine grained (UFG) steels with relatively simple chemical compositions have attracted much interest in replacing some conventional high strength alloyed steels. Methods to obtain UFG DP steels can be divided into two categories: (i) advanced thermo mechanical processing (ATMP) routes, which aim at improving conventional processing routes (ii) severe plastic deformation (SPD) techniques [Xue et al., 2013]. In order to develop new generation steels characterized by friendly environment, low cost and light weight, hot rolled ferrite-bainite/martensite dual phase steels are produced using simple C-Mn-Si chemistry without adding expensive alloys [Tan et al., 2012]. Thus, it can be said that still development is going on DP steels, using lean chemistry and different processing routes to manufacture these steels with enhanced mechanical properties.

1.8 Summary of the Chapter

This chapter includes the introduction of various Advanced High Strength Steels, various generations of AHSS, and their benefits. This chapter also discusses the most common types of AHSS being used. The details regarding the manufacturing aspects of Dual Phase steels along with effect of alloying elements has also been discussed. Finally, a brief overview of current developments in the area of DP steels has been discussed. The subsequent chapter will summarize the research done by various authors in the field and gaps in the existing literature.

Chapter 2

Literature Review

2.1 Introduction

In this chapter literature by various authors in the field of dual phase (DP) steels has been discussed. The work done by various researchers has been summarized which includes methods of producing dual phase steels, their properties and applications etc. In the last section, gaps in the present literature have been discussed.

2.2 Review of the Literature

Cornet and Herman (2003) invented a method for fabricating a multi-phase hot rolled steel strip comprising of an ultrafast cooling operation after the controlled slow cooling of the strip. In this method an ultrafast cooling operation was carried out (after slow laminar cooling) followed by final slow cooling operation. In the process, at end of the hot strip mills, temperature of the strip was kept equal to or greater than the Ar_3 temperature (dependent the composition of the steel). After hot rolling, the strip was subjected to a first slow cooling operation from end of roll temperature to an intermediate temperature (usually lying between 750 to 600 ℃). After the first slow cooling operation, ultrafast cooling operation was performed from intermediate temperature to a temperature referred as coiling temperature (lying between 600 ℃ to room temperature). Finally, a second slow cooling operation was performed from the coiling temperature to the room temperature. The first step cooling operation was performed at a high temperature under the conditions close to equilibrium conditions so that ferrite could form. The duration of the first step was dependent on the speed of the strip (during the process of hot rolling) and cooling rate was a function of degree of transformation required. The ultrafast cooling operation was performed at such a cooling rate that the product of thickness of the strip (in mm) and the cooling rate was greater than 600^{o} ℃ / s.mm e.g. for a 4mm thick strip, the cooling rate must be greater than 150 ℃ / s. In the course of final (second) slow cooling operation, residual austenite transformed to form the second phase (i.e. bainite or martensite) which was a function of the coiling temperature. For the experimentation work, authors applied the above discussed method for three different steels to obtain different microstructures. The different microstructures were obtained by careful choice and adequate control of intermediate temperature and coiling temperature.

Ferrite/Bainite and Ferrite/Martensite microstructures were obtained for different samples of all the three steels. However, using conventional methods, multiphase microstructure could not be obtained. Finally, from the results, it was concluded that the method presented by the authors can be used to obtain multiphase microstructure in different steels. Also, it was clear from the results obtained, that microstructure in steels not only depends upon the chemical composition but also on the application of combination of laminar and ultrafast cooling operations.

Adamczyk and Grajcar (2006) investigated the effect of heat treatment conditions on the structure and mechanical properties of Dual Phase (DP) type steel. For the experimentation steel (C:0.09; Mn:1.5; Si:0.26; Ni:0.07; P:0.014; S:0.009; B:0.003; Al:0.029; N:0.012: Fe: balance; all in wt %) was melted and continuous casting of 100x100mm slabs were done. After solidification the slabs were hot-rolled and forged in order to obtain the rods with a section of 24 x 24mm. The specimens for structure and mechanical properties investigations were prepared after the heat treatment. The heat treatment of the specimens was realized according to three routes. In the routes I and II, the steel was heated to a temperature of 910 ℃ ($\alpha + \gamma$ region), hold at this temperature for 30min. In route I specimen air cooled to room temp then again heated to 750 ℃ and water quenched. In route II specimen was water quenched from both temperatures viz: 910 ℃ and 750 ℃. The route III consists in austenitizing of steel at a temperature of 910 ℃ and air cooling for 45 s to a temperature of 750 ℃ in order to realize the partial α to γ transformation, followed by water quenching. The steel heat-treated according to the route I has the ferrite structure with an irregular envelope of martensite on grain boundaries. In route II during heating the steel to an under hardening temperature, the nucleation of austenite mainly occurs on the boundaries of martensite laths formed after primary quenching from a temperature of 910 ℃. The predominated martensite fraction occurs mainly as thin fibres located in surroundings of grain boundaries. Moreover, in surroundings of martensite, especially at a boundary zone of large grains of the alpha phase, small grains of the recrystallized ferrite can be identified. In route III Martensite was located on grain boundaries of the alpha phase. The optimum fraction of martensite averaging 20% occurs after air cooling of the specimens for 45s. The used conditions of the heat treatment led in obtaining the DP-type steels of comparable fractions of ferrite and martensite. The optimum fraction of the martensite was from 21% to 24%, and a grain size of α phase equals from 7 μm to 10 μm. The diversified morphology of martensite had the influence on various mechanical properties of the steel and its deformability. The optimum

strength and ductile properties had the route II steel. The yield point of this steel was about 520 MPa, tensile strength about 800 MPa, total elongation 20%, and uniform elongation about 16%.

Bhattacharya (2006) reviewed various developments in the area of Advanced High Strength Steels (AHSS) which included Dual Phase steels, Multi Phase steels, Transformation Induced Plasticity (TRIP) steels and Martensitic (MART) steels. The author discussed that AHSS are replacing the conventional steels (used to manufacture structural parts) to increase fuel efficiency and safety performance.

Among AHSS, the authors reported that dual phase steels provide an excellent combination of strength and ductility. All the dual phase steels developed have been based on annealing in the two-phase (inter-critical) temperature region and the consequent increase in carbon content in austenite. Higher carbon content in austenite after inter-critical annealing results in a significant shift of M_s to a lower temperature. Direct quenching from inter-critical temperature range allows achieving very high strength of steels without expensive alloying.

Multiphase steels, also referred to as complex phase steels are steels with a higher level of yield strength at the same comparable tensile strength levels of dual phase steels. The only way to gain yield strength in multiphase structure is to obtain appropriate mixture of pearlite, bainite as well as ferrite straightened by grain refinement and precipitation strengthening.

TRIP steels, based on the Transformation Induced Plasticity effect, offer the highest combination of strength and elongation, which is a measure of high level of energy absorption. In addition, they also show high bake hardening compared to dual phase steels. The relatively slow initial cooling and rather rapid cooling down to the temperature of isothermal holding results in further enrichment of the remaining austenite by carbon and enhancing its stability. Further growth in its stability occurs during the austenite to bainite transformation in the presence of strong ferrite forming elements. This significantly retards the carbide formation part of the bainite reaction and helps to keep all carbon in the remaining austenite.

Using water quenching in a continuous annealing line, steels with 100% martensite are produced. These steels offer very high strength although ductility is lower than other AHSS steels. The strength of the steel is controlled by the carbon content and a complete austenitizing temperature is used to obtain a fully martensitic structure.

Park et al. (2007) studied the effect of heat treatment path on the cold formability of drawn dual phase steels. The composition of the steel was: 0.07C, 0.83Si, 1.51Mn and balance Fe (all in wt. %). After homogenization, the dual-phase steels were made by three different heat treatments, namely inter-critical quenching (IcQ), intermediate quenching (ImQ) and step quenching (SQ). During inter-critical quenching (IcQ), steel was first heated to 1000 ℃ and was held for 1 hour followed by air quenching which resulted in ferrite/pearlite structure. This steel was again reheated to an inter-critical temperature of 770 ℃ and held for 30 minutes and then water quenched to get ferrite/ martensite structure. In the process of intermediate quenching (ImQ), steel was first heated to 1000 ℃ and was hold for 1 hour followed by water quenching which led to martensite structure. This martensitic structured steel was again reheated to an inter-critical temperature of 770 ℃ and hold for 30 minutes and then water quenched to get ferrite/ martensite structure. The SQ specimen was heated to 1000 ℃ and was held for 1 hour and then slowly cooled to 750 ℃ and held for 30 minutes and then water quenched to get final ferrite/ martensite structure. Optical microscopy results showed that the ImQ specimen exhibited more ragged grain boundaries and smaller ferrite grains as compared to the IcQ specimen and the SQ showed two phase aggregates of large, blocky shaped martensite islands surrounded by the coarse ferrite matrix. Drawing was conducted on the draw bench with drawing speed of 3 m/min up to a drawing amount of 10% by a single pass. Cylindrical samples for tensile tests (having gauge length of 20 mm and 4 mm diameter) and compression tests (having height of 15 mm and 4 mm diameter) were machined from the drawn rods. The SQ specimen showed higher yield strength and tensile strength and less elongation as compared to IcQ and ImQ specimens. Work hardening rates of all three microstructures were greatly reduced when the drawing process was carried out, which resulted in similar deformation resistance of the three microstructures. IcQ microstructure showed an excellent forming limit compared to the other two microstructures, because of formation of voids instead of microcracks.

Prahl et al. (2007) studied the crack initiation and crack propagation phenomenon in multiphase steels. For the study, steel having composition as C: 0.19%, Mn: 1.50 %, Si: 0.26 %, P: 0.086 %, Al: 0.52 %, Ni: 0.004 and Fe: balance (all in wt. %) was used to obtain five different microstructures termed as A, B, C, D and E, using different annealing treatments. Effects of inter-critical annealing temperature and holding time in the bainitic regions were also investigated. During investigation, two inter-critical temperatures i.e. 785 ℃ and 825 ℃ were used to obtain two different ferrite volumes of 55% and 30% respectively. Rapid

cooling after holding at 785 ℃ for 5 minutes led to dual phase (DP) microstructure termed as steel A. Two type of transformation induced plasticity (TRIP) steels termed as B and C were obtained by holding the samples at 425 ℃ for 1 minutes and 2 minutes respectively which were held at 785 ℃ for 5 minutes formerly. Two additional dual phase steels with less ferrite (30 %) termed as D and E were also obtained using higher inter-critical temperature of 825 ℃. Steel D having ferrite/martensite dual phase microstructure was produced by direct quenching after holding at 825 ℃ for 10 minutes. Steel E having ferrite/bainite dual phase microstructure was produced by holding the sample for 20 minutes at 825 ℃ and later for 120 minutes at 425 ℃. Tensile test were carried at room temperature for all the specimens. The two TRIP steels B and C showed high stress and strain levels. Among dual phase steels A, D and E, steel D exhibited highest true stress and lower true strain levels due to high amount of martensite whereas steel E showed high strain-hardening level due to the high bainite amount. Scanning Electron Microscope (SEM) analysis was done to study the fractured surfaces of all the specimens. The results of SEM showed both dimples and cleavage fracture which existed in parallel. Finally, finite element calculations of representative elements were carried out. It was concluded that a model parameter study can be formulated for the damage study of the multiphase steels.

Ahmad et al. (2008) studied the effect of thermo-mechanical processing on the hardenability and tensile fracture behavior of dual-phase (DP) steels. Thermo-mechanical processing with various rolling reductions (0-50%) was applied in the inter-critical temperature range of 725–830 ℃ on low alloy hot rolled steel (0.09 C, 1.2 Mn, 0.78 Cr, 0.26 Si, 0.15 Ni, 0.2 Cu, 0.04 Mo and balance Fe, % wt) followed by quenching in the iced brine solution Metallographic examination of the as-received steel showed a microstructure comprising of ferrite and pearlite phases. Samples were inter-critically heat treated in an argon atmosphere in the range 725–830 ℃ for 20 min and then quenched in brine solution. Due to very fast cooling rate, the austenite phase almost fully transformed to martensite. Point counting method was used to determine the volume fraction of austenite. It was observed that at a temperature of 790 ℃, about 50% of austenite got formed; at this temperature, samples were rolled and cross section reductions in the range 0–50% (0, 20, 30 and 50 % reduction respectively) in lateral and longitudinal direction were achieved. All the specimens were quenched in iced brine solution, offering a cooling rate of about 500 ℃/s After grinding and polishing, specimens were etched with 5% picral followed by 2% nital solution and then immersed in a boiling alkaline chromate solution (8g CrO_3 + 40 g NaOH + 72 ml H_2O). It

was observed that with rolling at a temperature of 790 ℃ for 0 to 50% thickness reduction, about 6% of ferrite increased in rolled specimens even after quenching but not in the un-rolled condition which reflected that rolling in the inter-critical region decreased the hardenability. The increase in the rolling reduction resulted in more strain and martensite particles became more fibrous. In longitudinal direction, the martensite fibres were lengthened and got reduced in thickness by rolling. In the transverse direction, they did not lengthen but thinned in the direction normal to the rolling plane. Thus, the aspect ratio of the martensite fibres was more in the longitudinal than in the transverse direction, and this affected the tensile properties to a great extent. For 30% reduction, maximum true stress in longitudinal and transverse direction were 1023 MPa and 902 MPa respectively; similarly for 50%, values were 1021 MPa and 939 MPa respectively. The UTS almost remained equal in both directions. Total elongation was also significantly affected for 50% rolling in transverse and longitudinal directions with total elongation of 12% and 18% respectively. Hot rolling in the Inter-critical region increased the strength of the steel without an appreciable loss in ductility. Rolling also increased the aspect ratio of the martensite more in the longitudinal direction than in the transverse directions, which developed the tensile properties.

Kumar et al. (2008) examined the structure property relations for ferrite/bainite dual phase (FBDP) and ferrite/martensite dual phase (FMDP) steels and compared the results for both the steels. For the study, a series of FBDP and FMDP steels containing wide variation (20–90%) of the harder constituents i.e. bainite/martensite was prepared from a commercial low carbon micro-alloyed steel by suitable heat treatments. The composition of the steel used was C: 0.08%, Mn: 1.38%, Si: 0.49%, S: 0.006%, P: 0.017%, Al: 0.036%, Nb: 0.22%, N_2: 0.046% and Fe: balance. Cylindrical bars of 10 mm diameter and 120 mm length were cut from the steel plates and were subjected to heat treatment for achieving ferrite/bainite and ferrite/martensite structures. The heat treatment for the ferrite/bainite structure consisted of four steps: (a) austenitizing the steel at 1100 ℃ for 20 min, (b) cooling in air for different time durations (to alter the volume fraction of ferrite in the microstructure), (c) soaking in a salt bath at 500 ℃ for 1 h and finally (d) quenching in water. For obtaining ferrite/martensite microstructure, heat treatment comprised of three steps: (a) austenitizing the steel at 1100 ℃ for 20 min, (b) cooling in air for different time durations and finally (c) quenching in water. The employed heat treatment led to 11 different combination of ferrite/bainite microstructure having bainite volume fractions of 22.0, 26.0, 40.0, 50.2, 59.9, 65.0, 69.2, 76.1, 80.5, 85.2 and 90.3%, and 7 different ferrite/martensite microstructures having volume fractions of

martensite of 22.0, 26.0, 40.0, 52.1, 61.9, 71.9 and 90%. Metallographic examinations of all the heat treated samples were carried out with the help of a scanning electron microscope. Macro-hardness values of the differently heat-treated specimens were determined at a load of 30 kgf using a Vickers hardness tester and micro-hardness measurements were also done on ferrite, bainite and martensite phases using a load of 10 gf with the help of a micro-hardness tester. Cylindrical tensile specimens with 25mm gauge length and 5mm diameter were fabricated and tensile tests were carried out using a universal testing machine at room temperature. Results showed that the hardness of FBDP steels remained almost unchanged up to 50% bainite followed by monotonic increase with increasing bainite content greater than 50%, however hardness of FMDP steels increased continuously with increase in the martensite content. Ferrite/martensite steel possessed higher strength and lower ductility as compared to steels with ferrite/bainite microstructure having identical amount of ferrite. The minimum elongation of FBDP steels was ≈22% while that of FMDP steels was ≈8%. The strain-hardening exponent of FMDP steels decreased with increasing volume fraction of martensite whereas its change with volume fraction of bainite was insignificant. The fracture surfaces of FBDP steels revealed the presence of dimples which indicated typical ductile mode of fracture whereas FMDP steels exhibited cleavage mode of fracture. Finally it was concluded from the comparative assessment of strength and ductility values for these steels that FBDP steels with bainite content in the range of 60–70% is a potential candidate for application in structural components.

Kuziak et al. (2008) presented some basic concepts of Advanced High Strength Steels (AHSS) for use in the automobile industry, which included their chemical composition design, microstructure analysis, mechanical properties development during thermomechanical processing, production technology characterization, potential applications and performance in service. The authors reported that AHSS are characterized by improved formability and crash worthiness compared to the conventional steel grades. The category of AHSS covers the following generic types: dual phase (DP), transformation induced plasticity (TRIP), complex phase (CP) and martensitic steels (MART). As opposed to the conventional high strength steels in which ductility decreases with strength, modern AHSS steels combine high strength and formability/ductility.

Microstructure of dual phase steels is composed of soft ferrite matrix and 10–40% of hard martensite or martensite-austenite (M–A) particles which allows achieving the ultimate tensile strength in the range of 500–1200 MPa. The strength of the DP steel is controlled by

the amount of martensite and ductility by the size and distribution of this phase. DP steels possess low YS/UTS ratio (around 0.5) and high strain hardening characteristics (high n value).

Transformation-induced plasticity (TRIP) steels are based on the principle that the strain or stress induced transformation of retained austenite present in the microstructure in a sufficient amount can substantially harden the steel during deformation. The mechanical properties of TRIP steels are derived from their dispersed multi-phase microstructure which is composed of ferrite (0.50–0.55), bainite (0.30–0.35), retained austenite (0.07–0.15), and possibly martensite (0.01–0.05). To obtain the best mechanical properties in a product, carbon should be distributed to austenite and should enrich this phase as much as possible to preserve the M_s below the room temperature (generally 15−25 ^{o}C below room temperature).

Complex phase (CP) steels belong to a group of steels with very high ultimate tensile strength of 800 MPa or even greater. The chemical composition of CP steels contains some quantities of Nb, Ti and or V to cause the precipitation strengthening effect. CP steels have no retained austenite in the microstructure, but contain more hard phases like martensite and bainite. Their mechanical properties are characterized by continuous yielding and high uniform elongation.

Martensitic (MART) steels provide the highest ultimate strength in final products, up to 1500 MPa. Microstructure of martensitic steels is mainly composed of lath martensite, which is developed by the transformation of austenite during quenching after hot rolling or annealing.

AHSS are produced in complex processes involving thermomechanical processing followed controlled cooling. For producing DP steels, the cooling process after rolling starts with slow cooling stage (on the run out table) after rolling in which the desirable amount of ferrite is obtained as a result of the austenite transformation. The ferrite transformation allows the carbon content enrichment in the remaining austenite, which increases its hardenability and reduces M_S temperature. The optimal combination of strength and ductility of TRIP steels is achieved by grain refinement and obtaining a uniform distribution of fine second phase particles. The cooling stage in the strip rolling process of TRIP steels is more complicated than that for DP strips. After producing 50–60% of ferrite in the microstructure, accelerated cooling with cooling rate greater than 20 °C/s to the coiling temperature which lies in the bainitic transformation temperature range, is realized. During coil cooling, bainitic transformation proceeds, further increasing the carbon content in remaining austenite to around 1.2%. A part of this austenite, in the amount of 10–15%, remains untransformed

accounting for the TRIP effect. The concept of CP steels is essentially similar to those of TRIP steels, however less stringent cooling practice is imposed on the hot band during the last stage of processing as no presence of retained austenite is required in their microstructure. Martensitic steels are produced by applying rapid quenching from the austenitic phase to produce the laths martensite microstructure. Finally from the discussion it was concluded that a substantial progress has been achieved during the last same years in the development of AHSS.

Zhao et al. (2009) studied the microstructure evolution of cold rolled dual phase steel at the initial stages of the annealing process and the effects of overaging temperature. The composition of the experimental steel was: C: 0.14–0.17, Si: 0.40–0.60, Mn: 1.70–1.90, Nb: 0.02–0.04, Cr: 0.40–0.60, P: ≤ 0.010, S: ≤ 0.010, Al: 0.02–0.06, Fe: balance (all by wt. %). Steel samples (having size 35 mm× 100 mm× 100 mm) were hot rolled to 3.5 mm thickness and finally cold rolled to thickness of 1.0 mm. Finally cold rolled sheets were cut into the specimens for continuous annealing experiment. The specimens were heated at 10 ℃/s to different heating temperatures (550, 630, 670, 710, 730, 750 and 780 ℃) and held for 20 s followed by water-quenching. For the studying the effects of different overaging temperatures on the microstructures and mechanical properties of dual phase steels, steel specimens were heated to an inter-critical temperature of 800 ℃, were soaked for 80 seconds and after some slow cooling the samples were rapidly cooled to 240, 280, 320 and 360 ℃, respectively and soaked for 300 seconds followed by air cooling to the room temperature. The microstructures of specimens were analysed using scanning electron microscopy (SEM) and transmission electron microscopy (TEM). The results showed that after cold rolling, the microstructure of steel consisted of elongated grains of ferrite and deformed colonies of pearlite. After annealing, the microstructure of DP exhibited a mixture of ferrite, martensite and martensite/austenite (MA) constituents. Study of the microstructure evolution at the initial stages of continuous annealing process revealed that, when that sample was heated to 550 ℃, microstructure showed no visible changes as compared to cold rolled samples. When the heating temperature was 630 ℃, the recrystallization nuclei originated in the microstructure. With the increase in the heating temperature, the recrystallization nuclei started to grow. When the heating temperature was 670 ℃, the deformation structure still existed in the microstructure. When the heating temperature was 710 ℃, the deformation structure had already vanished and was replaced by equiaxed recrystallization grains. When the heating temperature was 730 ℃, microstructure entered into the two-phase region i.e.

ferrite and austenite. When the temperature reached 750 ℃, the pearlite dissolved rapidly. When the annealing temperature was 780 ℃, the austenite volume increased. The martensite transformed from austenite during the rapid cooling process. When the DP steel was annealed at 800 ℃ for 80 s and overaged at 280 ℃, the tensile strength and total elongation of dual-phase steel reached 1150 MPa and 13% respectively. When the overaging temperature reached 360 ℃ the tensile strength decreased while the yield strength did not change significantly.

Calcagnotto et al. (2010) studied the effect of grain refinement on the strength and toughness of dual phase steels. Large strain warm deformation at different temperatures and subsequent inter-critical annealing had been applied to obtain fine grained (2.4 μm) and ultrafine grained (1.2 μm) ferrite/martensite dual-phase (DP) steels. The mechanical properties of the produced steels were tested under tensile and impact conditions and were compared to a hot deformed coarse grained (12.4 μm) reference material. The chemical composition of the steel used was (in wt. %) 0.17 C, 1.49 Mn, 0.22 Si, 0.033 Al, 0.0033 N, 0.0017 P and 0.0031 S. To obtain the final ferrite/martensite dual-phase microstructure, the specimens were subjected to inter-critical annealing in a salt bath furnace. The temperature was held constant at 730 ℃. The samples were annealed for 3 min in the salt bath, before they were quenched in water to obtain a ferrite/martensite DP structure. The martensite volume fraction and grain size were determined using the scanning electron microscope (SEM). The coarse grained (CG) steel had a grain size of 12.4 μm and contained 31.3% martensite in ferrite matrix. Fine grained (FG) steel had grain size of 2.4 μm and comprised of 30.1% martensite while the ultrafine grained (UFG) steel had grain size of 1.2 μm with 29.8% martensite. Cylindrical tensile test specimens with a diameter of 4 mm and a gauge length of 20 mm were machined and tensile tests were conducted at room temperature. Impact tests were also carried out in the temperature range of -40 ℃ to 200 ℃. Results showed that with decrease in the grain size, ultimate tensile strength and yield strength increased remarkably while uniform elongation and total elongation were affected marginally. The ductile to brittle transition temperature (DBTT) was decreased from 127 ℃ to 100 ℃ for fine grained steels and for ultrafine grained steels it was decreased to 94 ℃ which showed the improvement in the impact toughness. The formation of the cracks and cleavage fracture was also suppressed in the fine grained and ultrafine grained steels. Therefore, it was concluded that the grain refinement affects the properties of dual phase

steels and ultrafine grained dual phase steels provide better properties as compared to fine grained and coarse grained dual phase steels.

Kwon et al. (2010) discussed the new trends in development of Advanced High Strength Steels and elaborated on the salient characteristics of the next generation AHSS having enhanced performance.

The conventional AHSS are high strength steels having tensile strength – elongation (TS-EI) product lower than 25,000 MPa.%. The typical steels in this group are DP, TRIP and martensite-based complex microstructure steels. The microstructure of these steels contains phase transformation products like retained austenite, martensite and bainite. In addition, various thermal cycles are generated to obtain the desired microstructure. These steels have their own advantages and disadvantages as compared to each other (e.g. a primary advantage of DP steels compared to TRIP steels is better weldability. However ductility of TRIP steels is more than DP steels). AHSS with higher hole expansion ratio value have been developed to enhance stretch flangeability and bendability. A few authors are focusing on the development of TRIP steels having TS-EI product greater than 25,000 MPa%. This group of steels are categorized as the so called X-AHSS (e.g M-TRIP (**m**artensite based TRIP) steel is defined as the TRIP steel with martensitic matrix). M-TRIP steel is produced by Q&P process in which austenite is formed at high temperature either by full austenitization or by inter-critical heat treatment, which is followed by rapid cooling to a temperature between M_s and M_f to control the fraction of martensite and retained austenite. The typical TS-El product value is slightly greater than 25,000 when conventional TRIP steels with lean alloying elements are Q&P processed and the microstructure consists of uniformly distributed annealed martensite matrix and retained austenite. In SB-TRIP (Super Bainite TRIP) steel, nano-sized bainitic microstructure is embedded with retained austenite. This steel has a tensile strength of 1187 MPa and an elongation of 39%. In order to enhance the ductility of AHSS, it is desired to have austenite as the matrix phase. For improved ductility, it is also important to utilize transformation hardening phenomenon and to control the mechanical stability of austenite phase properly. The typical TS-El product for ultra-AHSS is greater than 50,000 MPa·%. These steels have superior strength and ductility combination. TWIP (Twinning Induced Plasticity) is a potential mechanism to obtain the superior balance of tensile strength and elongation, and is extensively utilized to develop steels of the Ultra-AHSS class. The typical value of TS-El product for TWIP steels is about 65,000 MPa·%, more than three times greater than those of conventional AHSS. This superior mechanical performance has been

obtained by gradual twinning during deformation. The formation of twins partitions austenite grains and induces the continuous strain hardening, resulting in improved ductility.

Nadlene et al. (2011) studied the effect of volume fraction of martensite on the corrosion behavior and the hardness of a dual phase steel. A low carbon steel (C: 0.226; Mn: 0.928; Si: 0.219; Ni: 0.0941; P: 0.0296; S: 0.0359; Cr: 0.126: Fe: balance; all in wt %) was used for the study. Nine specimens were heated in the furnace at various intercritical temperatures for 25 minutes and quenched in cold water to produce martensite in the microstructure. The first specimen was heated at the lower intercritical temperature (Ac_1) which was 720 ℃ and the temperature was increased 12 ℃ for the following specimens until the upper intercritical temperature (816 ℃) was achieved. After the intercritical annealing process, microstructure of all specimens was observed. The corrosion test was done using the CMS 105^{TM} DC corrosion measurement system. The hardness of the specimens was determined using Vickers Hardness Testing Machine. Results revealed that the percentage volume fraction of martensite in dual phase steel was influenced by variation in the intercritical annealing temperature. Higher the inter-critical annealing temperature, more the volume fraction of martensite produced in the steel. It was also observed that the interfacial area between the ferrite (anode) and martensite (cathode) increased with increase in martensite fraction. Hence the corrosion rate increased with increase in the volume fraction of the martensite. From the hardness tests it was observed that the hardness of the steel increased with increase in the volume fraction of the martensite. The hardness of martensite was the result of severe lattice distortion produced due to formation of this phase. From the above results, it was concluded that the volume fraction of martensite has great influence on the hardness and corrosion properties of a dual phase steels.

Nie et al. (2012) studied the effect of soft phase (ferrite) content on the work hardening behavior of a series of ferrite/bainite multiphase steels containing different volume fractions of ferrite. A low carbon micro alloyed steel was used to obtain the multi-phase microstructure by thermo-mechanical control process (TMCP). The composition of the steel was 0.07% C, 1.7% Mn, 0.25% Si, 0.09% Nb, 0.6% (Cu + Cr + Ni), and balance Fe. The Ar_3 and Ar_1 temperatures for the steel were 678 ^oC and 575 ^oC respectively. Five different microstructure steels termed as No.1 to No.5 were obtained by TMCP. After the controlled cooling, the steel samples were cooled first in air and then were cooled at a higher rate (i.e. more than 30 ^oC/sec) to a temperature lower than the bainitic ferrite transformation finish (B_f) temperature. The accelerated-cooling start temperature (ACST) was decreased from higher temperature to

lower temperature to control the volume fraction of ferrite. The ACST of No.1 steel was above Ar_3 temperature, and the ACSTs of No.2, No.3 and No.4 were between the Ar_3 and Ar_1 temperature. No.5 steel specimen was cooled in air with a cooling rate of about 1 ^oC/sec to obtain an acicular/granular ferrite microstructure. The microstructure of the experimental steels was observed using optical microscope. The stress-strain curves and nano-hardness measurements for the steel specimens were obtained. Results showed that the microstructure of No.1 steel was lath bainite/ferrite and for steel No.5 it was granular ferrite. Microstructure of the steels No.2, No.3 and No.4 comprised of acicular ferrite, bainite and MA constituents. The fraction of acicular ferrite in No.2 steel was about 30%, while the fraction of ferrite in No.3 and No.4 steels was about 50% and 70%, respectively. Thus it was concluded that, with decrease in the ACST, there was an increase in the ferrite volume. Results also revealed that with increase in the ferrite volume, the strength and the stress ratio ($R_{t1.5}$ / $R_{t0.5}$) decreased while the uniform elongation and total elongation increased. As compared to single phase steel the multiphase steels showed excellent anti-deformability such as higher stress ratio ($R_{t1.5}$ / $R_{t0.5}$), higher uniform elongation and lower yield to tensile strength ratio. Finally it was concluded that the volume of the soft phase i.e. ferrite influences the work hardening behaviour of the steel.

Tan et al. (2012) studied the effects of chemical composition and various parameters of thermo-mechanical controlled processing (TMCP) like finish rolling temperature, isothermal temperature and coiling temperature on the microstructure and mechanical properties of some economical dual phase steels. Three different steels with varied Mn and Si contents were used for the study. Steel 1 and 2 contained higher amount of silicon (0.60 wt. %), however steel 2 had higher Mn content (1.55 wt. %) as compared to steel 1 (1.20 wt. %). Steel 3 contained low silicon (0.20 wt. %) and Mn (1.20 wt. %) content. The carbon content in all steels was 0.050 wt. %. The strip finish rolling thickness was 4 mm and rolling temperature was 790−860 ℃. After rolling was completed, first laminar cooling was done at the rate (φ_1) of 5−30 ℃/s from rolling finish temperature (FT7) to ferrite transformation temperature (Ar_3) which was a function of φ_1. Isothermal holding (φ_2) process with air cooling was conducted after first step cooling to control the fraction of ferrite. Rapid cooling with cooling rate (φ_3) ≥ 100 ℃/s was conducted when adequate ferrite fraction was obtained. Strip was quenched down to martensite formation temperature (M_s) with dense water and coiled at two temperatures Tc_1 = 300 ^oC and $Tc_2 \leq 250$ ℃. Quantitative metallographic studies were carried out using an optical microscope. Ferrite grain size was found to be insensitive to chemical

compositions and martensite volume varied slightly (and was 18 %, 21.11 and 20% for steel 1, 2 and 3 respectively). With Mn content increasing and Si content decreasing, martensite volume increases slightly. Yield strength and tensile strength were dependent on the martensite volume. With FT7 decreasing, both the dislocation density in ferrite matrix and martensite volume fraction increased, which led to the strength increasing and elongation slightly decreasing. With isothermal temperature T_{iso} decreasing from 740 to 620 ℃ yield strength increased sharply and tensile strength decreased slightly. The optimal coiling temperature T_c was lower than 250 ℃ for C-Mn-Si DP steel production because lower strength and higher elongation were obtained with higher T_c.

Li et al. (2013) investigated the effect of heating rate on the ferrite recrystallization and austenite formation in a cold rolled dual-phase steel. The material used in this study was the cold-rolled DP590 steel sheet having thickness of 1 mm with 70 pct cold rolling. . The composition of the experimental steel was: C: 0.1, Si: 0.4, Mn: 1.6, Cr: 0.017, P: 0.013, S: 0.006, Fe: balance (all by wt. %). For recrystallization and austenite formation study, rapid annealing simulations were performed using a Gleeble 3500 simulator. Samples were heated to the desired annealing temperatures of below 700 ℃ and intercritical temperatures with different heating rates (5, 50 and 500 ℃/ s) and holding time (0–40 s) respectively, and then quenched into water of room temperature. Scanning Electron Microscope (SEM) and Transmission Electron Microscope (TEM) were used for the microstructure characterization. In the cold rolled structure alignment of ferrite grains and pearlite colonies into the rolling direction were observed. Results showed that the increase in heating rate from 5 to 500 ℃/ s resulted in variety of microstructures ranging from fully recrystallized to almost totally non-recrystallized structures prior to austenite nucleation temperature of 720 ℃. The ferrite recrystallization and austenite formation processes overlapped under faster heating rate, which further affected the spatial distribution and morphology of austenite. The morphology of martensite was observed from network structure to a chain shape with the heating rate under lower annealing temperatures. The steel heated at 50 ℃/ s produced less volume fractions of austenite than the other two heating rates (5, 500 ℃/ s), which might be caused by the fact that the nucleation of austenite was unfavourable at moving ferrite boundaries at low temperature. But higher annealing temperature minimized the microstructure difference. Finally it was concluded that the heating rate affects the microstructure considerably and rapid heating with high temperature results in the refinement of the grains and further improves the strength as well.

Meng et al. (2014) performed fast-heating annealing on a cold rolled dual phase steel in order to explore the possibility of fast-heating routine on large scale production. A cold rolled dual phase steel (Fe – 0.07C, –1.7Mn, – 0.429Si) sheet with 70 pct cold rolled ratio was investigated for the study. Same composition steel produced through continuous annealing was also used for the comparison. From the dilatometer study, the lower and upper critical temperatures were found out to be 1023 K and 1193 K respectively for the heating rate of 500 K/ s. Specimen was heated at 500 K/ s to 1123 K, soaked for 2 s and then cooled down to 323 K. Microstructure evaluation and tensile testing was done for both the steels i.e. fast heated (FH) and continuous annealed (CA). Tensile tests showed that the yield strength for the fast heated sample increased from 277 MPa to 372 MPa and ultimate strength increased from 625 MPa to 666 MPa. The total elongation was also increased from 23.3 % to 26.6 % as compared to the continuous annealed sample. Compared to the continuous annealed sample, the ferrite grains were observed to be refined strikingly in the fast heated sample. The fine and fibrous morphology of the martensite in the FH sample resulted in the improvement of strength. Hence, it was concluded that the simplified fast heating process can be an alternative route for the production of the dual phase steels.

2.3 Gaps in the Existing Literature

The following gaps have been identified after the review of literature:

1. Considerable work has been done in the past decades in the area of the Dual Phase steels. Various authors have produced dual phase steels through the inter-critical annealing of low carbon steels. Since every author has used different steel chemistry; the working parameters obtained by them have also been different. Hence, the overall all approach appears to be one of hit and trial to select the optimized annealing parameters to produce the required volume fraction of martensite in the microstructure.
2. In literature, the effect of heating rates on the microstructure and properties of DP steels has been discussed vastly in the past few years in order to reduce the processing times. However, if it is not feasible to achieve very high heating rates then it is reasonable to adjust the other parameters like annealing temperature and the soaking times. However, in literature there is no clarity on the soaking time. Some authors have used very less soaking periods [Li et al., 2013; Meng et al., 2014] whereas others have used very larger soaking periods [Nadlene et al., 2011].

3. Most of the authors have used water quenching as the cooling medium (as it provides very high cooling rates) to transform austenite formed during inter-critical annealing into martensite. But water quenching produces some adverse effects also and to avoid them, industry is moving towards the concept of controlled cooling achieved through various cooling mediums. However, there is difference in the volume fraction and morphology of the martensite produced through the two methods discussed above. No considerable literature has been reported showing the combined effect of all annealing parameters viz. heating rates, annealing temperature, soaking times, and cooling rates on the volume fraction and morphology of martensite during the production of dual phase steels.
4. During the production of dual phase steel from a cold rolled steel sheet, two main phenomena occur viz. recrystallization of deformed ferrite grains and formation of austenite. Very few authors have discussed the occurrence of these two phenomena during the heating cycle but the effect of other annealing parameters viz. annealing temperature and soaking time has not been discussed.

Chapter 3

Design of the Study

3.1 Introduction

This chapter includes the detail of overall design of the study which includes objective of the research work, the key issues, methodology, experimental procedure followed, details of machines, equipment and the commercial software used during the experimental work.

3.2 Establishing the Objective Function

From the review of existing literature, it was observed that substantial amount of research work has been reported on the production of the 'dual phase' (DP) steels containing the ferrite/ martensite dual phase structure. However, there exists uncertainty in achieving the same microstructure (and mechanical properties) consistently from the same alloy chemistry during production of dual phase steels through continuous annealing process. Thus, the main focus of the present work is to study the effect of annealing parameters viz. annealing temperature, soaking time periods, cooling rates on the recrystallization kinetics, austenite formation and stabilization, and the final microstructure obtained in a cold rolled low carbon DP steel. The present research work is an effort to address the following:

- To study the kinetics of recrystallization, formation and stabilisation of austenite phase during the inter-critical annealing of a low carbon cold rolled steel under fast heating.
- To determine the appropriate process parameters for the annealing cycle in order to produce ferrite-martensite dual phase microstructure with varied volume fraction of martensite.

The key issues to be taken up during the research work:

- To investigate the microstructure of the as-received low carbon steel using optical microscopy and SEM analysis for studying the morphology of pearlite phase mixture.
- To obtain the inter-critical annealing parameters (annealing temperature, holding time, cooling rates etc.) for the given alloy chemistry using JMat-Pro and Thermo-Calc

software. Also to compare the above obtained results through subsequent annealing experiments.

- To provide inter-critical annealing (through air cooling) to the samples in the range 700–850 ^{o}C for time periods in the range 30–180 s for observing the recrystallization process. Also, to quantify the recrystallization fraction through micro-hardness testing.
- To provide inter-critical annealing (through water quenching) to the samples in the range 775–850 ^{o}C for time periods in the range 30–300 s for observing formation of austenite phase. Also, to quantify the austenite volume fraction through optical microscopy.
- To select the optimum annealing parameters from the recrystallization and austenite formation studies (above steps).
- To subject the samples to intercritical annealing process at the selected (optimum) annealing parameters using an annealing simulator.
- To conduct microstructure characterization of the annealed specimens through optical microscopy and hardness measurements. Also, to determine the volume fractions of ferrite and martensite phases using Image Analyser 'ImageJ' software.
- To conduct tensile testing of the annealed sample treated under optimum process parameters for determining its ultimate tensile strength and percentage total elongation.

3.3 Experimental Procedure

The details of experimental procedure followed in the present research work have been described as follows:

3.3.1 Material and Processing

A) Starting Material

The as-received material was a 57% cold rolled low carbon steel sheet having a final thickness of 1.6 mm. A detailed microstructure characterization was carried out by using both an optical microscope and a scanning electron microscope. The main focus of this characterization was to observe the distribution of pearlite and ferrite phases in the as-received material.

Table 3.1 presents the chemical composition of the as received cold rolled steel sheet.

Table 3.1: Chemical composition of the investigated steel

Element	C	Mn	Si	Al	P	S	N	Fe
% wt.	0.08	1.82	0.40	0.042	0.017	0.005	0.0035	Balance

Microstructure of the as-received cold rolled sheet was investigated both in the direction of rolling and the transverse section using standard metallographic procedure. For this purpose, the samples were prepared following the standard steps viz. specimen cutting, mounting, grinding and polishing. A 3% nital solution was used as etchant to draw out the microstructure. A Leica DM 2500M metallographic microscope was used for the microstructure characterization. Optical micrographs at different resolutions were recorded.

B) Characterization of Pearlite Phase Mixture

Microstructure characterization of the as-received cold rolled steel samples was carried out using a SEM set-up to investigate the morphology and distribution of pearlite phase mixture. Copper mounted specimens were prepared and utilized for the stated purpose and images were taken at high magnifications of upto 5000X.

3.3.2 Estimation of Annealing Parameters

After microstructure analysis of the as-received steel, the next step was to investigate the inter-critical annealing process for recrystallization and austenite formation. For this, the suitable temperature range and time span for the annealing process needed to be found out. For this purpose, commercial software like JMAT-Pro and Thermo-Calc were used for obtaining the CCT and TTT diagram, equilibrium diagram, phase fraction diagram etc. for the given steel. These graphical tools were used to select the suitable temperature-time conditions for producing the desired microstructure (i.e. to obtain required amount of austenite in the steel which could be transformed to martensite for producing ferrite-martensite dual phase structure). Both JMAT-Pro and Thermo-Calc provided information based on the chemical composition of the steel.

3.3.3 Recrystallization Studies

For the study of recrystallization phenomenon in the investigated steel, various annealing experiments were conducted. Small steel samples were cut **(**$15\times10\times1.6\ mm^3$**)** and heated at

the different temperatures between the lower and upper critical temperature of the steel (starting from 700 ℃ to 850 ℃ with steps of 25 ℃) for time steps of 30 s followed by the air cooling. A muffle furnace was used for heating the specimens. After the heat treatment, samples were prepared using standard metallographic technique for microstructure analysis and micro-hardness evaluation. Optical micrographs were taken using an optical microscope and microhardness of the soft ferrite phase was measured using a Vickers microhardness testing machine with load of ranging 15−50 g force and a dwell time of 15 s. The indenter speed was kept as 30 μm/s. The recrystallization volume fraction was measured through hardness measurements and activation energy for recrystallization of ferrite was determined by the standard JMAK analysis.

3.3.4 Study of Austenite Formation

Using the theoretically selected heat treatment parameters, various steel samples were annealed followed by water quenching to understand the phase transformation kinetics in the given steel. Quenching was done to induce martensitic phase transforms of austenite phase formed at high temperature for estimating the austenite content formed at that temperature. Samples were heated at different temperatures in the range 775–850 ℃ with increments of 25 ℃ . After heat treatment, the samples were prepared for the microstructural investigation using an optical microscope. 'Image J' software was used for the calculation of austenite phase fraction. Also, microhardness data was obtained to confirm the presence of ferrite and martensite in the microstructure after the annealing process.

3.3.5 Tensile Properties Evaluation

After the completion of recrystallization and austenite formation studies, optimum values for the annealing process parameters were selected to produce the ideal dual phase microstructure (40–45 % martensite, based on the literature). The steel sample annealed under the optimum heat treatment conditions was subjected to tensile testing to evaluate the ultimate tensile strength and the total percentage elongation. Tensile testing of as-received cold rolled steel was also done and properties of steel in the both the conditions (i.e. as-received as well as annealed) were compared.

3.4 Machines and equipment

This section describes the detail of various machines, equipment, commercial software etc. that have been used for the present experimental work. A brief outline and description of the characteristic features of these is described as below:

3.4.1 Precision Cutter

The precision cutter (Make: Mecatome T 255/300, Metal Power Analytical (I) Pvt. Ltd, Andheri, India) is a compact, multi-purpose cutter for cutting a variety of materials. The sheet of the given steel was mounted between the two clamping vices. The sheet was positioned in any starting position relative to the cutting wheel and then the arm was gently lowered until the cutting wheel had cut the sample from the steel sheet. Figure 3.1 shows the precision cutter used in the present work.

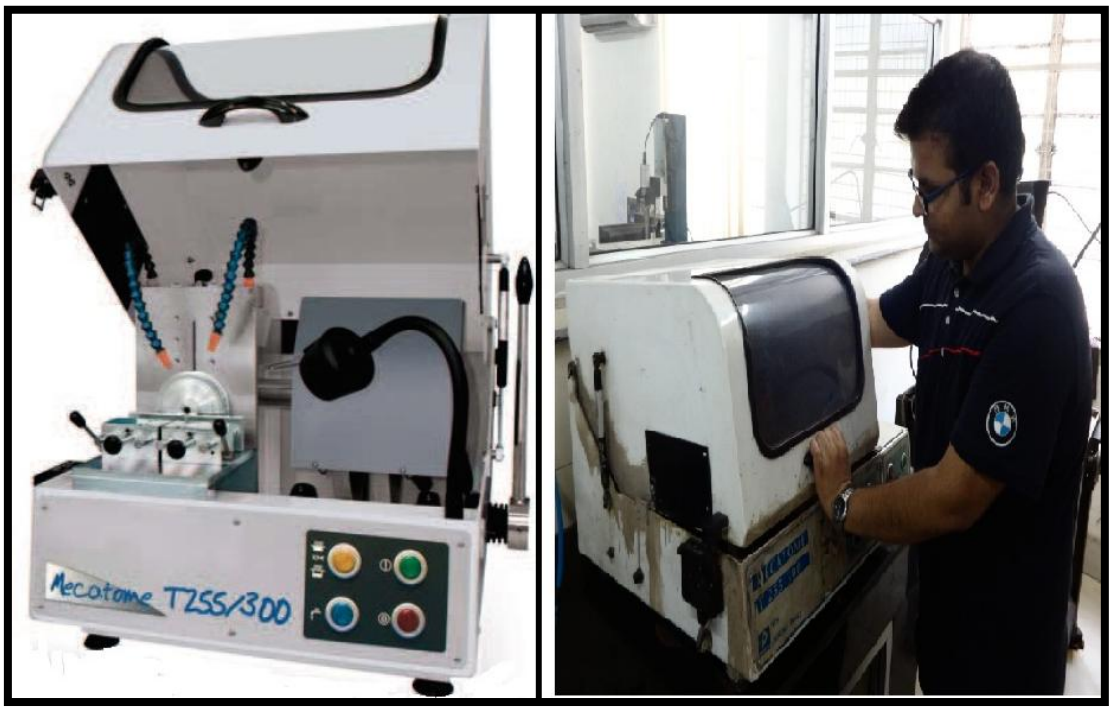

Fig. 3.1 Low Speed Precision Cutter (Courtesy: NML, Jamshedpur)

3.4.2 Tensile Testing Machine

The primary use of the tensile testing machine is to create the stress-strain diagram. After the diagram is generated, a computer algorithm calculates the yield strength, young's modulus, tensile strength and total elongation of the tested specimen. Figure 3.2 shows the setup of tensile testing machine used in the present work. A flat dog-bone shaped specimen of 35 mm

gauge length (Fig. 3.3) was machined from the cold rolled (CR) sheet and was given inter-critical annealing at the selected annealing conditions.

Tensile tests were conducted at room temperature under displacement control at a strain rate of 1 x 10^{-3} s^{-1} using a tensile testing machine (Make: Instron 8501 System, *Instron Engineering Corporation*, Norwood, USA) of 100 kN capacity in the region of uniform elongation. Elongation was measured by an extensometer of 25 mm range.

Fig. 3.2 Tensile testing machine (Courtesy: NML, Jamshedpur)

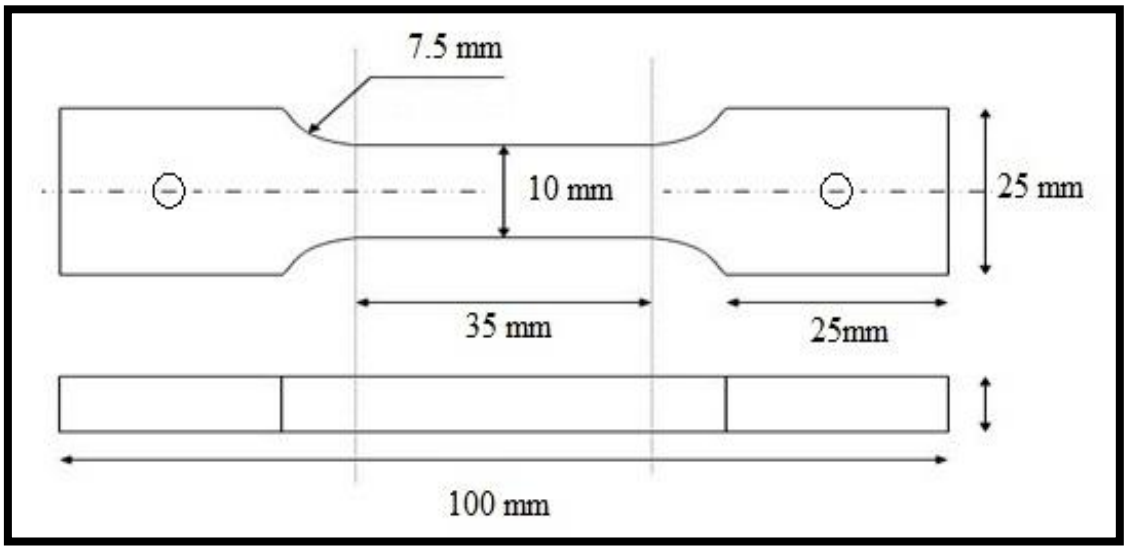

Fig. 3.3 Drawing of the Tensile Testing Specimen

3.4.3 Hardness Testing Machine

Vickers Hardness Tester is a key piece of equipment that is vital to metallographic research. In Vickers micro-hardness test procedure, indentation is made with a range of loads using a diamond indenter which is then measured and converted to a hardness value. For this purpose, test samples are carefully and properly prepared by grinding and polishing. Two types of indenters are generally used for Vickers test family; a square base pyramid shaped diamond indenter for Vickers hardness testing and a narrow rhombus shaped indenter for Knoop hardness testing. The Vickers hardness test method requires a pyramidal diamond with square base having an angle of 136° between the opposite faces. Upon completion of indentation, the two diagonals are measured and the average value is considered. Vickers Hardness Number is obtained by dividing the applied load in kilogram-force by surface area of indentation.

Figure 3.4 shows the hardness tester used in the present work (Make: Leica Q550MW VMHT Auto, *Leica Microsystems*, Wetzlar, Germany). In the present study, the micro-hardness tester was operated at a low load of 15–50 g-force for a dwell time of 15 s and with an indenter speed of 30 μm/s.

Fig. 3.4 Hardness Testing Machine (Courtesy: NML, Jamshedpur)

3.4.4 Muffle Furnace

Muffle furnace is a front loading box type oven or kiln for high temperature applications such as for fusing glass, creating enamel coating, ceramics soldering and brazing of articles etc. The inner chamber is made of stainless steel and heaters are clamped to its outside and

operated at low heat. Glass wool insulation is used between the two walls. Temperature control is provided by a capillary thermostat which possesses excellent durability and accuracy. Heaters are made of 80/20 nichrome wire, uniformly wound on the muffle. The safety fuse limits the temperature from exceeding the value of set temperature. Mild steel control box is fitted at the bottom of the furnace and consists of indicating lamps, On/Off switch, digital temperature controller along with Cr/Al thermocouple sensor. The furnace is electrically operated at 230 Volts (AC), single phase, and 50 Hz supply. The muffle furnace used in the present work is shown in Fig. 3.5.

Fig. 3.5 Muffle Furnace (Courtesy: NML, Jamshedpur)

3.4.5 SAMPLE PREPARATION FOR METALLOGRAPHY

After the heat treatment, all samples were prepared for metallographic examination. In order to prepare samples for material characterization, some basic steps need to be followed carefully. These include mounting, planar grinding, rough polishing, final polishing, etching, and microscopic analysis. These steps are discussed in brief as follows:

A) Mounting

Mounting of samples is usually done in order to facilitate their easy handling. Mounting is done either with copper or with bakelite. Copper is mostly used as a mounting material when specimen is used for SEM analysis. Specimens were hot mounted at a temperature of 160 ℃ by following the procedure similar to powder metallurgy. The edges of the mounted samples were rounded to minimize the damage to grinding/polishing discs. The mounting press

(Make: BAINMOUNT METCO, *Chennai Metco Pvt. Ltd.*, Chennai, India) was used in the present work and is shown in Fig. 3.6.

Fig. 3.6 Mounting Press (Courtesy: NML, Jamshedpur)

B) Grinding

Grinding is required to planarize the specimen. The surface to be examined by microscope is polished with abrasive papers of successive finer grades such as 80, 120, 220, 320, 400, 600, 800, 1000, 1200, 1500 and 2000 mesh abrasive paper (shown in Fig. 3.7). Each time the sample is rubbed on SiC paper, it produces scratch marks and therefore polishing is continued till the scratches from earlier stages (SiC paper) have been obtained in uniform one direction. Then, the direction of scratching or rubbing is switched perpendicular to previous scratches on the next paper with finer grade. Again this is repeated until all scratches get oriented uniformly in one direction. The over-heating of sample is avoided as it may cause modification in the microstructure. Further, the pressure needs to be adjusted wisely as high pressure applied can lead to introduction of deep scratches and low pressure applied can result in elongated time consumption. Starting from the coarse grade paper (80 grit size), the procedure was carried up to fine grade paper (2000 grit size).

C) Polishing

The next step in preparation of sample is polishing on a horizontal rotating wheel. Polishing wheels are covered with a soft cloth (velvet, canvas, suede or selvet etc.) which need to be impregnated with a polishing medium (alumina or colloidal).

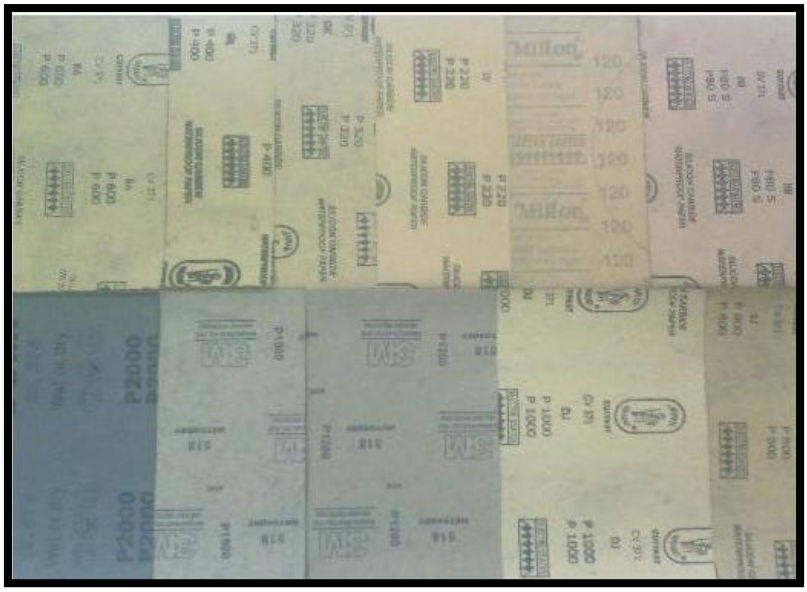

Fig. 3.7 Abrasive Papers (Courtesy: NML, Jamshedpur)

The polishing medium is spread on to the rotating disc and specimen is held on the rotating disc in order to obtain a scratch free surface with mirror like finish. Precautionary measures such as washing the specimen, and also the polishing cloth thoroughly with water prior to initiating polishing should be done. This would divert any chances of introduction of contaminants or abrasive particles (from abrasive paper during grinding) which may lead to more deep scratches. Polishing medium is spread on to a well washed cloth and as soon as the specimen starts to stick or friction starts to act between the specimen and cloth, water is poured on to the rotating wheel. Polishing machine (Make: BANIPOL METCO, Model No: PMV018, *Chennai Metco Pvt. Ltd.*, Chennai, India) of 0.37 kW capacity was used in the present work. Polishing machines have been shown in Fig. 3.8.

Fig. 3.8 Polishing Machine (Courtesy: NML, Jamshedpur)

D) Etching

Etching is done in order to reveal the microstructure of the metal/alloy system through selective chemical attack as the constituents mostly show similar reflectivity, causing difficulty in distinguishing them. Etching occurs by electrolytic action at structural variations on the sample surface. Chemical etchants produce either a metallographic contrast as grains etch at different rates because of variation in their crystallographic orientation which produces steps at grain boundaries and reflectivity difference or by grain or phase-boundary etching, which produces grooves. The sample must be thoroughly cleaned before etching. A satisfactory etchant must be selected and prepared, and etchant may be applied using a cotton bud wiped over the surface for a few times (necessary precautions must be taken while etching, as there is only a hair line difference between etching and over-etching). Nital (a solution of 3% nitric acid (HNO_3) in ethanol) was used as etchant in the present work. The specimens were immediately washed with alcohol after applying the etchant and were dried.

E) Levelling

Ideally, the surface to be examined optically should be perfectly flat and levelled. If not, then, as the viewing area is moved across the surface it passes in and out of focus. In addition, it makes it difficult to have the whole of field of view in focus - while the centre is focused, the sides go out of focus. By using a specimen levelling press (shown in Fig. 3.9) this problem can be avoided, as it presses the mounted specimen into clay or plasticene on a microscope slide, making it levelled. A small piece of paper or cloth covers the surface of the specimen to avoid scratching.

3.4.6 Microstructural Evaluation

The important mechanical properties are strongly influenced by the microstructure, so microstructural evaluation and its understanding is important for development of metallic materials. In the present research work, optical microscopy and scanning electron microscopy (SEM) were used for microstructure assessment.

A) Optical Microscope

Optical microscope is used for the purpose of magnifying small samples by using visible light and a system of lenses. The image from an optical microscope is captured by normal light sensitive cameras to generate micrographs. Metallic materials are usually opaque and therefore investigations of plane cross-sections by incident light prevail in metallography.

While amplitude objects become visible owing to differences in light absorption and thus appear in different grey shades or even colours, phase objects only differ in the refractive indices which cannot be recognized without additional provision. Starting from the cross-section preparation, to etching of the specimen, and setting up of microscope, all steps should be carefully optimized in order to get maximum information from a microscopic study. The optical microscope (Make: Leica DM2500 M; *Lieca Microsystems*, Wetzlar, Germany) used in the study is shown in Fig. 3.10.

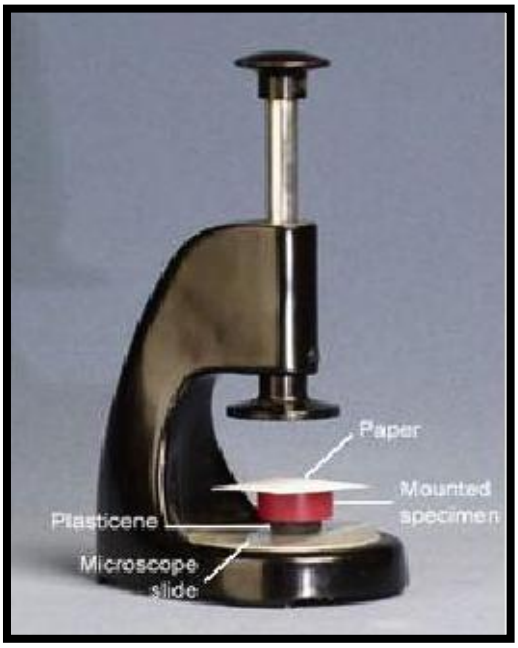

Fig. 3.9 Levelling Machine (Courtesy: NML, Jamshedpur)

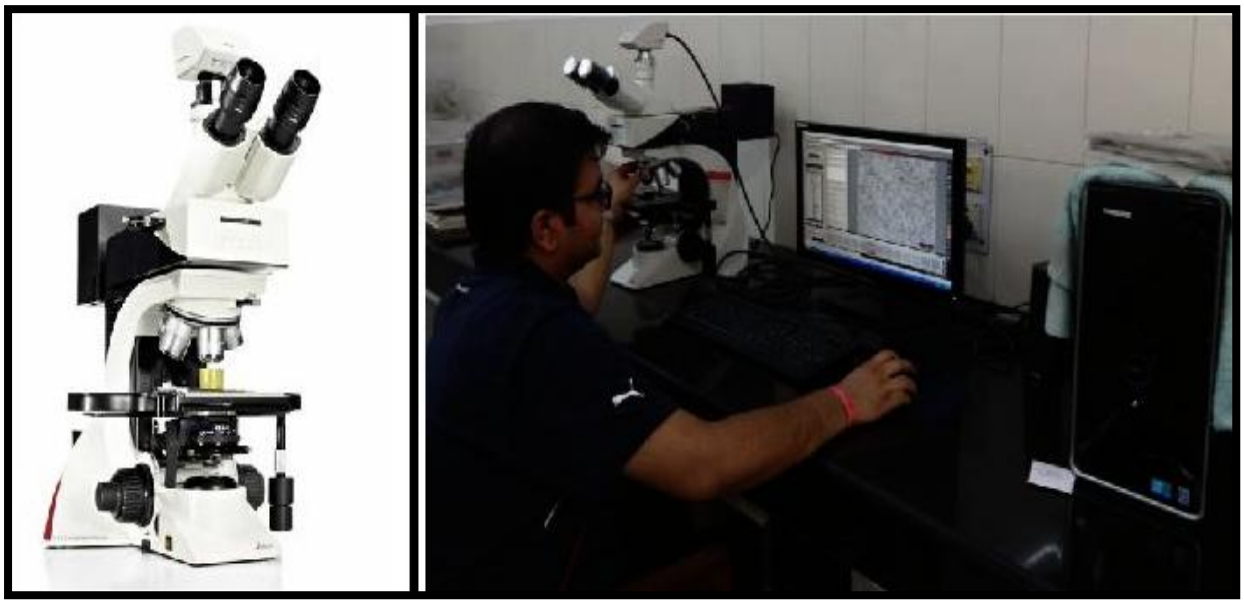

Fig. 3.10 Optical Microscope (Courtesy: NML, Jamshedpur)

B) Scanning Electron Microscope

A scanning electron microscope (SEM) is a type of electron microscope that images a sample by scanning it with a high-energy beam of electrons in a raster scan pattern. The electrons interact with the atoms that make up the sample and produce signals that contain information about the sample's surface topography, composition, and other properties such as electrical conductivity etc. SEM can produce very high-resolution images of the sample's surface, revealing details less than 1 nm in size. Due to the very narrow electron beam, SEM micrographs have a large depth of field yielding a characteristic three-dimensional appearance useful for understanding the surface structure of a sample. Figure 3.11 shows the scanning electron microscope (Make: Nova Nano SEM 430; *Field Emission Inc.*, Hillsboro, USA) used in the present study.

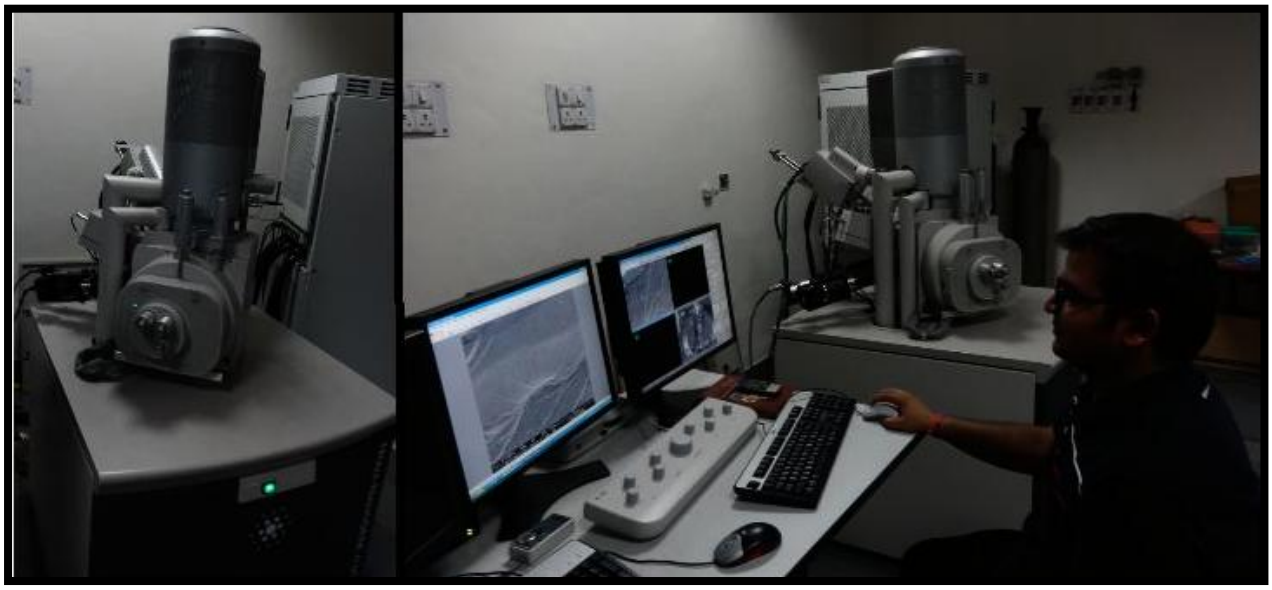

Fig. 3.11 Scanning Electron Microscope (Courtesy: NML, Jamshedpur)

3.4.7 Annealing Simulator

Annealing simulator is a specialized equipment for annealing of steel samples in a controlled environment. In this simulator, samples to be annealed can be heated in a controlled environment and can be cooled under controlled cooling rates. The simulator has been designed and developed as a joint venture of CSIR-NML and Tata Steels, Jamshedpur. The simulator system (as shown in Fig. 3.12) consists of three main sub-systems (or parts) viz. a heating system, a cooling system and a PLC based digital control system. Heating system consists of a heating chamber in which the sample is placed and a movable furnace is provided to heat the chamber. A reducing environment is provided in the chamber so as to

avoid oxidation of the sample. Cooling system consist of a mixing tank in which hydrogen (H_2) and nitrogen (N_2) gases are mixed. This mixture of gases is supplied to the chamber through the supply lines. Pressure of the gas mixture is varied to achieve different cooling rates. Multiple options for cooling medium are available, such as hydrogen, nitrogen, or mixture of these, atomized water, air humidification etc. For the measurement of heating and cooling rates, thermocouples are provided inside the chamber which determine the specimen temperature and chamber temperature at very instance. All these thermocouples are connected to the digital control system.

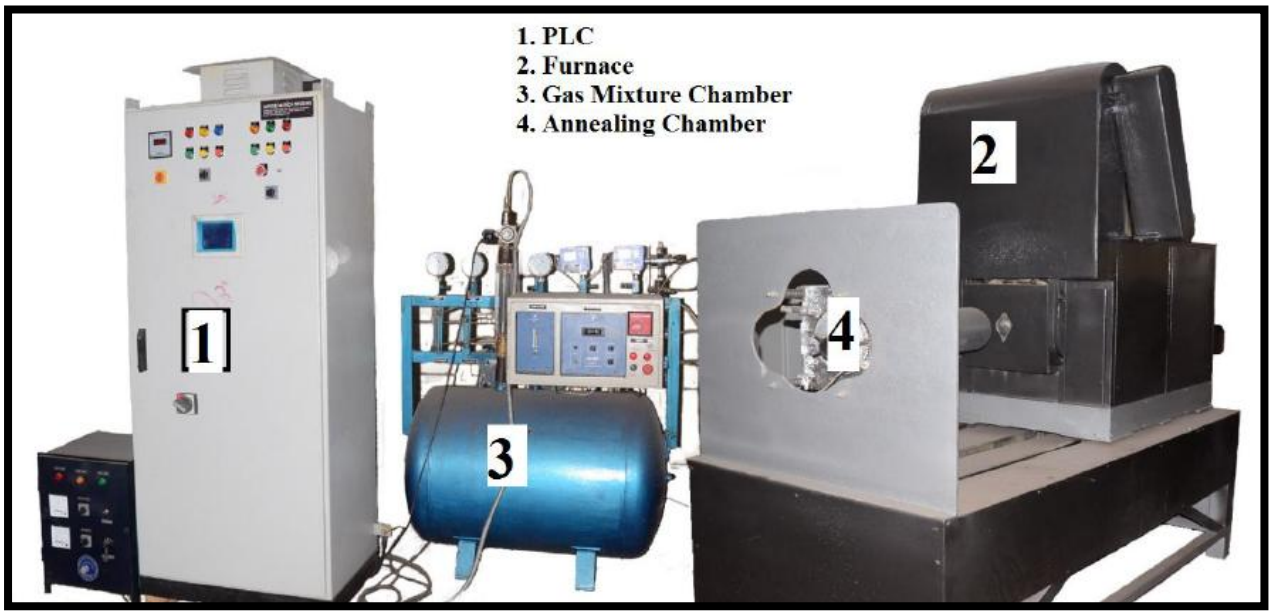

Fig. 3.12 Annealing Simulator (Courtesy: NML, Jamshedpur)

3.4.8 Commercial Software

The various commercial software that were used in the present study are Thermo-Calc, JMAT-Pro, Dictra and ImageJ. The details of these software are given as follows:

A) Thermo-Calc

To investigate the critical temperatures of the given steel and to determine the phase fractions at various inter-critical temperatures (during heating), Thermo-Calc software (*Thermo-Calc 3.0*; developed by *Thermo-Calc Software AB*, Stockholm, Sweden) was used to obtain the phase fraction diagram and equilibrium diagram. Equilibrium diagram provides data both on critical temperatures (Ac_1 and Ac_3) as well on phase fractions of ferrite and austenite at the inter-critical temperatures. Phase fraction diagram presents the volume fraction of constituent phases at a given inter-critical temperature.

B) JMat-Pro

To investigate the effect of heating rates on austenite formation (TTA diagram) and to construct the CCT, TTT, and phase fraction diagram, JMat-Pro software (*JMat-Pro 7.0;* developed by *Sente Software Limited,* Guildford, United Kingdom) was used. CCT diagram explains the effect of different cooling rates on the microstructure and hardness of samples, TTT diagram provides information on isothermal transformation of austenite phase, and phase fraction diagram presents the volume fraction of constituent phases at a given inter-critical temperature.

C) ImageJ

ImageJ (*ImageJ*; developed by *National Institutes of Health*, Bethesda, Maryland, USA) is an image processing program that can display, edit, analyze, process, save, and print 8-bit color and gray scale, 16-bit integer and 32-bit floating point images. ImageJ can calculate area and pixel value statistics of user-defined selections and intensity threshold objects. It can measure distances and angles. It can create density histograms and line profile plots. It supports standard image processing functions such as logical and arithmetical operations between images, contrast manipulation, convolution, Fourier analysis, sharpening, smoothing, edge detection and median filtering. For the present study ImageJ was used to measure the volume fraction of the martensite phase from the optical micrographs for the various samples.

3.5 Summary of the Chapter

This chapter describes the design of the study that was adopted for present work. In this chapter of the report, the objective function with key issues has been discussed. An overview of the experimental procedure that was followed and machines and equipment has been provided. This chapter also includes the procedure for sample preparation for metallography, microstructural analysis and mechanical properties evaluation etc. In the last section of the chapter information about the commercial softwares that were used in the present study has also been provided.

Chapter 4

Results and Discussion

4.1 Introduction

This chapter deals with the theoretical predictions with regards to annealing parameters using commercial software, results of various experiments performed and the calculations regarding recrystallization fraction, activation energy etc. using empirical relations and equations from available literature. The phase diagram, CCT & TTT diagram, phase fraction diagram were developed for the given steel. These were used along with various micrographs, recrystallization curves, and tensile curves etc. draw conclusions regarding the recrystallizations phenomenon, austenite formation and stabilization during the intercritical annealing of the given low carbon steel for producing dual phase ferrite-martensite microstructure. The overall objective of the present study was to determine the appropriate process parameters viz. temperature, holding time, and cooling rate etc. during the annealing cycle for production of dual-phase steel from a low carbon cold rolled steel sheet.

4.2 Microstructure of the As-received Steel

Cold rolled sheet of a low carbon steel with very lean chemistry (Table 3.1) was used for the present study. Microstructure of the as-received cold rolled sheet in the rolling and the transverse section was investigated using micrographs from a metallographic microscope at different magnification levels (100, 200, 500 and 1000X). Optical micrographs showed presence of pearlite and pro-eutectoid ferrite. There was alignment of deformed ferrite grains and the pearlite colonies in the rolling direction. Figure 4.1 shows the optical images of the as received steel in the rolling and transverse directions.

Further, for detailed investigation of the distribution and morphology of pearlite phase mixture in the as-received cold rolled steel, SEM images were recorded at relatively high resolutions. SEM images in Fig. 4.2 show various pearlite colonies and their different shapes and distribution in the as-received steel. It was observed that distribution of pearlite phase mixture was not uniform in the ferrite matrix. Further, the shape and size of pearlite colonies was also not uniform showing the effect of cold working. Cold deformation resulted in destruction of lamellar pearlite colonies into a non-uniform shape and size. This type of

microstructure leads to non-uniform dissolution of pearlite phase during the course of austenite formation. Thus, this

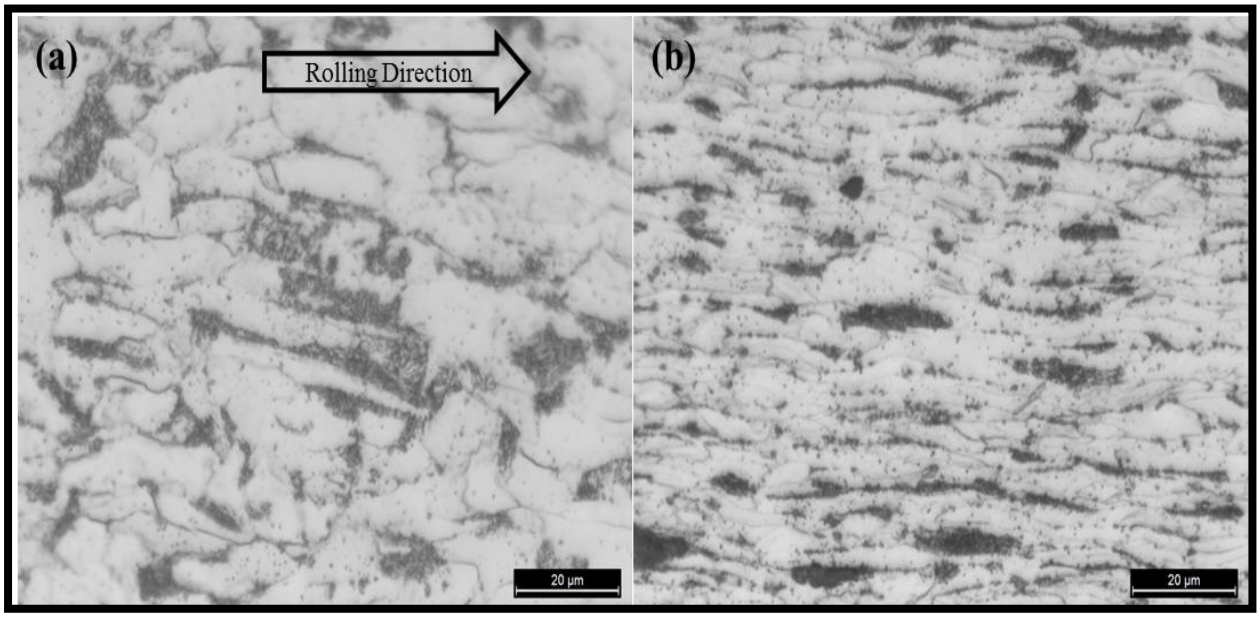

Fig. 4.1 Optical micrographs of as-received steel in (a) rolling plane and (b) transverse plane

anomaly in the microstructure due to prior cold rolling can show delayed formation of austenite at the ferrite-pearlite interfaces during the annealing process.

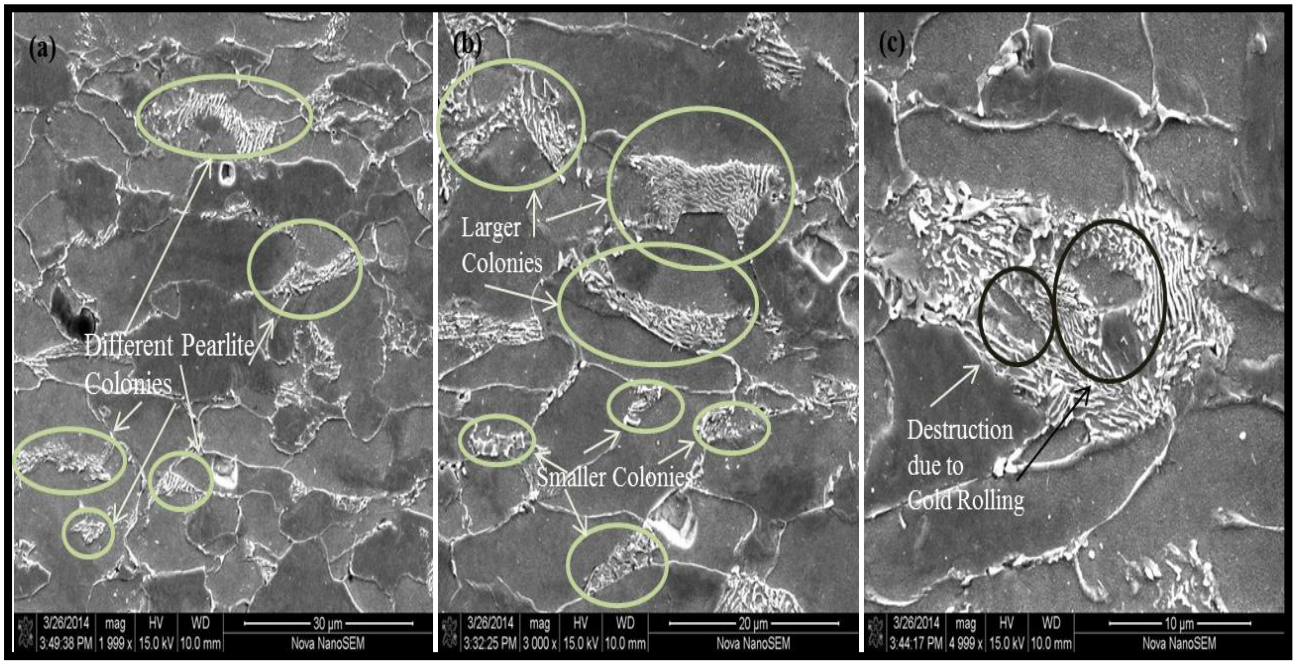

Fig. 4.2 SEM micrographs of as-received steel showing (a) different pearlite colonies (b) distribution of colonies (c) destruction of lamellar structure

4.3 Prediction of Annealing Parameters

The annealing temperature range (lower and upper critical temperatures), soaking periods, cooling rates etc. to be followed during annealing were predicted using commercial software viz. JMat-Pro 7.0 and Thermo-Calc 3.0.

4.3.1 Thermo-Calc Predictions for Annealing Parameters

Commercial software Thermo-Calc was used for obtaining the equilibrium diagram, and phase fraction diagram for the given cold rolled steel. Figure 4.3 (a and b) show the phase diagram and phase fraction diagram (obtained using Thermo-Calc) for the given steel. From the equilibrium diagram, the intercritical temperatures were obtained. The lower critical and the upper critical temperatures were obtained as 682.2 ℃ and 839.7 ℃ respectively**.** Hence, the temperature range for the experimental study was determined.

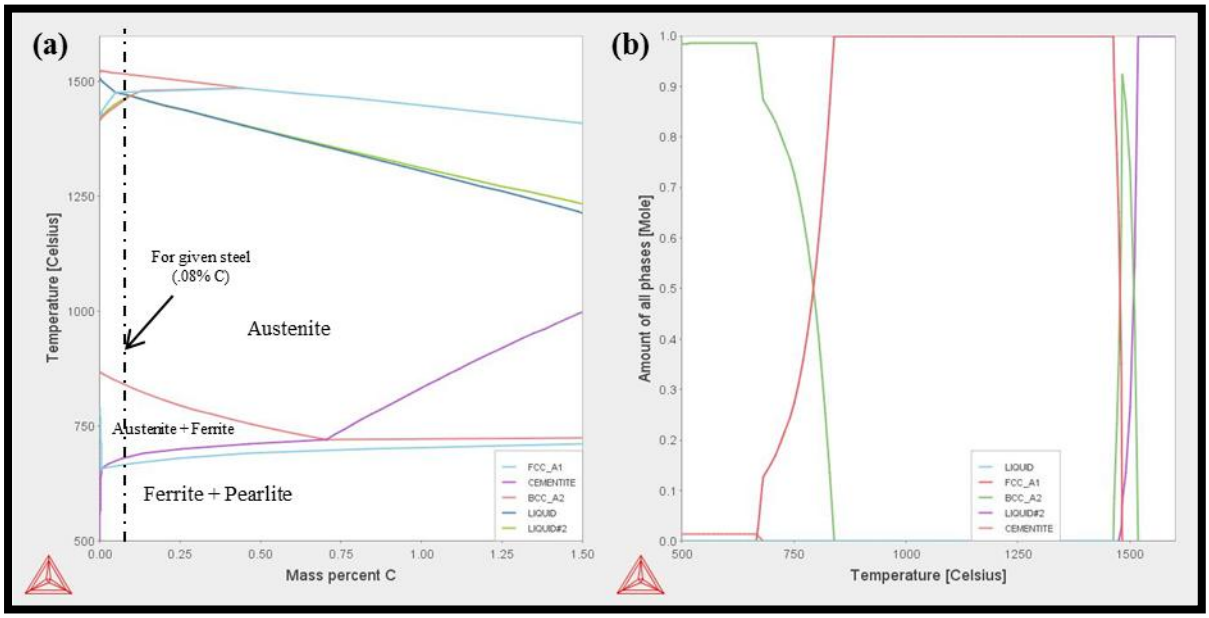

Fig: 4.3 Result window of Thermo-Calc for a) Equilibrium phase diagram b) Phase fraction diagram for the as-received material

4.3.2 JMat-Pro Predictions for Annealing Parameters

JMat-Pro was used to obtain the phase fraction diagram again, TTA diagram and the CCT and TTT diagrams for the given steel. Figure 4.4 (a–c) show the various diagrams obtained using JMat-Pro software. From these diagrams, the intercritical temperature range, and the cooling rates required for producing various microstructures were obtained. TTA diagram

(Fig. 4.4c) showed that with increase in heating rate, the lower and upper critical temperatures also increase.

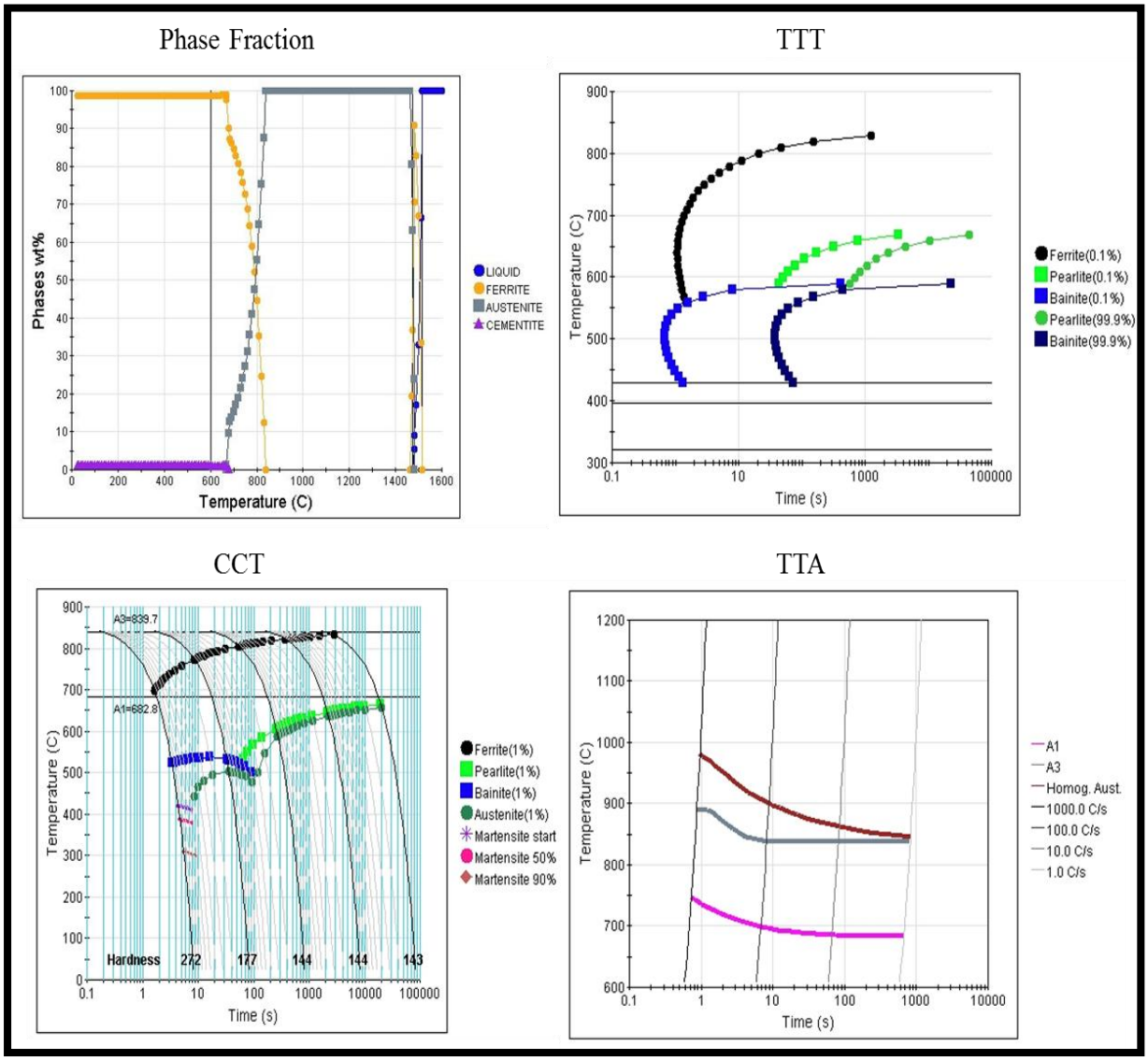

Fig. 4.4 Result window of JMat-Pro (a) Phase Fraction diagram (b) TTT diagram (c) TTA diagram (d), CCT diagram for equilibrium heating conditions

The volume fraction of austenite phase in the steel during equilibrium heating was also predicted from the phase fraction diagram at different annealing temperatures as shown in Table 4.1.

4.4 Recrystallization Kinetics

For the investigation of recrystallization phenomenon in the given steel, annealing experiments were conducted for small sized specimens (15×10×1.6 mm^3) in the inter-critical temperature range. Samples were annealed in a muffle furnace at different temperatures

(700 ℃ to 850 ℃ with steps of 25 ℃ each) with different holding time periods at each temperature (30 s to 180 s in steps of 30 s each) followed by air cooling. After the heat treatment, samples were prepared using standard metallographic technique for microstructure analysis and micro-hardness evaluation. The recrystallization volume fraction was measured through hardness measurements and activation energy for recrystallization of ferrite was determined by the standard JMAK analysis.

Table 4.1 Austenite phase fraction at different inter-critical temperatures from JMat-Pro

Temperature (℃)	Austenite Phase Fraction (wt.%)
700	15.24
725	20.21
750	27.28
775	38.28
800	55.40
825	81.22
850	100

4.4.1 Calculation of Recrystallization Fraction

Recrystallization volume fraction (X) for each annealed sample was calculated using the microhardness data as per equation 4.1 [Li et al., 2013].

$$X = \frac{(H_0 - H_t)}{(H_0 - H_{Rex})} \qquad 4.1$$

where, H_0 stands for the initial microhardness (of the ferrite phase) of the as-received cold rolled material, H_t is the microhardness after the heat treatment and H_{Rex} is the micro-hardness of the fully recrystallized steel.

Recrystallization fraction was calculated for all annealed samples subjected to different temperature-time conditions, (Appendix I)**.** The microhardness of the fully recrystallized ferrite structure was obtained by normalizing the sample at 750 ℃ with 30 min holding and was measured to be 150 Hv and the hardness of the as-received cold rolled steel (comprising of deformed ferrite with non-uniformly distributed pearlite colonies) was found to be 284.4 Hv. It was observed that the recrystallization fraction increased with increase in annealing

temperature, or holding time at a given temperature, or both. Figure 4.5 shows the ferrite recrystallization fraction plot for different temperature-time annealing conditions.

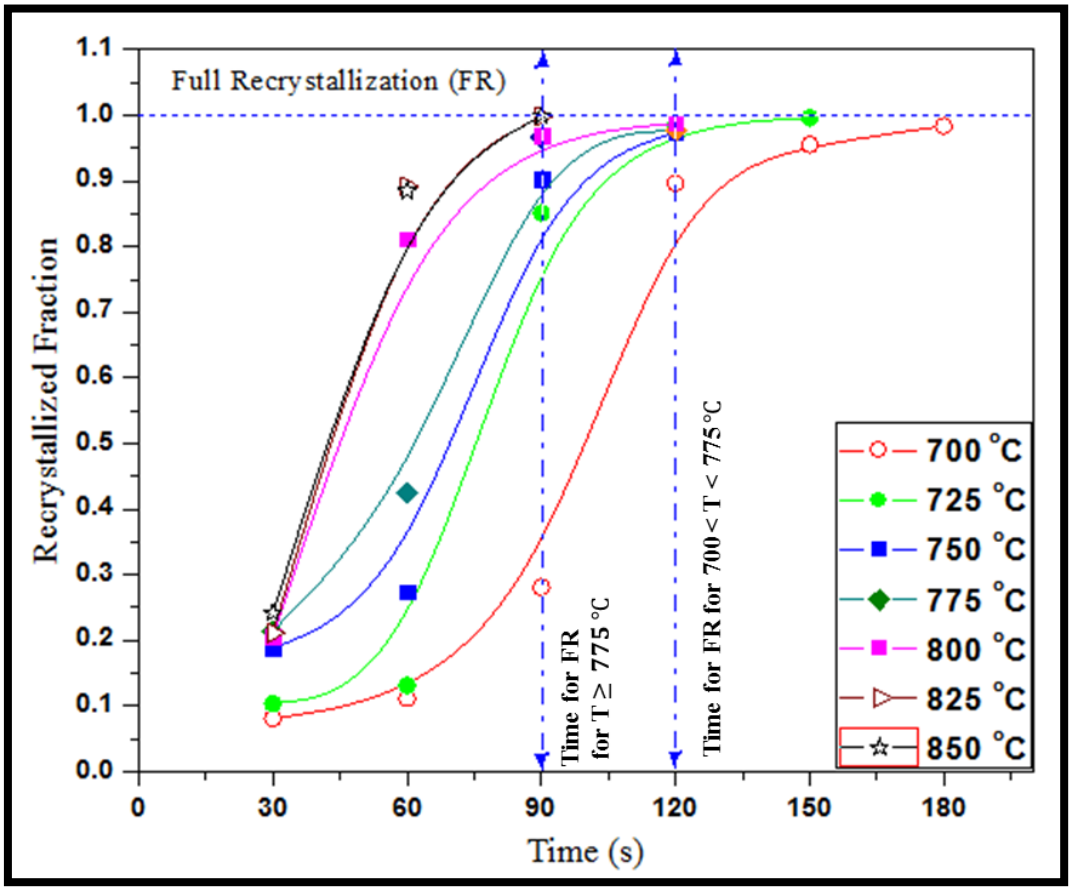

Fig. 4.5 Variation in recrystallization fraction with different annealing temperatures and holding time periods. T= annealing temperature

The recrystallization fraction obtained using microhardness data was again confirmed by observing the recrystallized ferrite phase in the optical micrographs recorded for this study. Appendix II shows all the micrographs for annealed samples under various temperature-time conditions. Table 4.2 shows some selected micrographs representing non-recrystallized, partially recrystallized and fully recrystallized microstructures at a given annealing temperature with different holding time periods. The micrographs support the results of microhardness testing and represent increase in fraction of recrystallization with increase in annealing temperature, or holding time, or both. The micrographs reveal that at higher temperatures, the rate of recrystallization becomes very fast which can also be noted from the hardness calculations. For temperatures of 775, 800, 825 and 850 ℃, the rate of recrystallization was very fast and even with less holding time of 1 min, the recrystallization fraction (X) was considerably high.

Table 4.2 Optical Micrographs for the Recrystallization Studies

Temp. (℃)	Non-Recrystallized Structure	Partially Recrystallized Structure	Fully Recrystallized Structure
700	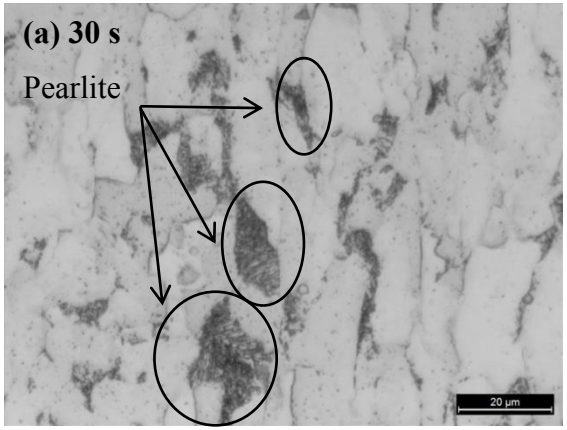	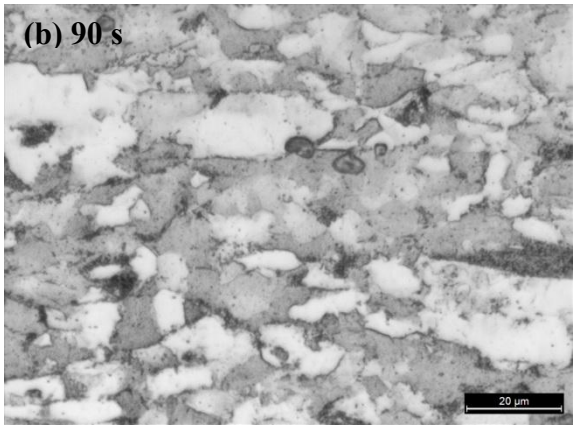	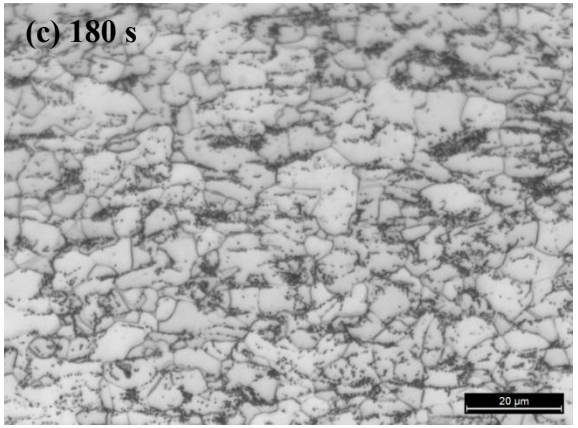
725	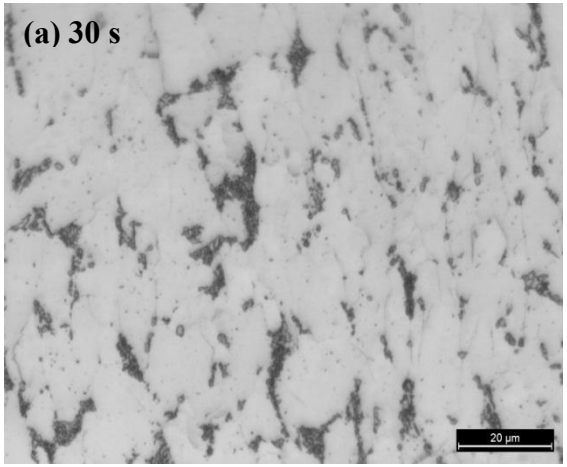	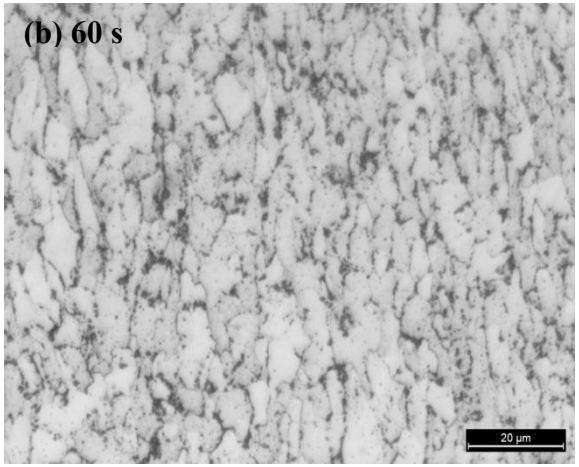	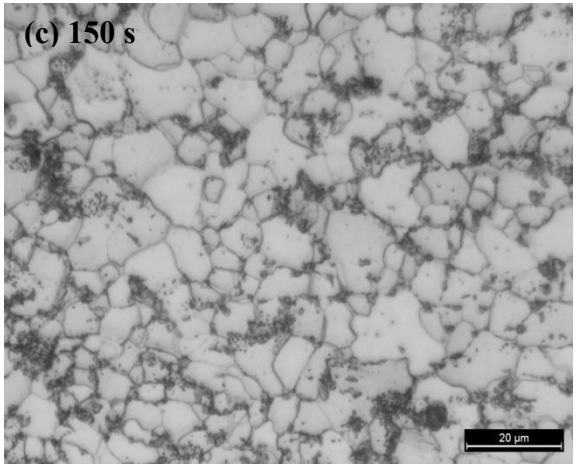

Temp. (℃)	Non-Recrystallized Structure	Partially Recrystallized Structure	Fully Recrystallized Structure
750	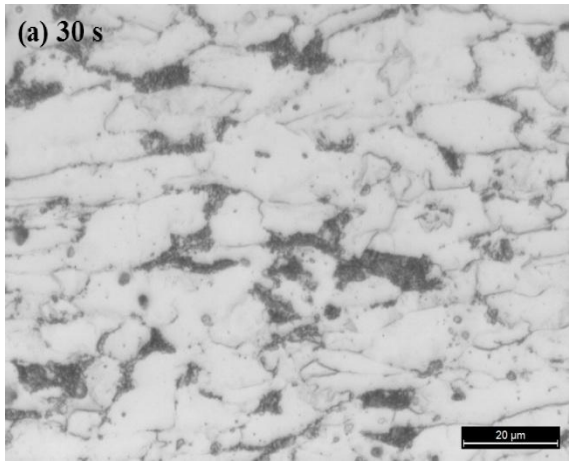	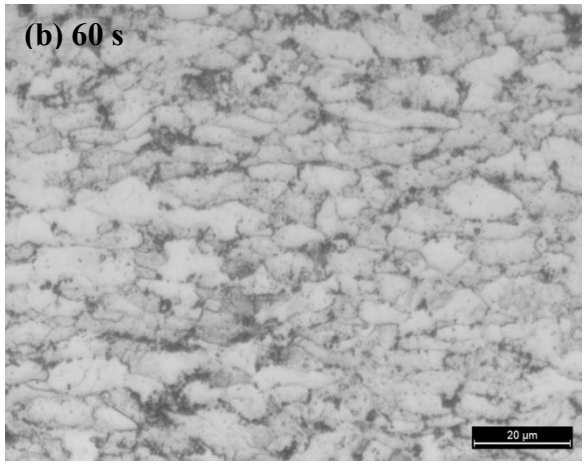	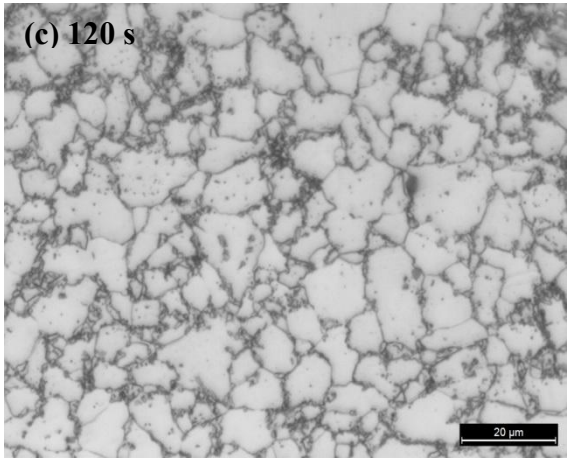
775	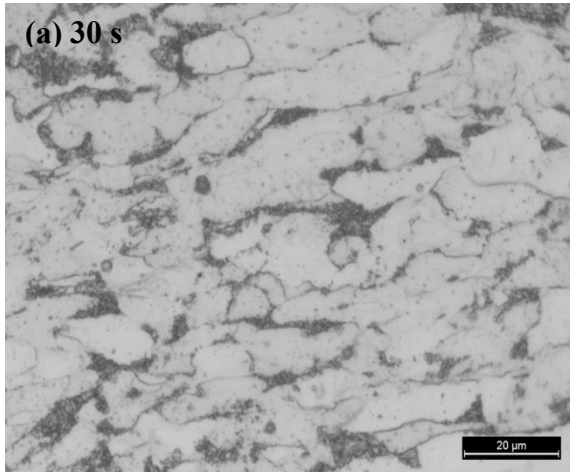	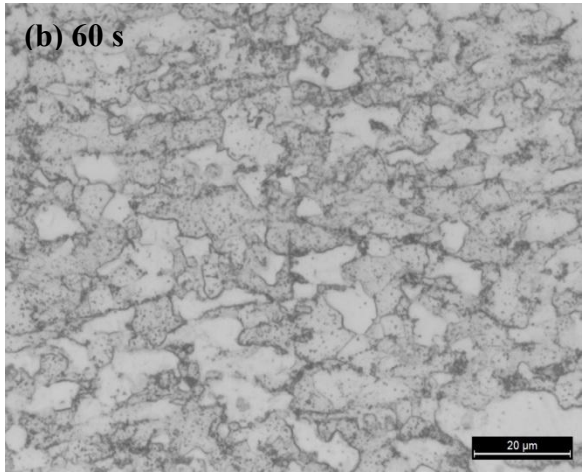	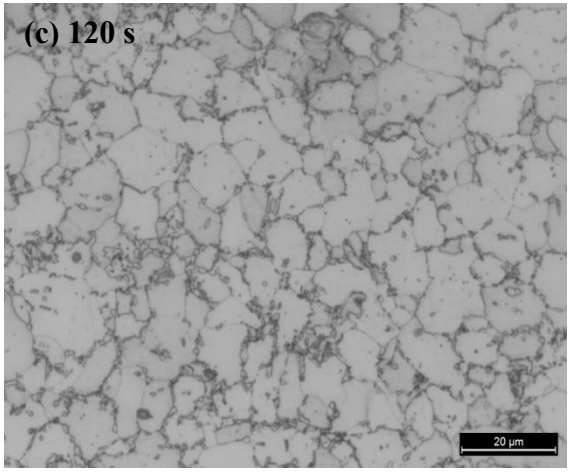

Temp. (℃)	Non-Recrystallized Structure	Partially Recrystallized Structure	Fully Recrystallized Structure
800	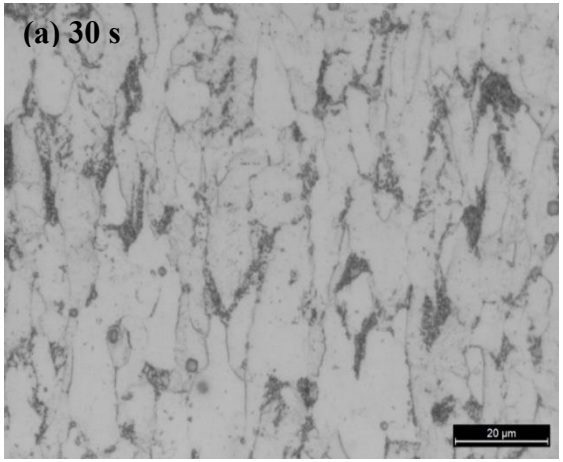	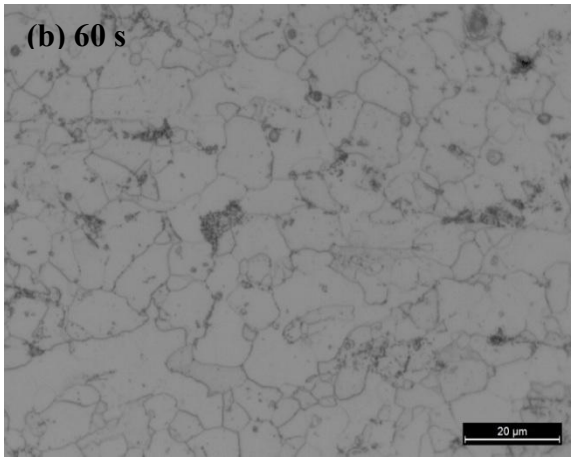	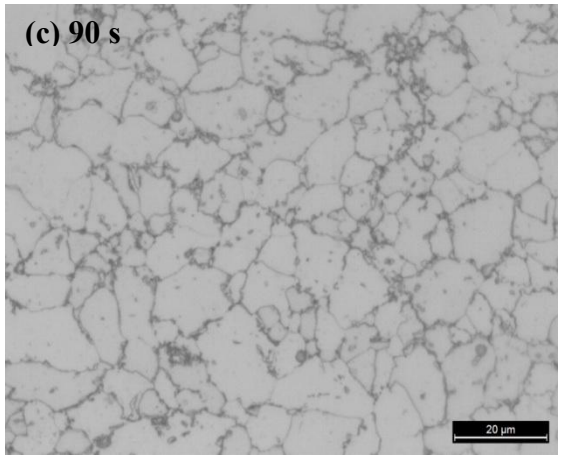
825	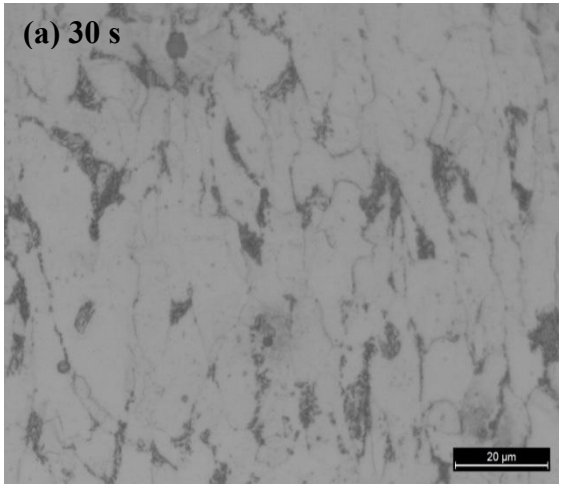	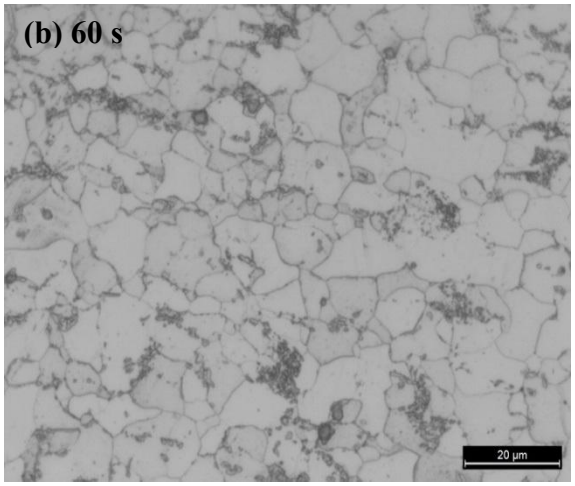	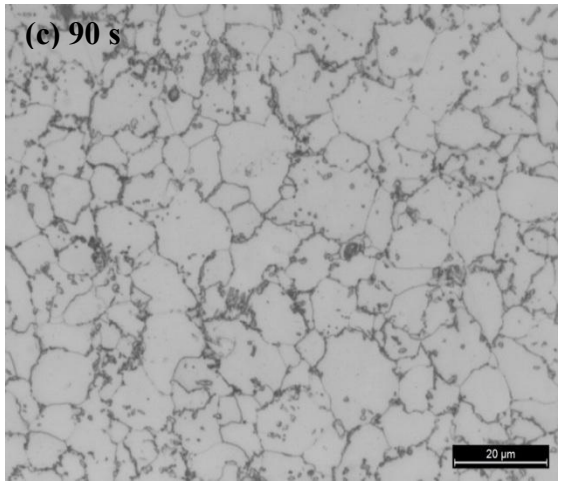

Temp. (℃)	Non-Recrystallized Structure	Partially Recrystallized Structure	Fully Recrystallized Structure
850	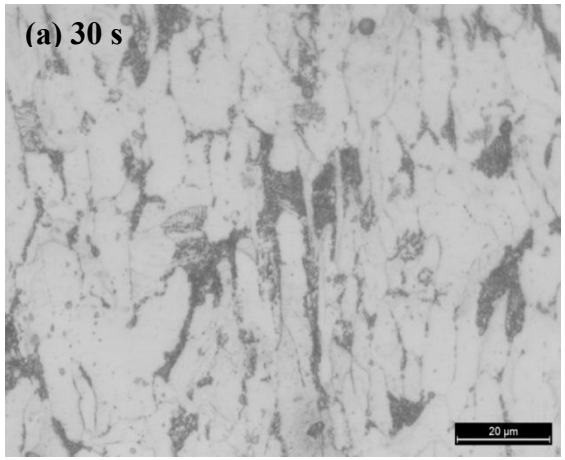	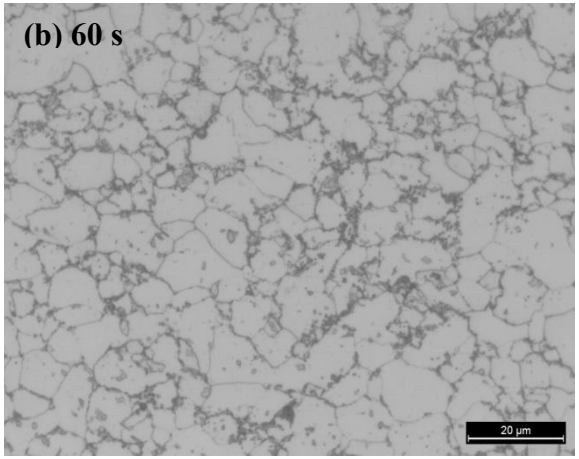	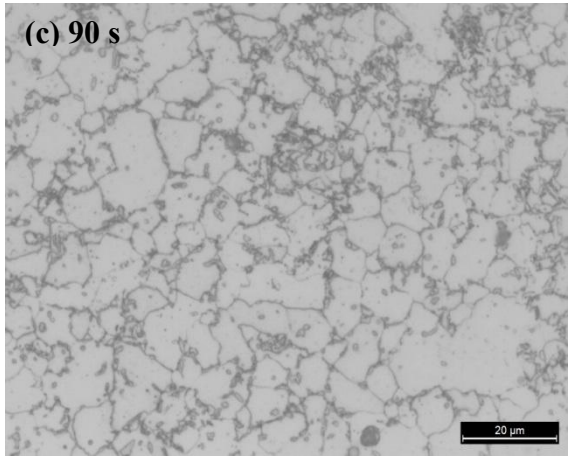

It was clear both from the optical micrographs and recrystallized fraction calculations that no subtle changes were observed during the early stages of annealing (0–30 s) which is the recovery stage of the annealing process. The duration of this recovery period depends upon the annealing temperature. At low annealing temperatures, long recovery periods are required and vice versa [Kalu and Waryoba, 2007].

4.4.2 Calculation of Activation Energy

Activation energy for recrystallization of ferrite was determined using the standard JMAK analysis (Avrami equation) which is expressed as Equation 4.2 This equation is valid only when the recrystallized grains are distributed randomly and when the grains are growing independently of each other [Kalu and Waryoba, 2007; Li et al., 2013].

$$X = 1 - e^{[-bt^n]} \quad 4.2$$

where, X is the recrystallized volume fraction of ferrite as a function of annealing time for a particular temperature, n is JMAK constant/ Avrami constant and b is the temperature dependent value which is expressed as equation 4.3.

$$b = b_0 e^{[-\frac{Q}{RT}]} \quad 4.3$$

here, b_0 is a constant, Q is recrystallization activation energy (kJ/mol), R is the universal gas constant (J mol^{-1} K^{-1}) and T is the annealing temperature (K).

Equation 4.2 can be rewritten as:

$$\ln(1 - X) = -bt^n \quad 4.4$$

Equation 4.4 can be further expressed as:

$$\ln(\ln\left(\frac{1}{1-X}\right) = \ln(b) + n\ln(t) \quad 4.5$$

Equation 4.5 was used for calculating the value of parameters b and n. For this, a plot between $ln(ln(1/(1-X))$ and $ln(t)$ for each annealing temperature was obtained. The values of JMAK constant (n) and temperature dependent factor (b) were calculated from these plots for each temperature. Figure 4.6 shows these plots (JMAK plot) for different annealing temperatures. The values of *b* and *n* calculated from the JMAK plot (Fig. 4.6) are shown in Appendix III.

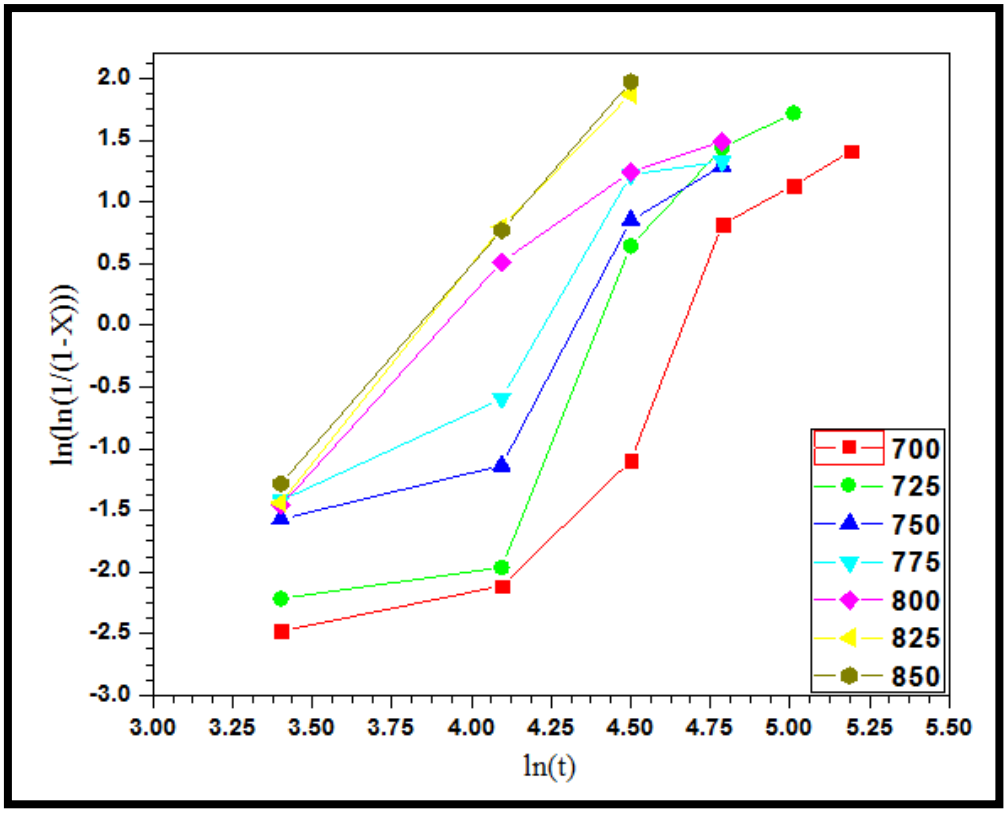

Fig. 4.6 JMAK plot of $\ln(\ln(1/(1-X))$ vs. ln(t) for different temperatures

Taking the natural log of Equation 4.3, the equation became linear as shown in Equation 4.6.

$$\ln(b) = \ln(b_0) - \frac{Q}{RT} \qquad 4.6$$

Plot of $ln\ (b)$ vs. $1/T$ was drawn for determining the value of activation energy (Q) for the recrystallization of ferrite. Figure 4.7 shows the plot of $ln\ (b)$ vs. $1/T$. The slope of the plot was equal to $(-Q/R)$. This slope from Fig. 4.7 was calculated as -26065 (K) from which the activation energy (Q) for recrystallization was calculated as 216.7 kJ/mol. The plot (Fig. 4.7) also gave the value of $\ln(b_0)$ from the intercept value. From this, the value of b_0 was calculated as 1.24×10^7 respectively.

Using the values of constants n and b_0 and using Equation 4.2 and Equation 4.3, the holding time needed for full recrystallization of ferrite can be predicted for any annealing temperature. However, it may be noted that the time period calculated as discussed here does not include the recovery time. The total time required for recrystallization will also include the recovery time (30 s approximately in the present work.).

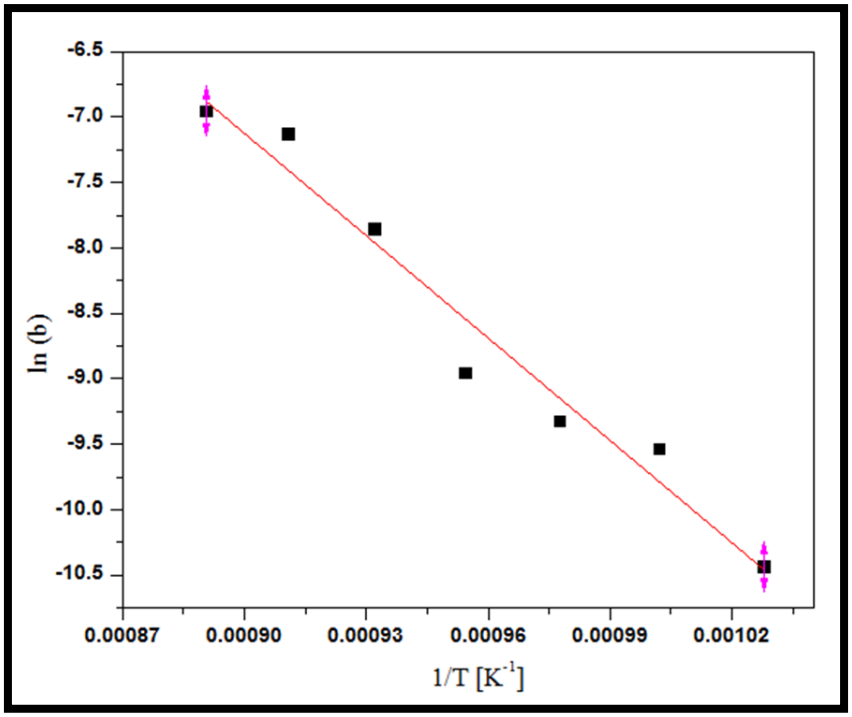

Fig. 4.7 Plot of $ln(b)$ vs. $1/T$

4.5 Kinetics of Austenite Formation

In the present work, dual phase microstructure comprising of ferrite and martensite phases was to be investigated. As discussed in Section 4.3.2, the JMat-Pro data revealed that for annealing temperatures of less than 775 ℃, austenite was not formed in an appreciable amount (Table 4.1). Thus, annealing experiments were not conducted for such temperatures (T< 775 ℃) because they would not form martensite in an appreciable amount because of lack of austenite available in them at the annealing temperature. So, the annealing experiments for the study of austenite formation kinetics were conducted at higher temperatures, in the range of 775–850 ℃ followed by water quenching (so that required amount of austenite and hence martensite could be obtained). It was observed during the annealing experiments that martensite did not form in the quenched samples which were soaked for short holding times at a given annealing temperature. This was because of the reason that for austenite formation to begin during the annealing cycle, there is a certain amount of holding time required at the inter-critical annealing temperature for processes viz. recovery, recrystallization, pearlite dissolution etc. followed by austenite formation and stabilization. For a relatively lower annealing temperature of 775 ℃, it was observed that with increase in holding time, austenite phase started getting stabilized. Martensite phase was observed in the annealed samples only after an initial holding of 3 min at 775 ℃. SEM

images were recorded for recognizing the fine martensite obtained from austenite. Figure 4.8 presents the SEM micrographs showing fine martensite phase produced (along grain boundaries in the ferrite matrix) in the samples annealed at 775 ℃ with 3 min holding.

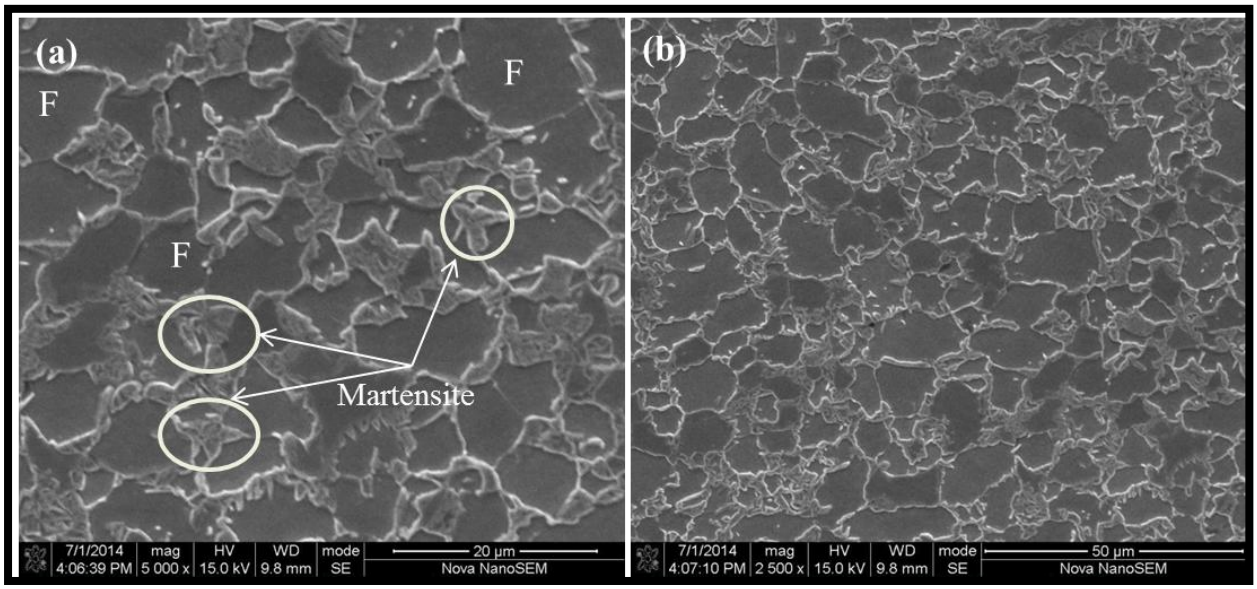

Fig. 4.8 SEM micrographs of sample annealed at 775 ℃ for 3 min showing martensite along grain boundaries. F = ferrite

Microhardness tests were done to verify the presence of martensite and ferrite phases in the annealed samples. For this, first the hardness of individual phases of ferrite and martensite was determined. Microhardness of ferrite phase was already determined in Section 4.4.1 during the recrystallization studies. For determining the microhardness of martensite phase, a reference was prepared by annealing at 900 ℃ with 6 min holding followed by water quenching to obtain a fully martensitic microstructure. Figure 4.9 (a–b) show the optical micrographs of steel containing fully ferritic and fully martensitic microstructures respectively. Microhardness measurements of these samples determined the average microhardness of ferrite and martensite phases as 150 Hv and 405 Hv respectively. Now, microhardness measurements were made for the sample annealed at 775 ℃ with 3 min holding for measuring the hardness of primary (ferrite) phase and secondary (martensite) phase. Hardness results showed that the hardness of the primary phase (i.e. ferrite) was about 150–225 Hv and that of the fine secondary phase (i.e. martensite) along the grain boundaries was 375–425 Hv. These results confirmed the presence of martensite phase in the ferritic matrix.

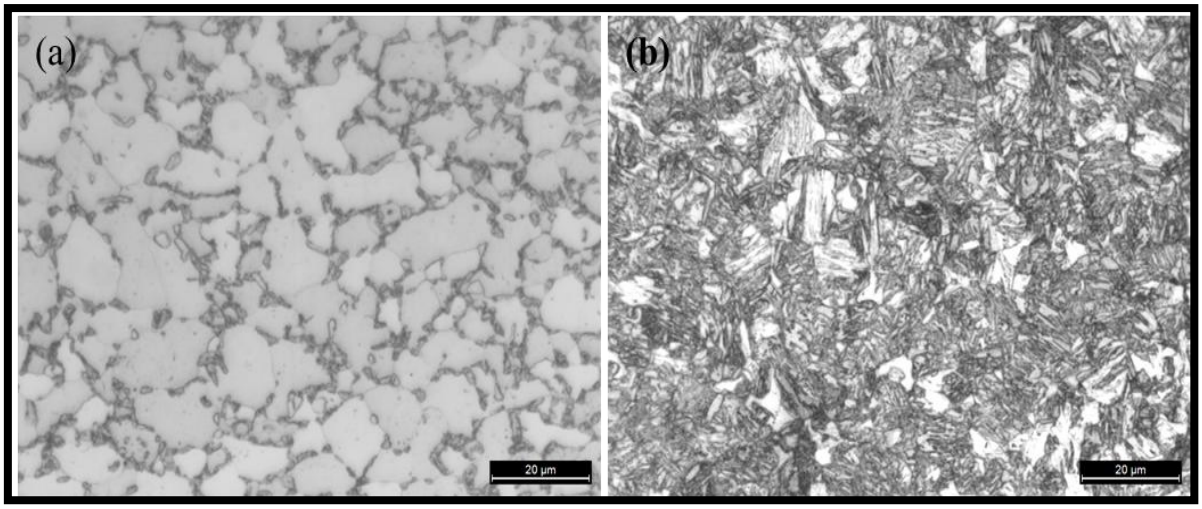

Fig. 4.9 Optical micrographs of steel containing (a) fully ferritic and (b) fully martensitic microstructures

After confirming the presence of martensite phase in the annealed steel, the next step was to compare the austenite fraction (at a given annealing temperature) obtained through actual annealing experiments with the amount predicted by JMat-Pro software. The austenite amount was determined from martensite fraction present in the room temperature microstructure after annealing under given conditions. It was observed that volume fraction of martensite formed (and hence the austenite volume fraction) was lesser actually than what was predicted by JMat-Pro. This difference exists because the phase fraction values predicted through JMat-Pro and Thermo-Calc are based on the equilibrium conditions i.e. extremely slow rates of heating etc. Further, these software take no consideration of the holding time a given temperature during the annealing process. However, during the experimental work, time was an important parameter. The samples were soaked isothermally at the annealing temperature and the rate of heating was much higher (than equilibrium rates) as samples were directly placed in the muffle furnace which was already maintained at a high inter-critical temperature. Also, the software do not include the effect of parameters like the initial microstructure of the steel to be annealed, the time needed for uniform heating of specimens (especially with thicker sections), heating rates etc. For example, for the first sample annealed at 775 ℃ for 3 min soaking time, annealing experiment revealed martensite (and hence austenite fraction) as 33.19% (Table 4.3).whereas JMat-Pro predicted austenite fraction as 38.28% under the same annealing conditions. This revealed that for obtaining the same austenite fraction (as is predicted by JMat-Pro) under actual experimental annealing conditions, larger soaking time periods, or higher annealing temperatures, or both are required.

The annealing experiments were now performed at each annealing temperature with relatively larger holding periods in excess of 3 min. Thus, the annealing of samples was conducted at 775, 800, 825, and 850 ℃ for holding time periods of 3, 4, and 5 min respectively. Table 4.3 presents the austenite volume fraction obtained (through Image J software) under various annealing conditions and also through JMat-Pro predictions. The results of annealing experiments were recorded as optical micrographs and are presented in Table 4.4.

Table 4.3 Austenite fraction obtained under various annealing conditions and JMat-Pro predictions

Temp. (℃)	Holding Time			JMat-Pro
	3 min	4 min	5 min	
775	33.19	35.94	37.71	38.28
800	37.57	39.65	42.60	55.40
825	44.42	47.13	54.21	81.22
850	55.28	63.09	67.43	100

Figure 4.10 presents the martensite fraction-temperature plots showing martensite (and hence austenite fraction) obtained after annealing at a given annealing temperature with different soaking periods. It can be noted from the plots that with increase in annealing temperature, or holding time, or both, the fraction of austenite formed in the steel increases. Further, the plots also show that an adequate amount of martensite is formed in the steel for annealing temperatures in the range 775 – 800 ℃ with time periods in the range 3–5 min. One of the objectives of the present work was to obtain a dual phase microstructure with martensite fraction in the range of 40–50% providing a good combination of strength and ductility. As reported in literature, the maximum martensite content in DP steels lies in the above mentioned range only. Obtaining this range of martensite in dual phase microstructure, the ultimate tensile strength of 1000 MPa with total elongation of about 10 % can be obtained [Zhao et al. 2009; Wang and Wei, 2013; Krajewski and Nowacki, 2014]. Such steels are used in the automotive industry.

Table 4.4 Optical micrographs for austenite fraction under various annealing conditions

Time (min) / Temp. (℃)	3	4	5
775	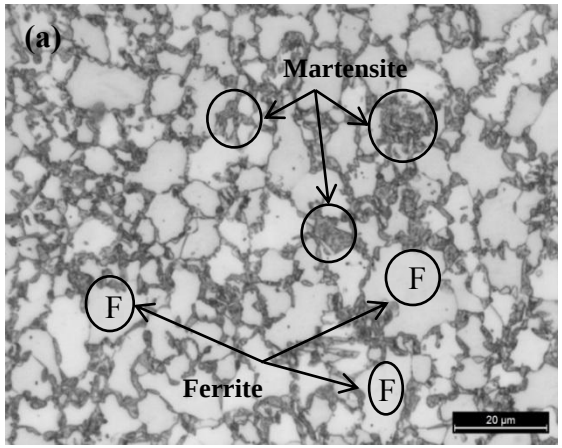	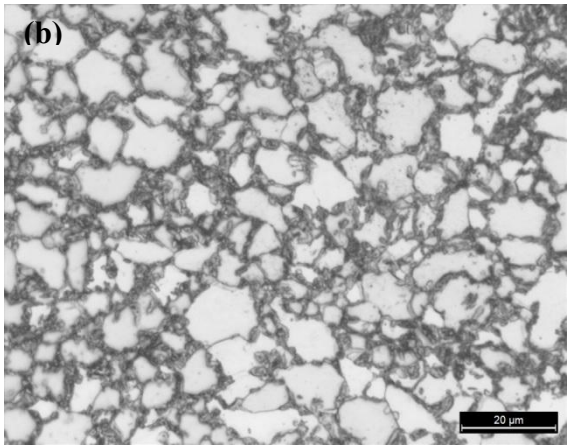	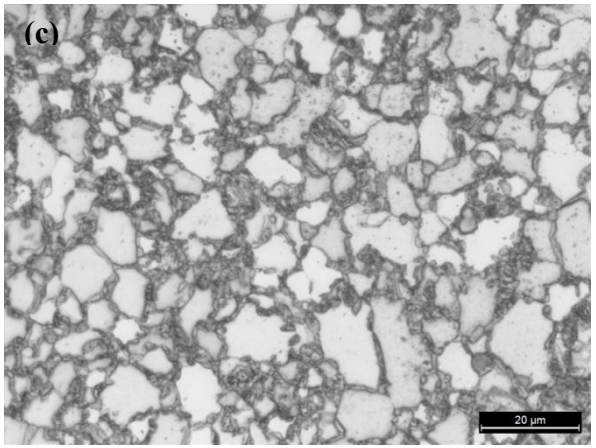
800	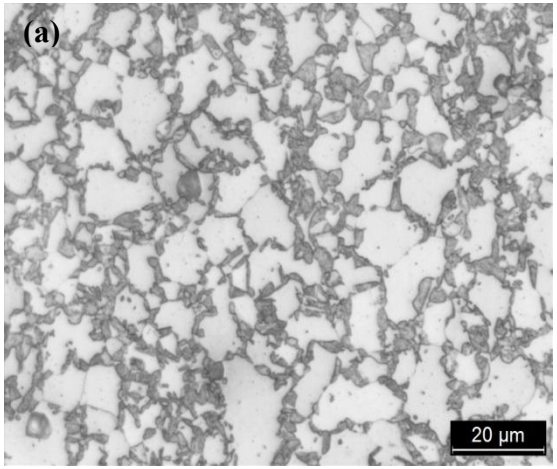	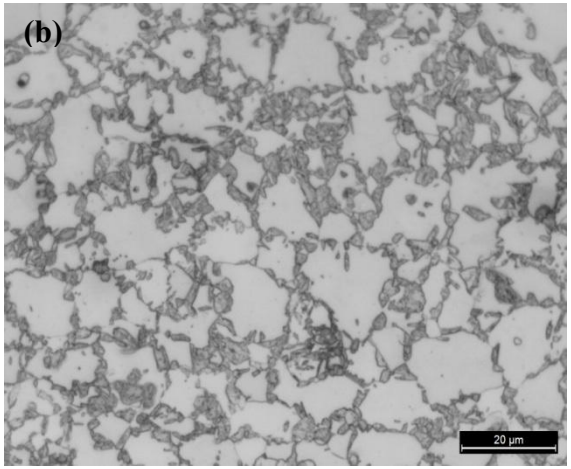	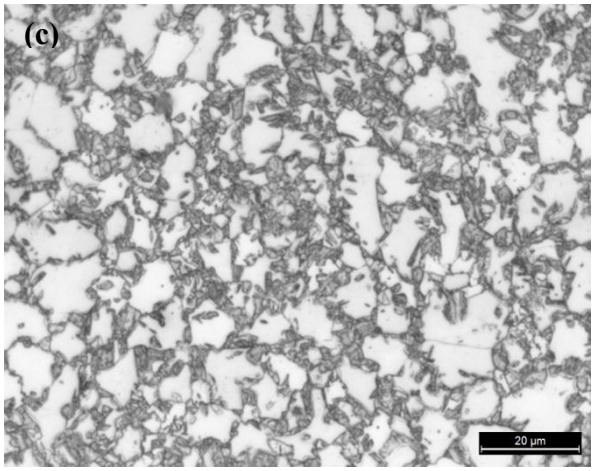

Time (min) / Temp. (℃)	3	4	5
825	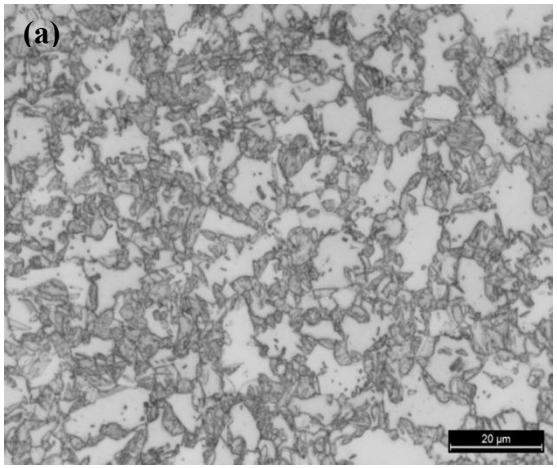	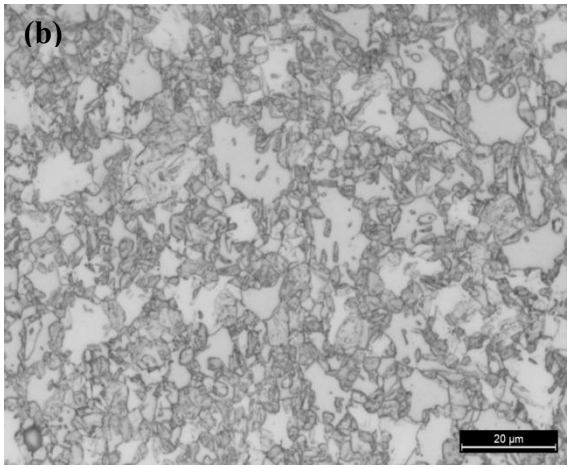	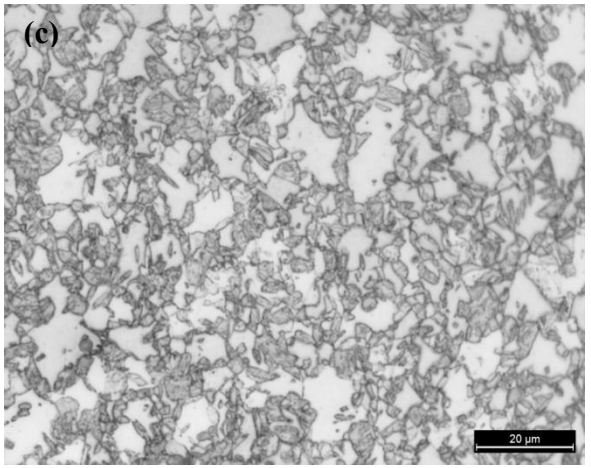
850	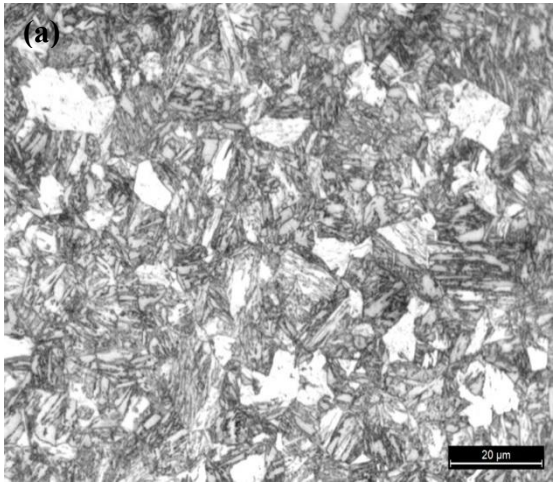	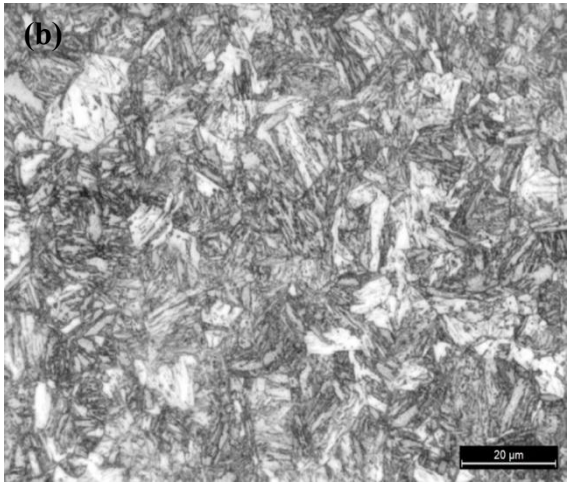	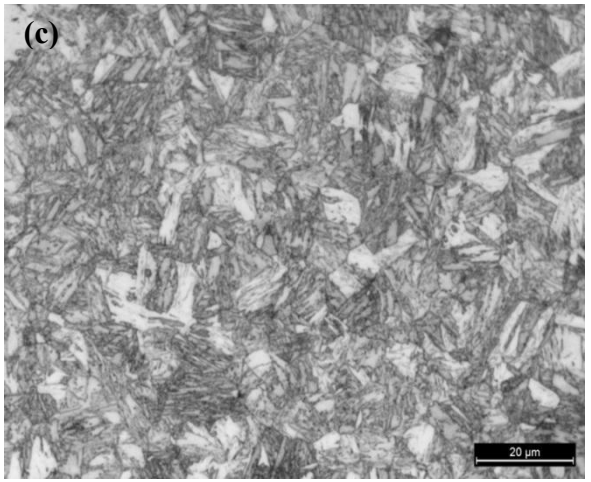

In the light of aforesaid, the annealing temperature-time combination which obtained martensite in this range (40–50%) with a reasonable holding time was to be selected. It was observed from Fig. 4.10 that this requirement was best met with an annealing temperature of 825 ℃ with a holding time of 3 min. Though, the annealing temperature of 800 ℃ was also resulting in the desired microstructure containing required fraction of martensite (40–50%) but with comparatively very large holding time of 6 min. At a higher temperature of 850 ℃, the amount of martensite formed in the dual phase structure was not meeting the requirement of desired fractions of ferrite and martensite phases. Martensite fraction obtained at 850 ℃ was higher (55–68%) than the required range (40–50%). Hence, the optimum annealing conditions selected in the present work comprised of 3 min holding at an annealing temperature of 825 ℃ which yielded a dual phase ferrite-martensite microstructure with martensite volume fraction in the range (40–50%).

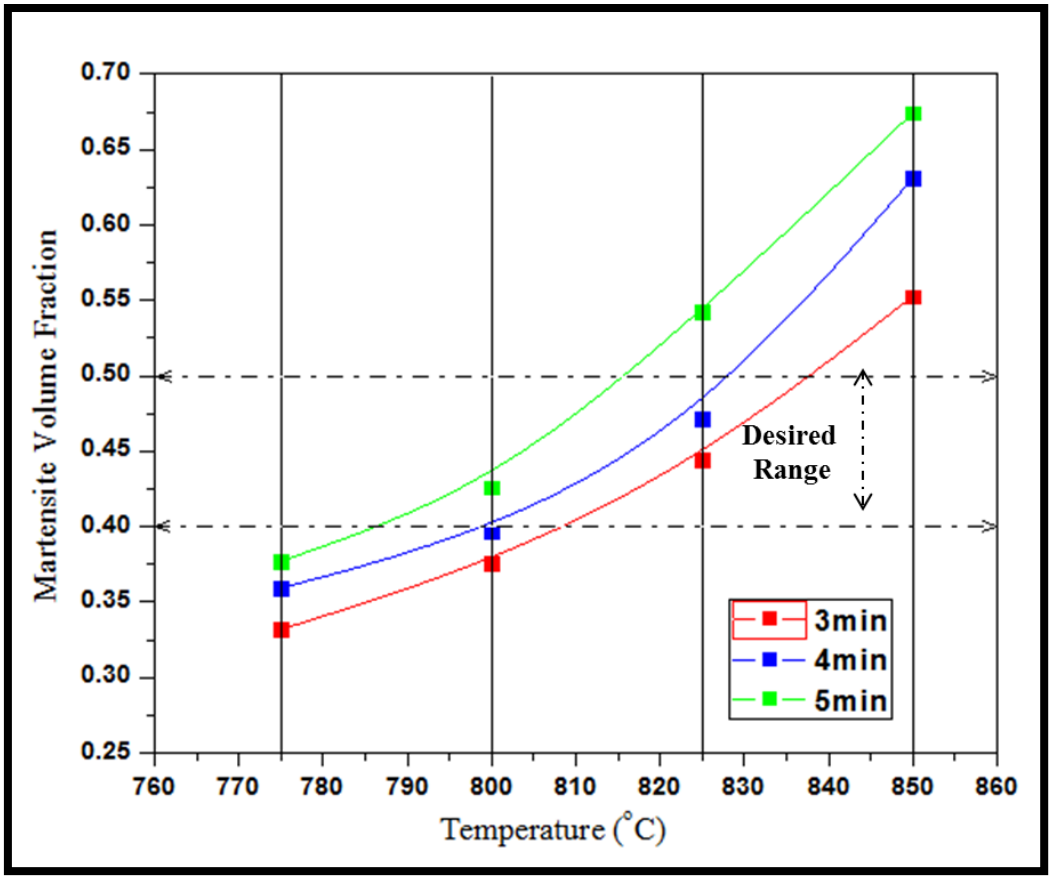

Fig. 4.10 Martensite volume fraction obtained at a given annealing temperature with different soaking periods

4.6 Annealing under Optimum Conditions in the Simulator

As discussed in section 4.5, the annealing parameters selected for the given steel were 825 ℃ as the annealing temperature with 3 min of holding. Dog-bone shaped tensile specimen was prepared and was annealed under the selected conditions in the annealing simulator. The tensile specimen is shown in Fig. 4.11 (a–b).

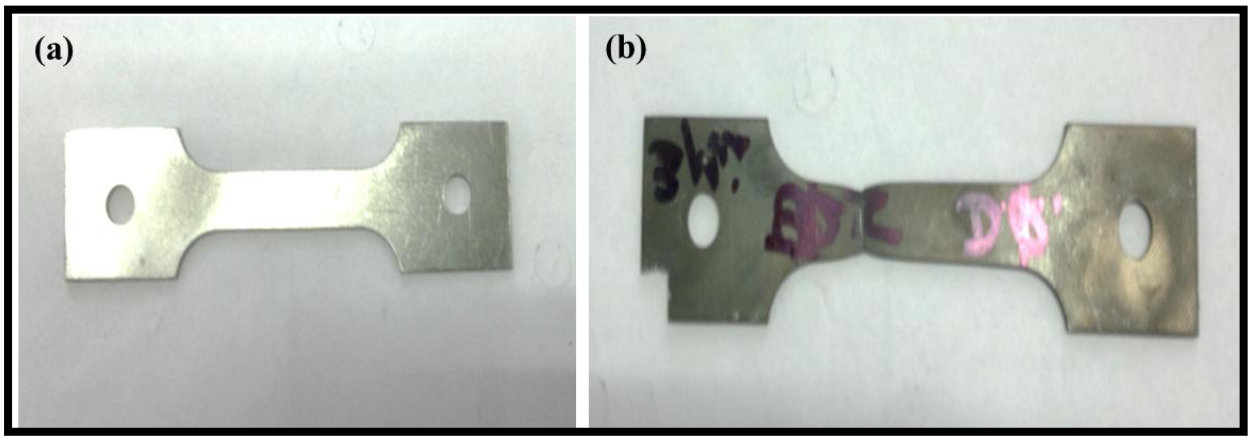

Fig. 4.11 Tensile specimen (a) before annealing (b) after annealing and tensile testing

Annealing was done in the simulator in order to realize the conditions in which steels are actually annealed for industrial applications. Thus, direct water quenching was avoided here because of its adverse effects viz. distortion and failure due to cracking due to the severe water quench. In the simulator, the specimen was heated and soaked under a controlled environment using inert gases in order to avoid oxidation of the sample. Cooling was achieved in the annealing chamber through a mixture of hydrogen and nitrogen gases (H_2+N_2 gas mixture). Further, to achieve, maximum cooling rates, N_2 assisted water spray and atomized air were also utilized. The maximum cooling rate achieved in the simulator was about 60 ℃ /s. Figure 4.12 shows the cooling curve for the specimen annealed at 825℃ with 3 min holding. The curve represents the cooling of specimen in the simulator from the intercritical temperature down to the room temperature. The slope of this curve (obtained through OriginPro 8.0 software) gave the value of cooling rate achieved as 60 ℃/ s.

After the annealing experiment, optical microscopy of the sample was done to obtain the volume fraction of constituent phases present in the annealed steel. The optical micrographs revealed the presence of ferrite and martensite phases with volume fraction of martensite (determined through Image J) as 35 %.

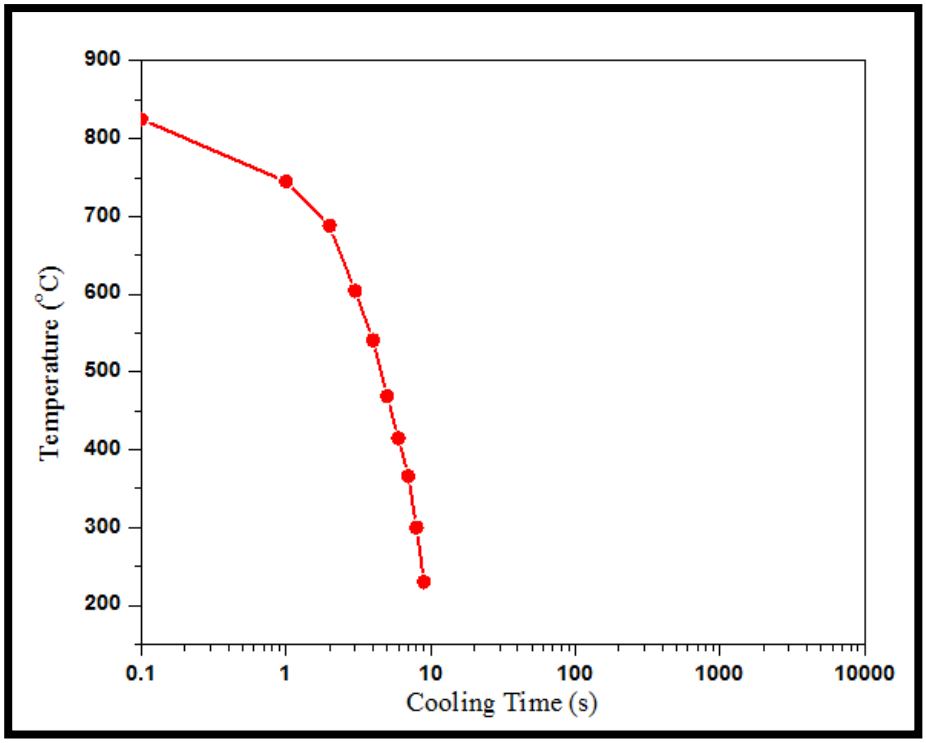

Fig. 4.12 Cooling curve for sample annealed in the simulator

The volume fraction of martensite obtained by annealing in the simulator (35 %) was less as compared to what was obtained (44.43 %; Fig. 4.10) by annealing under same conditions in muffle furnace followed by water quenching. Figure 4.13 (a–b) shows the optical micrographs of the steel annealed (at 825 ℃, 3 min) in annealing simulator and muffle furnace respectively. Figure 4.13b represents a typical necklace type martensitic structure obtained because of the severe water quench.

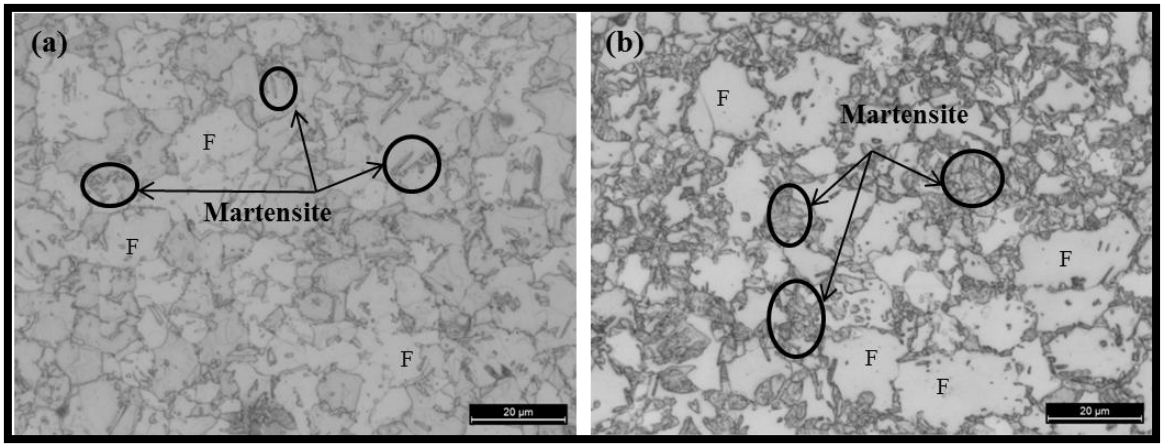

Fig. 4.13 Optical micrographs of the specimen annealed at 825 ℃, 3 min holding (a) annealing simulator (b) muffle furnace. F = ferrite

There was difference in the martensite fraction obtained in the two cases (cooling in annealing simulator and water quenching) because of the different cooling rates achieved. The cooling rate achieved in the simulator (60 ℃/s) was lower than the rate followed during water quenching. Because of the slower cooling in the simulator, the entire austenite phase present at the intercritical annealing temperature of 825 ℃ (with 3 min holding) did not transform solely into martensite and some fraction of austenite transformed to ferrite.

4.7 Tensile Property Evaluation

Tensile tests were performed in order to evaluate the tensile properties of the as-received cold rolled steel and the sample annealed in the simulator under the selected time-temperature conditions. Figure 4.18 shows the stress-strain curves for the as-received and the annealed sample (Appendix IV).

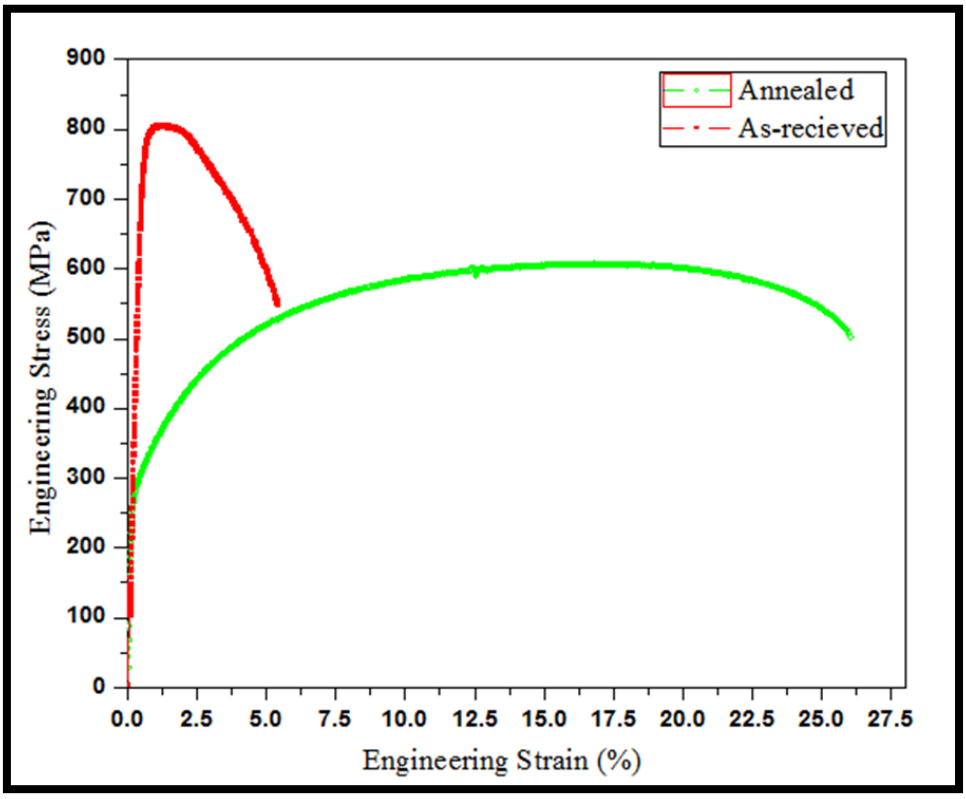

Fig. 4.14 Stress-strain curves for the as-received and annealed steel

From the above stress-strain curves, it can be seen that the tensile properties of the as-received steel changed considerably after the annealing process. As expected, the as-received cold rolled steel showed high ultimate tensile strength (~810 MPa) with a very low total elongation (~5.3%) because of the cold deformation effect. However, the annealed specimen

showed high total elongation (~26%) with a moderate ultimate strength (~610 MPa). The 0.2 % offset yield strength for annealed sample was calculated to be (~300 MPa). Hence, the YS/ UTS ratio was found to be about 0.5. Thus, with suitable heat treatment, the as-received steel with poor ductility was transformed to steel with good combination of strength and ductility. This clearly shows the effect of microstructure on the mechanical properties of steel. The as-received cold rolled steel initially contained deformed ferrite/pearlite microstructure. After annealing, the microstructure of the annealed specimen consisted of recrystallized ferrite grains with fine martensite phase. This type of microstructure resulted in good combination of strength and ductility which is a desired property for dual phase steels.

4.8 Summary of the Chapter

In this chapter of thesis, the results of various experimental studies have been presented. Various optical and SEM micrographs of the as-received as well as annealed steels have been given and discussed. The chapter also includes the calculations regarding recrystallization kinetics and austenite formation kinetics. In the last section, the results of tensile testing of the as-received steel and the annealed steel under selected conditions have been discussed.

Chapter 5

Conclusions

5.1 Introduction

As the need of improving the fuel efficiency and safety in the automobile industry is growing, the demand for advanced high strength steels is increasing. Dual-Phase steels are most common and demanding steel grades in this category as these can be produced very easily by annealing a low-carbon steel in the inter-critical region followed by fast cooling to produce the ferrite-martensite microstructure. Final mechanical properties of DP steel depend upon the volume fraction, morphology and distribution of martensite phase which in turn is influenced by the inter-critical annealing parameters viz. annealing temperature, soaking time and cooling rate etc. As far as industry is concerned, continuous annealing is more preferred because of short processing times and more uniform mechanical properties. The present study is an effort to study the effect of inter-critical parameters on the ferrite recrystallization and austenite formation and stabilization during the production of a dual phase steel.

5.2 Results and Conclusions

The main results and conclusions from the present experimental work are as follows:

As-received material

- The microstructure of the as-received low carbon cold rolled steel featured deformed ferrite grains and destructed pearlite colonies that were distributed non-uniformly in the ferrite matrix. This microstructure (due to different size and shape of the pearlite colonies) required larger soaking periods (for dissolution of pearlite colonies) leading to delay in formation and homogenization of austenite formed.

Recrystallization of ferrite during inter-critical annealing process

- During annealing, the recrystallization of deformed ferrite grains was a significant event. The general rule is that recrystallization of ferrite grains gets completed before the sample reaches the inter-critical region under equilibrium conditions. However, in the present study, the ferrite recrystallization was delayed to above Ac_1 because the rate of heating was much higher than equilibrium rates.

- During the early stages of annealing (i.e. 0–30 s), especially at lower annealing temperatures, ferrite phase did not recrystallize in any significant amount. This time was referred to as time required for the recovery stage of the annealing process.
- At lower annealing temperatures (i.e. below 775 ℃), the rate of recrystallization was slow which resulted in longer time periods for full recrystallization of ferrite. For temperature of 700 ℃, it took 3 minutes for full recrystallization. As the temperature increased, the time needed for full recrystallization of ferrite decreased. At higher temperatures (i.e. 775 ℃ and above) the rate of recrystallization became very fast and recrystallization of ferrite completed almost within 90 s.

Austenite formation and stabilization

- Austenite formed and stabilized after the isothermal soaking time of 3 min at the intercritical temperature of 775 ℃ in the muffle furnace. However, the amount of austenite formed was lesser than what was predicted through JMat-Pro. This difference was attributed to the different heating rates under the two conditions.
- With increase in annealing temperature, or holding time, or both, the fraction of austenite formed in the steel increased. The appropriate amount of austenite (40–50 %) was obtained at temperatures of 800 ℃ and 825 ℃ with soaking time periods of 5 min and 3 min respectively.

Annealing under optimum conditions in the simulator

- Under the optimum conditions (i.e. 3 min soaking at 825 ℃) in the annealing simulator, dual-phase microstructure with martensite fraction of 35 % was obtained. The martensite fraction obtained was lesser than what was obtained through water quenching. The cooling rate achieved in the simulator was 60 ℃/ s which was less than the cooling achieved through water quenching. This difference in the cooling rate led to formation of lesser martensite in the annealing simulator. Hence, for the industrial production of DP steel, if it is not possible to achieve high cooling rates, then annealing can be done at higher annealing temperatures with longer soaking time periods for producing required amount of martensite.
- Microstructure of the steel annealed in the simulator consisted of fine martensite phase dispersed in the recrystallized ferrite matrix. However, water quenching led to a typical

necklace type microstructure, in which martensite was observed on the ferrite grain boundaries.

Tensile Properties

- Due to the effect of cold rolling, the as-received steel showed a high ultimate tensile strength of 810 MPa with a low total elongation of 5.3 %. However, the sample annealed under the optimum conditions in the simulator (having 35 % martensite) showed high total elongation of 26.5 % with a moderate ultimate strength of 610 MPa. Increased ductility was obtained by transforming deformed ferrite grains to recrystallized ferrite grains. However, the strength did not reduce drastically because of the formation of martensite phase in the ferrite matrix. Thus, by obtaining an appropriate microstructure through the selection of inter-critical annealing parameters, a good combination of strength and ductility was obtained in the given low carbon steel.

5.3 Major Conclusions and Recommendations

- Inter-critical annealing parameters clearly affect the phenomenon of ferrite recrystallization, and austenite formation and its stabilization during the production of dual phase steel from low carbon steel. The parameters like annealing temperature, soaking time, and heating rate affect the rate of recrystallization, time needed for full recrystallization of ferrite and formation and stabilization of austenite phase. At lower annealing temperatures, it takes longer time for full recrystallization of ferrite after which the formation of austenite starts. At higher temperatures, it takes very short time to complete the full recrystallization of ferrite and formation of austenite starts simultaneously along the process ferrite recrystallization.
- There were variations in the annealing results obtained through annealing experiments and those obtained through software predictions. The variations are attributed to the reason that software predictions are made on the assumption of equilibrium heating which is seldom followed during actual industrial heating. Further, the software does not take into account the effect of holding time, heating rates, initial microstructure of the steel etc.
- The cooling rate affects the volume fraction of martensite obtained during the cooling of the sample. Water quenching offers a very high cooling rate through which the entire austenite formed during the annealing can be transformed to martensite. With cooling

through annealing simulator the cooling rate achieved was lesser (60 ℃/ s) which yielded further drop in the volume fraction of martensite obtained in the microstructure.

- There is a clear evidence of the effect of microstructure on the tensile properties. DP steel containing fine martensite in the ferrite matrix yielded good combination of strength and ductility and a YS/ UTS ratio, typically in the range reported for DP steels (~0.5). However, the as-received cold rolled steel yielded high strength but with very poor total elongation.
- The present study demonstrates a simple approach that can be followed in order to find the optimum combination of annealing parameters to produce dual phase structure in low carbon cold rolled steel. The study does not include the use of expensive and sophisticated equipment like Gleeble Simulator etc. to study the effect of annealing parameters on the recrystallization kinetics, austenite formation and stabilization. Hence, the procedure and results presented in the present experimental work clearly define a systematic approach for the industrial sector to analyze and select the appropriate annealing parameters for the production of dual phase steels.

5.4 Scope of Future Work

In the present work, the effect of intercritical parameters viz. annealing temperature and holding time on the ferrite recrystallization and austenite formation and stabilization have been discussed. However, the effect of different heating rates on the recrystallization kinetics of ferrite and the kinetics of austenite formation has not been discussed in the present study. Heating rate is also an important factor that affects these two phenomena comprehensively. Further, in this study water quenching was used for the cooling of samples and the cooling rate achieved through simulator was not enough to transform the whole austenite into the martensite. Hence, further work can be done by considering high cooling rates in the simulator. The effect of martensite morphology on the properties was also not studied which can be done further using specialized equipment like SEM and EBSD. Further, studies can also be done to include tailoring of the microstructure consisting of different volume fractions of martensite, bainite and retained austenite through varied cooling routes to obtain different properties.

References

- Adamczyk, J., Grajcar, A. (2006), 'Effect of heat treatment conditions on the structure and mechanical properties of DP-type steel', *Journal of Achievements in Materials and Manufacturing Engineering*, Vol. *17*, pp. 305–308.
- Ahmad, E., Manzoor, T., Hussain, N., Qazi, N.K. (2008), 'Effect of thermomechanical processing on hardenability and tensile fracture of dual-phase steel', *Materials and Design*, Vol. *29*, pp. 450–457.
- Bhattacharya, D. 'Developments in advanced high strength steels', presented at *Advanced High Strength Steel Workshop, Arlington, Virginia, USA*, 22–23 October, 2006.
- Cai, X., Liu, C., and Liu, Z. (2014), 'Process design and prediction of mechanical properties of dual phase steels with prepositional ultra fast cooling', *Material and Design*, Vol. *53*, pp. 998–1004.
- Calcagnotto, M., Ponge, D., and Rabbe, D. (2010), 'Effect of grain refinement to 1 μm on strength and toughness of dual-phase steels', *Materials Science and Engineering A*, Vol. *527*, pp. 7832–7840.
- Cornet, X. and Herman, J. C. 'Method for making a multiphase hot-rolled steel strip', *U.S. Patent 0041933 A1*, March 6, 2003.
- Dziedzic, M. and Turczyn, S. (2010), 'Experimental and numerical investigation of strip rolling from dual phase steel', *Archives of Civil and Mechanical Engineering*, Vol. *10*, pp. 21–30.
- Homberg, D., Krumbiegel, K. and Togobytska, N. 'Modelling, simulation and control of multiphase steel production', presented at *19th International Congress on Modelling and Simulation, Perth, Australia*, 12–16 December, 2011.
- Huang, J., Poole, W. J., Militzer, M. (2004) 'Austenite formation during intercritical annealing', *Metallurgical and Materials Transactions A*, Vol. *35(A)*, pp. 3363–3375.
- Kalu, P. N., Waryoba, D. R. (2007), 'A JMAK-microhardness model for qualifying the kinetics restoration mechanisms in inhomogeneous microstructure', *Materials Science and Engineering A*, Vol. *464*, pp. 68–75.

- Krajewski, S., Nowacki, J. (2014), 'Dual-phase steels microstructure and property consideration based on artificial techniques', *Archives of Civil and Mechanical Engineering*, Vol. *14*, pp. 278-286.
- Kang, Y. L., Han, Q. H., Zhao, X. M. and Cai, M. H. (2013), 'Influence of nanoparticle reinforcement on the strengthening mechanism of an ultrafine-grained dual phase steels containing titanium', *Materials and Design*, Vol. *44*, pp. 331–339.
- Kumar, A., Singh, S. B. and Ray, K. K. (2008), 'Influence of bainite/martensite-content on the tensile properties of low carbon dual-phase steels', *Materials Science and Engineering A*, Vol. *474*, pp. 270–282.
- Kuziak, R., Kawalla, R. and Waengler, S. (2008), 'Advanced high strength steels for automotive industry', *Archives of Civil and Mechanical Engineering*, Vol. *8*, pp. 103–117.
- Kwon, O., Lee, K., Kim, G. and Chin, K. G. (2010), 'New trends in advanced high strength steel developments for automotive applications', *Materials Science Forum*, Vol. *638–642*, pp. 136–141.
- Li, P., Li, J., Meng, Q., Hu, W.; Xu, D. (2013) 'Effect of heating rate on ferrite recrystallization and austenite formation of cold-roll dual phase steel', *Journal of Alloys and Compounds*, Vol. *578*, pp. 320–327.
- Martis, C. J., Putatunda, S. K. and Boileau, J. (2013), 'Processing of a new high strength high toughness steel with duplex microstructure (Ferrite + Austenite)', *Materials and Design*, Vol. *46*, pp. 168–174.
- Matlock, D. K., Speer, J. G., Moor, E. D. and Gibbs, P. J. (2012), 'Recent developments in advanced high strength sheet steels for automotive applications: an overview', *JESTECH*, Vol. *15(1)*, pp. 1–12.
- Meng, Q., Li, J., Zheng, H. (2014), 'High-efficiency fast-heating annealing of a cold-rolled dual-phase steel', *Materials and Design*, Vol. *58*, pp. 194-197.
- Nadlene, R., Esah, H., Norliana, S., Irwan, M. A. M. (2011), 'Study on the effect of volume fraction of dual phase steel to corrosion behaviour and hardness', *World Academy of Science, Engineering and Technology*, Vol. *5*, pp. 501–504.
- Nie, W.J., Wang, X. M., Wu, S. J., Guan, H. L. and Shang, C. J. (2012), 'Stess-strain behaviour of multi-phase high performance structural steel', *Science China Technological Sciences*, Vol. *55*, pp. 1791–1796.

- Park, K. S., Park, K. T., Lee, D. L. and Lee, S. L. (2007), 'Effect of heat treatment path on the cold formability of drawn dual-phase steels', *Materials Science and Engineering A*, Vol. *449–451*, pp. 1135–1138.
- Prahl, U., Papaefthymiou, S., Uthaisangsuk, V., Bleck, W., Sietma, J. and Zwaag, S. V. D. (2007), 'Micromechanics-based modelling of properties and failure of multiphase steels', *Computational Materials Science*, Vol. *39*, pp. 17-22.
- Saleh, M. H. and Priestner, R. (2001), 'Retained austenite in dual-phase silicon steels and its effects on mechanical properties', *Journal of Materials Processing Technology*, Vol. *113*, pp. 587–593.
- Sayed, A. A. and Kheirandish, S. (2012), 'Affect of tempering temperature on the microstructure and mechanical properties of dual phase steels', *Materials Science and Engineering A*, Vol. *532*, pp. 21–25.
- Souza, M. M., Guimaraes, J. R. C., Chawla, K. K. (1982) 'Intercritical austenitization of two Fe-Mn-C steels', *Metallurgical Transactions A*, Vol. *13(A)*, pp. 575–579.
- Tan, W., Han, B., Wang, S. H., Yang, Y., Zhang, C. and Zhang Y. K. (2012), 'Effects of TMCP parameters on microstructure and mechanical properties of hot rolled economical dual phase steel in CSP', *Journal of Iron and Steel Research, International*, Vol. *19(6)*, pp. 37–41.
- Tian, Y., Tang, S., Wang, B. X., Wang, Z. D. and Wang G. D. (2012) 'Development and industrial application of ultra-fast cooling technology', *Science China Technological Sciences*, Vol. *55*, pp. 1566–1571.
- Wang, W. and Wei, X. (2013), 'The effect of martensite volume and distribution on shear fracture propagation of 600–1000 MPa dual phase steels in the process of deep drawing', *International Journal of Mechanical Sciences*, Vol. *67*, pp. 100–107.
- Xue, P., Xiao, B. L., Wang, W. G., Zhang, Q., Wang, D., Wang, Q. Z., Ma, Z. Y. (2013) 'Achieving ultrafine dual-phase structure with superior mechanical property in friction stir processed plain low carbon steel', *Materials Science and Engineering A*, Vol. *575*, pp. 30–34.
- Zhao, Z. Z., Jin, G. C., Niu, F., Tang, D., Zhao, A. M. (2009) 'Microstructure evolution and mechanical properties 1000 MPa cold rolled dual-phase steel', *Transaction of Nonferrous Metals Society of China*, Vol. *19*, pp. 563–568.

Appendix I

Microhardness and Recrystallization Ferrite Fraction data under various Annealing Conditions

Annealing Temp. (℃)	Time (s)	Hardness Values (Hv)	Average Hardness	Recrystallized Fraction
700	30	274, 276, 274, 284, 262, 282, 265, 270, 278, 271	274	0.08
700	60	271, 257, 276, 279, 264, 264, 265, 276, 269, 270	269	0.11
700	90	255, 240, 245, 240, 253, 241, 257, 237, 242, 253	246	0.28
700	120	160, 164, 168, 160, 168, 164, 160, 166, 164, 165	164	0.89
700	150	160, 150, 164, 151, 164, 150, 153, 164, 152, 152	156	0.95
700	180	152, 152, 151, 151, 154, 150, 140, 159, 153, 160	152	0.98
725	30	264, 289, 270, 274, 264, 276, 271, 255, 270, 271	270	0.10
725	60	287, 266, 267, 267, 267, 257, 271, 260, 269, 257	267	0.13
725	90	166, 169, 167, 180, 168, 163, 166, 185, 170, 166	170	0.85
725	120	150, 152, 151, 152, 157, 155, 149, 151, 152, 151	152	0.98
725	150	156, 152, 153, 154, 157, 152, 149, 145, 143, 144	150	0.99
750	30	271, 262, 260, 259, 255, 255, 255, 257, 265, 253	259	0.18
750	60	260, 249, 244, 245, 245, 245, 250, 245, 247, 245	247	0.27
750	90	163, 164, 165, 167, 160, 170, 160, 158, 157, 165	163	0.90
750	120	155, 155, 153, 165, 154, 162, 136, 158, 152, 145	153	0.97
775	30	260, 270, 260, 255, 257, 252, 254, 251, 246, 251	256	0.21
775	60	229, 227, 225, 228, 234, 231, 240, 209, 216, 235	227	0.42
775	90	143, 160, 155, 154, 152, 149, 161, 157, 156, 158	155	0.96
775	120	155, 150, 153, 154, 152, 151, 157, 149, 159, 151	153	0.97
800	30	259, 265, 268, 249, 254, 262, 251, 246, 255, 257	256	0.20

800	60	166, 183, 178, 166, 171, 176, 181, 174, 183, 175	175	0.81
800	90	159, 149, 152, 163, 155, 148, 153, 155, 152, 156	154	0.96
800	120	158, 159, 151, 149, 147, 155, 157, 142, 153, 145	152	0.99
825	30	251, 258, 252, 259, 258, 257, 253, 260, 255, 257	256	0.21
825	60	168, 166, 164, 162, 165, 167, 163, 170, 161, 160	167	0.88
825	90	151, 153, 150, 149, 153, 147, 149, 145, 151, 154	150	0.99
850	30	260, 245, 260, 257, 255, 257, 241, 247, 243, 254	252	0.24
850	60	159, 179, 165, 166, 163, 157, 165, 170, 169, 162	166	0.89
850	90	149, 153, 151, 145, 157, 150, 143, 153, 149, 151	150	0.99

Appendix II

Optical Micrographs for the Recrystallization Studies

Annealing Temperature - 700 ℃

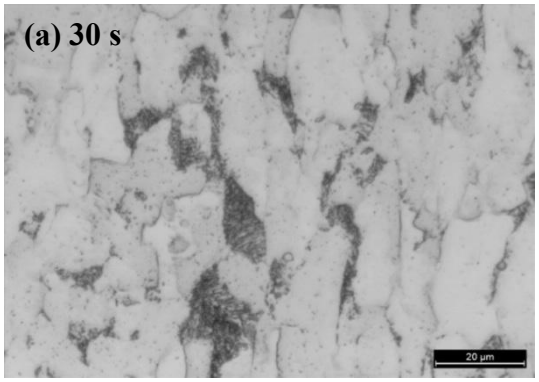

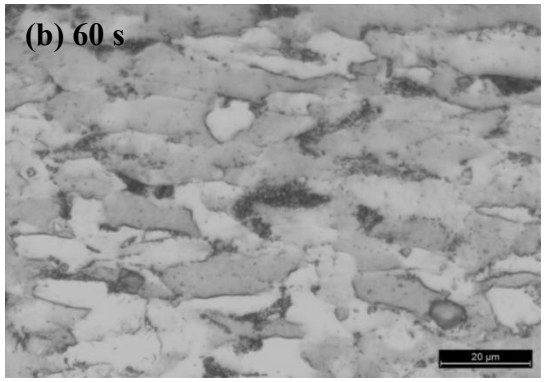

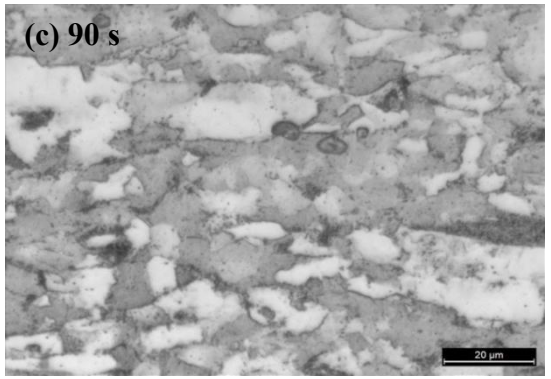

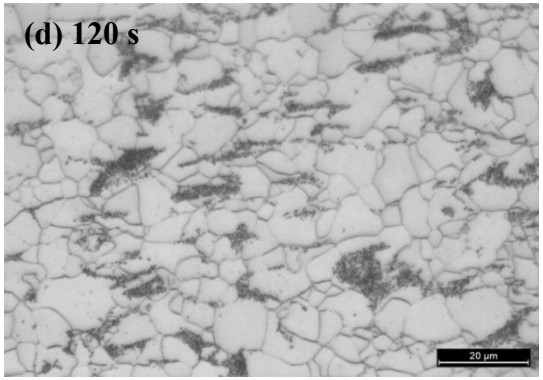

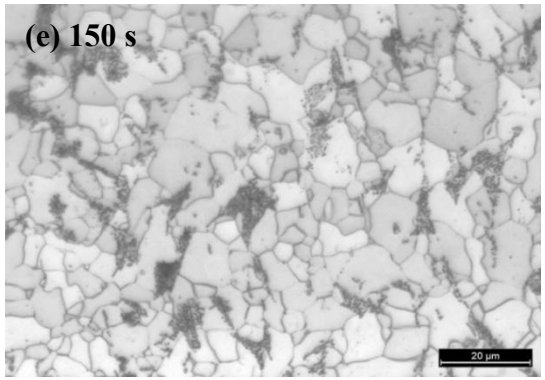

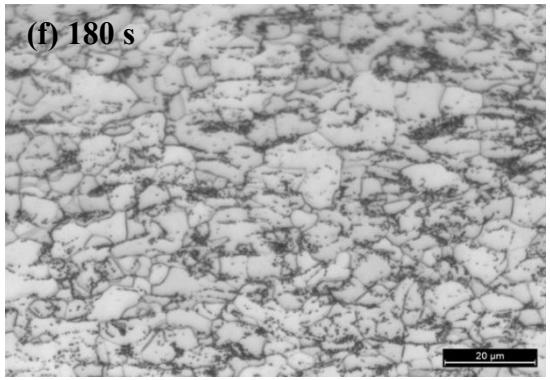

Annealing Temperature - 725 ℃

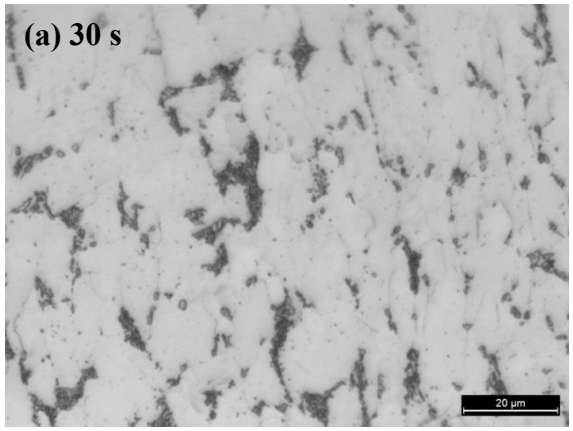

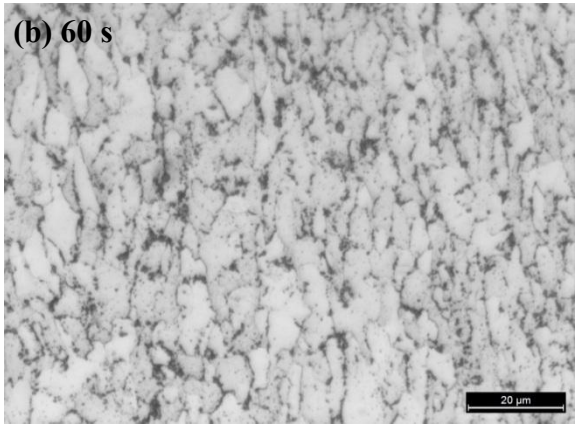

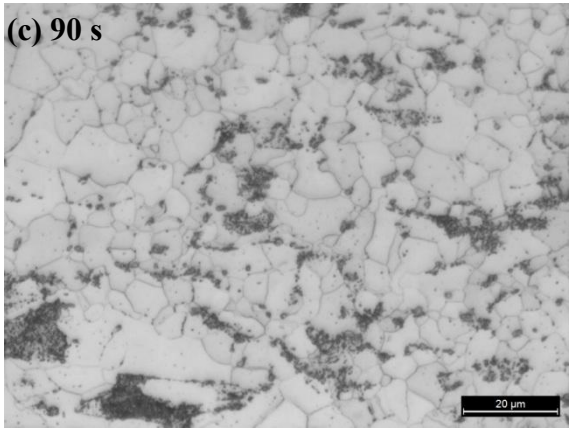

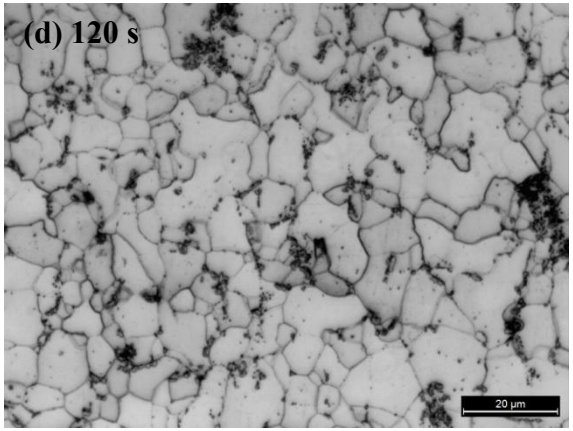

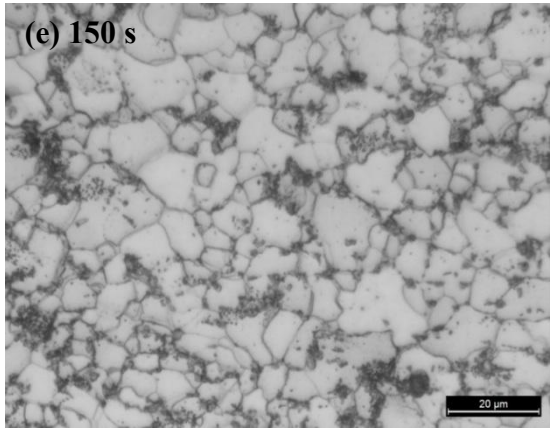

Annealing Temperature - 750 ℃

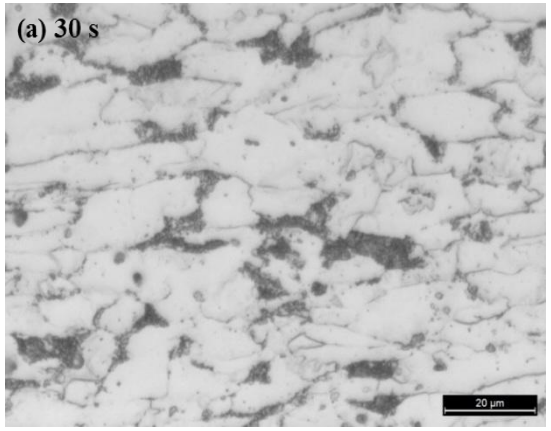

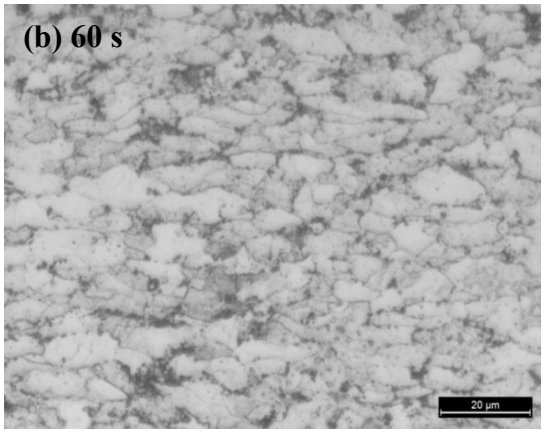

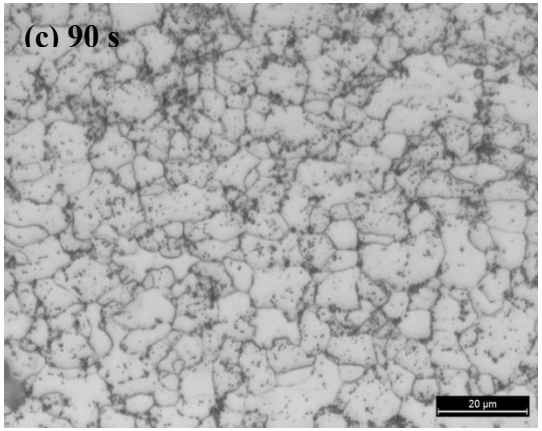

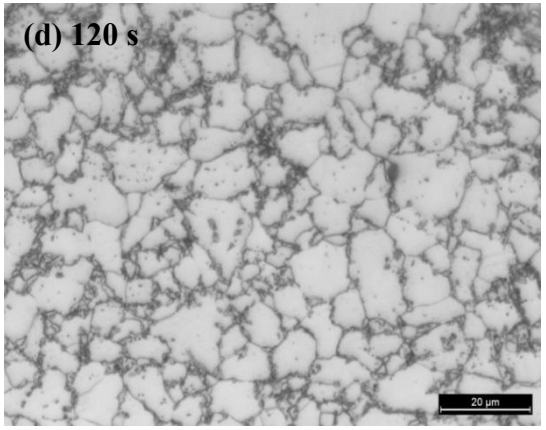

Annealing Temperature - 775 ℃

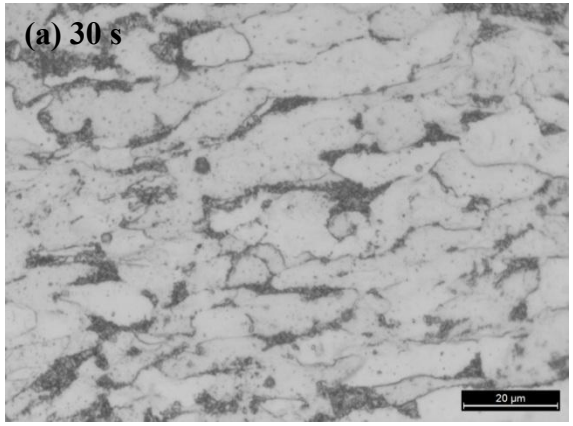

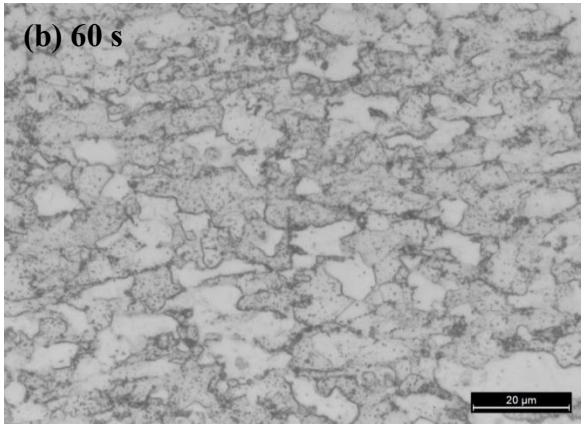

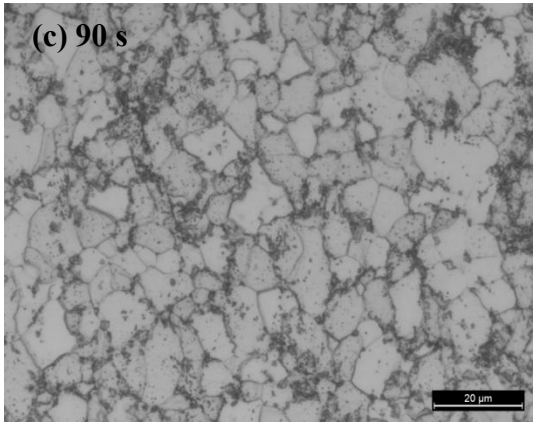

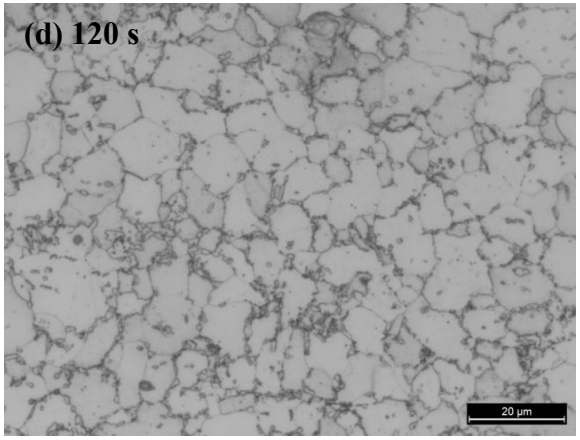

Annealing Temperature - 800 ℃

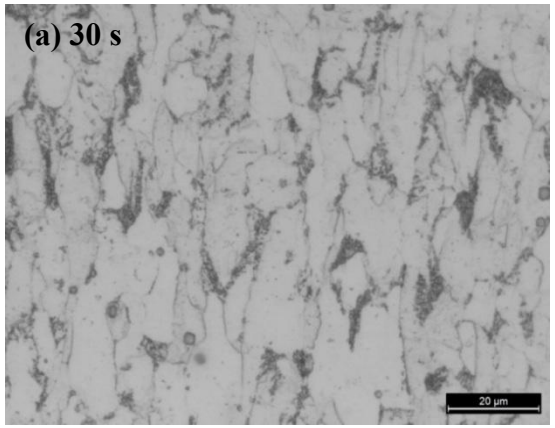

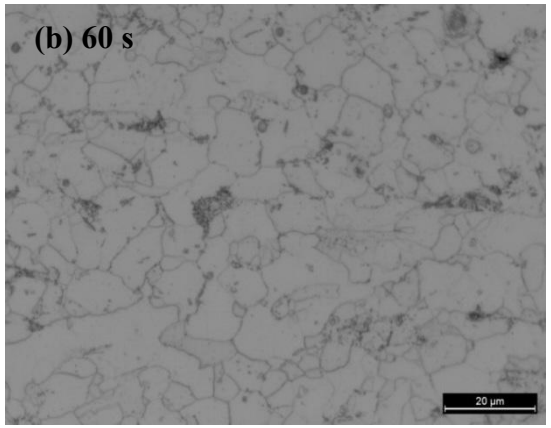

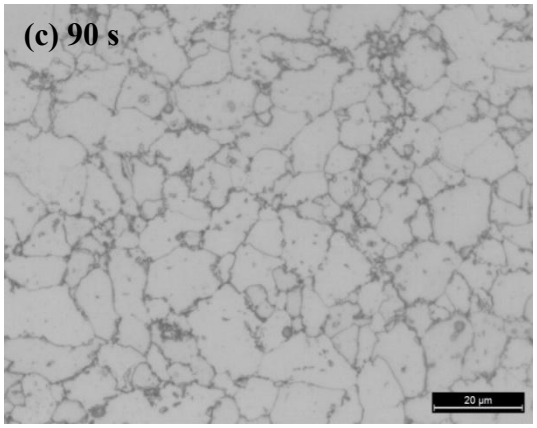

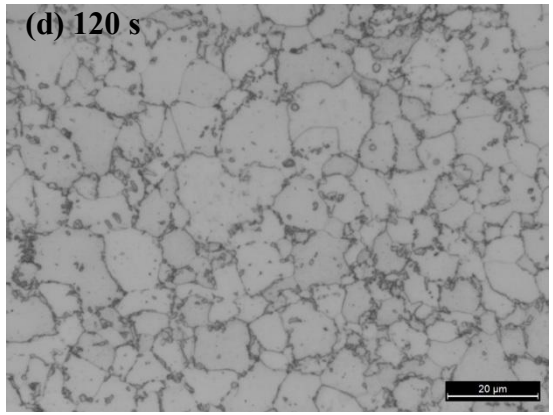

Annealing Temperature - 825 ℃

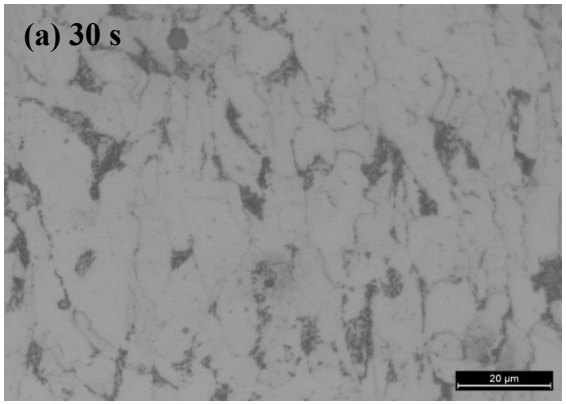

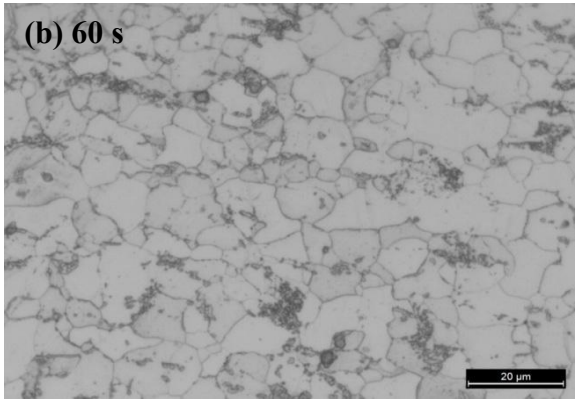

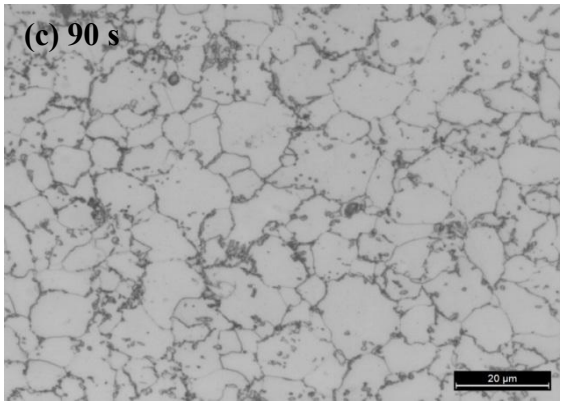

Annealing Temperature - 850 ℃

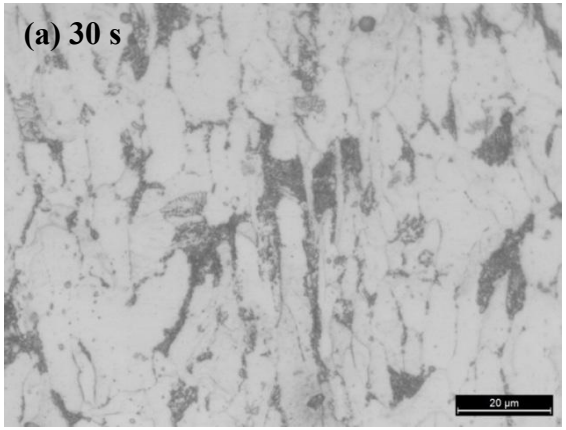

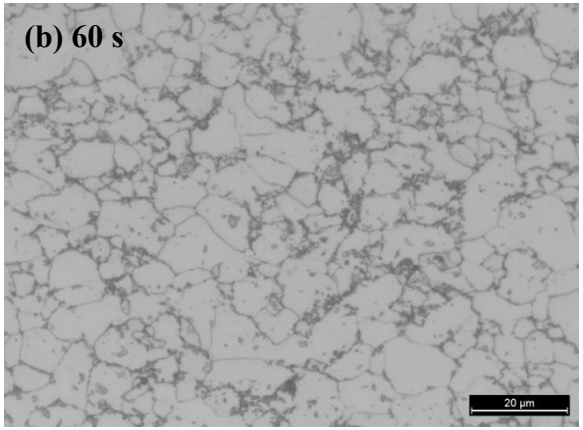

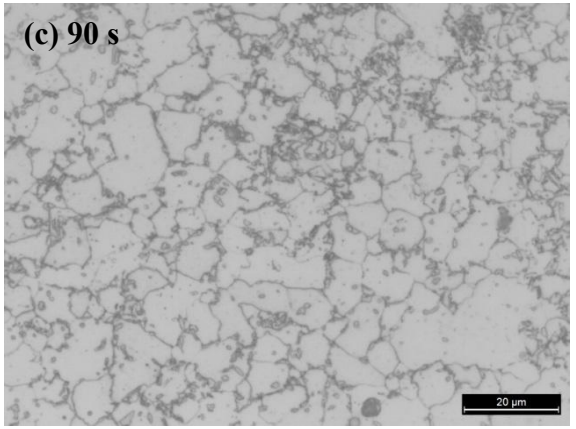

Appendix III

Values of *b* and *n* calculated from the JMAK plot

Temperature (℃)	***b***	***n***
700	2.97×10^{-5}	2.15
725	7.24×10^{-5}	2.27
750	8.95×10^{-5}	2.29
775	1.29×10^{-4}	2.35
800	3.88×10^{-4}	2.36
825	8.06×10^{-4}	2.41
850	9.55×10^{-4}	2.43

Appendix IV

Data for determining the Stress-Strain Curve

(As-received Cold Rolled Steel)

Strain (%)	Stress (MPa)	Strain (%)	Stress (MPa)	Strain (%)	Stress (MPa)	Strain (%)	Stress (MPa)
0.00314	4.795	0.25854	442.76	1.38115	805.28	2.62687	767.17
0.06217	105.62	0.26631	452.25	1.39772	805.33	2.64732	765.88
0.06447	109.43	0.2776	463.12	1.41991	806.00	2.65777	764.47
0.06611	116.09	0.28639	472.65	1.4401	805.81	2.66616	762.58
0.06852	122.62	0.29216	485.97	1.4509	804.18	2.67681	762.28
0.07071	131.62	0.26631	452.25	1.46317	803.80	2.69068	762.12
0.07991	141.18	↓	↓	1.47408	804.31	2.62687	767.17
0.08532	150.27	↓	↓	1.49091	804.58	2.64732	765.88
0.09096	159.11	↓	↓	1.51351	805.33	2.65777	764.47
0.09718	169.51	0.85684	799.31	1.53405	805.24	↓	↓
0.10194	180.33	0.8665	800.01	1.54459	803.66	↓	↓
0.10406	191.60	0.88471	801.71	1.56044	803.37	↓	↓
0.11317	202.94	0.90306	802.98	1.56776	803.57	3.10538	738.06
0.12486	215.62	0.9174	803.59	1.38115	805.28	3.12553	736.82
0.13019	225.91	0.93375	803.60	↓	↓	3.14294	736.39
0.13267	236.41	0.94292	802.47	↓	↓	3.15447	735.99
0.13509	246.07	0.96046	802.50	↓	↓	3.16991	735.07
0.14464	258.19	0.97838	804.01	1.94607	797.75	3.18546	734.36
0.15515	269.13	0.99057	804.54	1.96365	797.67	↓	↓
0.16485	283.99	1.00918	805.09	1.97663	798.26	↓	↓
0.17357	293.25	1.02302	805.92	1.98897	797.77	↓	↓
0.17415	302.44	1.03803	804.40	1.99977	797.741	5.10476	582.69
0.17666	312.97	1.05435	803.97	2.01274	795.65	5.11276	581.66
0.18182	324.18	1.07357	804.90	2.03186	795.16	5.12573	580.30
0.19568	335.27	1.08379	805.71	2.04512	795.66	5.13798	578.81
0.20836	349.95	1.10115	806.56	2.05333	795.74	5.15849	578.33
0.2119	359.94	1.1188	806.88	2.06606	795.30	5.1877	577.26
0.21237	368.31	1.13256	806.26	2.08076	794.79	5.21566	573.64
0.21904	377.87	1.1947	806.39	2.09905	793.48	5.24741	570.33
0.22457	390.03	1.20824	806.68	2.11211	792.66	5.27821	565.41
0.23779	402.30	1.22865	806.56	↓	↓	5.30148	560.60
0.24853	412.89	1.34144	805.70925	↓	↓	5.32641	557.50
0.25077	423.32	1.35834	804.56282	↓	↓	5.35008	555.12
0.25312	433.86	1.37126	805.0403	2.61084	767.14	5.36824	552.26

(Specimen Annealed under Optimized Conditions using Simulator)

Strain (%)	Stress (MPa)	Strain (%)	Stress (MPa)	Strain (%)	Stress (MPa)	Strain (%)	Stress (MPa)
0.03934	28.29	1.07957	358.81	↓	↓	14.40667	603.19
0.02673	45.41	1.0942	360.012	↓	↓	14.4157	604.42
0.02735	56.96	1.13602	360.85	↓	↓	14.43887	604.12
0.06008	68.08	1.11709	361.06	11.89959	595.59	14.45362	605.04
0.03495	88.40	1.15091	362.48	11.90289	595.71	14.46495	604.08
0.05929	104.53	1.07957	358.81	11.92471	595.51	14.49545	603.54
0.07484	115.54	1.0942	360.01	11.94455	596.33	↓	↓
0.05516	125.26	↓	↓	11.9507	596.67	↓	↓
0.08795	136.00	↓	↓	11.98793	595.91	↓	↓
0.07694	148.32	↓	↓	11.98689	596.47	17.71418	606.71
0.08198	161.05	5.50766	529.96	12.01251	596.05	17.72428	606.20
0.11215	175.66	5.49969	530.36	12.02619	596.61	17.74267	606.38
↓	↓	5.52405	530.72	12.03528	596.95	17.76641	605.96
↓	↓	5.5442	530.79	12.0726	596.81	17.77968	606.90
↓	↓	5.54249	531.62	12.0694	597.21	17.80247	606.70
0.77161	331.76	5.58371	531.71	12.10557	596.55	17.82259	606.72
0.75961	333.41	5.57607	531.34	12.11379	596.48	17.83714	606.17
0.79384	335.38	5.58904	531.87	12.12615	596.35	17.85573	605.85
0.8152	336.10	5.61667	532.30	11.89959	595.59	17.86947	605.70
0.81345	336.99	↓	↓	11.90289	595.71	17.88532	605.87
0.85206	338.53	↓	↓	11.92471	595.51	17.90869	605.75
0.84684	339.34	↓	↓	↓	↓	17.92443	606.02
0.861	340.59	9.36778	579.40	↓	↓	↓	↓
0.89442	342.35	9.35296	580.08	↓	↓	↓	↓
0.88419	343.58	9.36852	580.05	14.36713	603.85	↓	↓
0.91785	344.57	9.41365	580.02	14.38085	603.47	25.80713	515.41
0.93228	344.92	9.38174	580.50	14.40667	603.19	25.82349	514.11
0.92463	345.66	9.44513	580.94	14.4157	604.42	25.84384	513.84
0.96453	347.25	9.42995	580.77	14.43887	604.12	25.86356	513.55
0.95439	348.70	9.45296	580.51	14.45362	605.04	25.88437	512.38
0.97139	350.18	9.49309	580.29	14.46495	604.08	25.9051	511.02
1.00827	351.79	9.46533	581.15	14.49545	603.54	25.9228	510.40
0.99795	353.49	9.53074	581.44	14.49488	604.06	25.93857	509.15
1.03258	353.47	9.5054	581.04	14.52069	604.03	25.95937	508.43
1.04076	354.95	9.54177	581.78	14.53739	604.25	25.97697	507.70
1.04448	355.66	9.56911	582.23	14.36713	603.85	25.99994	506.42
1.08288	357.58	9.55152	581.27	14.38085	603.47	26.03387	502.12